MAGNETIC AND SUPERCONDUCTING QUANTUM CRITICAL BEHAVIOR OF ITINERANT ELECTRONIC SYSTEMS

by

RASTKO SKNEPNEK

A DISSERTATION

Presented to the Faculty of the Graduate School of the

UNIVERSITY OF MISSOURI–ROLLA

in Partial Fulfillment of the Requirements for the Degree

DOCTOR OF PHILOSOPHY

in

PHYSICS

2004

Dr. Thomas Vojta, Advisor	Dr. Massimo Bertino
Dr. Carsten Ullrich	Dr. Gerald Wilemski

Dr. Jörg Schmalian

To my mother, father, and sister...

PUBLICATION DISSERTATION OPTION

This dissertation contains two parts, a general introduction (chapter 1) and preprints of four research papers (chapters 2-4) that have already been published or that are submitted for publication. In the first half of the introduction (sections 1.1. and 1.2.) we briefly summarize the theory of classical and quantum phase transitions. In the second half of the introduction we outline the main results of the theory of magnetic quantum phase transition of itinerant electrons (section 1.3.) and we discuss classical and quantum phase transitions in the presence of quenched disorder (section 1.4.). We also summarize the main results of the four research projects of this dissertation. The introductory chapter is written in normal dissertation style.

The second part of this dissertation contains preprints of four research papers. The article on pages 49-59 is published in the *Phys. Rev. B*, vol. 64, p. 052404, 2001. The articles on pages, 60-86 and 87-111 are submitted for publication in the *Phys. Rev. B*. The article on pages 112-122 is submitted for publication in the *Phys. Rev. Lett.* All articles are written in the style (*REVTEX4*) of the American Physical Society.

ABSTRACT

Quantum phase transitions occur at zero temperature as a function of some non-thermal parameter, e.g., pressure or chemical composition. In addition to being of fundamental interest, quantum phase transitions are important because they are believed to underlie a number of interesting low temperature phenomena.

Quantum phase transitions differ from the classical phase transitions in many important aspects, two of them being *(i)* the mode-coupling effects and *(ii)* the behavior in the presence of disorder. We devote two projects of this dissertation to each of the two.

First, we investigate the quantum phase transition of itinerant electrons from a paramagnet to a state which displays long-period helical structures due to a Dzyaloshinskii instability of the ferromagnetic state. In particular, we study how the self-generated effective long-range interaction recently identified in itinerant quantum ferromagnets is cut-off by the helical ordering. Second, we discuss a quantum phase transition between a disordered metal and an exotic (non-$s-$wave) superconductor. Like in the case of ferromagnetic quantum phase transition mode coupling effects lead to an effective long-range interaction between the anomalous density fluctuations. We find that the asymptotic critical region is characterized by run–away flow to large disorder. However, for weak coupling, this region is very narrow, and it is preempted by a wide crossover regime with mean-field critical behavior.

Then, we present results of large-scale Monte Carlo simulations for a $3d$ Ising model with short range interactions and planar defects. We show that the phase transition in this system is smeared, i.e., there is no single critical temperature, but different parts of the system order at different temperatures. Our Monte-Carlo results are in good agreement with a recent theory. Finally, we present large-scale Monte-Carlo simulations of a $2d$ bilayer quantum Heisenberg antiferromagnet with random dimer dilution. In contrast to the exotic scaling scenarios found in many other random quantum systems, the quantum phase transition in this system is characterized by a finite-disorder fixed point with power-law scaling. After accounting for strong corrections to scaling, we find universal, i.e., disorder-independent, critical exponents.

ACKNOWLEDGMENT

It is needless to say that not much of this would have been possible without the patient guidance and help of my adviser Dr. Thomas Vojta. During the past four years his admirable passion for physics and his true love to teach served me as a bright guiding light. Thank you for the invaluable journey!

Many thanks go to my parents Radmila and Dragan Sknepnek for their endless love. Their support was decisive for me to take the path of science when everyone else thought that a bright high school kid should not waste his time on physics.

I owe a deep gratitude to my childhood friend Ivan Dživdžanovski. Ivan and I spent countless hours in often naive discussions about philosophy, politics, mathematics, physics, musics, poetry, movies... Those hours made me keep my sanity and the purpose of studying physics in a crumbling society of a post-communist eastern European country. Thank you for your friendship!

I wish to thank my girlfriend Harshani for her love and support. Her kindness and serenity are the source of priceless happiness and inspiration. Thank you for loving me!

My gratitude goes to Dr. Rajesh Narayanan for the close collaboration on one of the topics of this dissertation and numerous illuminative discussions about quantum phase transitions.

Also, I wish to thank Prof. Dr. Michael Schreiber and the members of his research group at Physics Department, Chemnitz University of Technology, Germany for creating an inspiring scientific environment. Many thanks go, as well to the chairman of Physics Department, University of Missouri - Rolla, Dr. Paul Parris for allowing me to transfer to UMR and continue research with Dr. Vojta. In the past two years, to me the UMR Physics Department has been much more than the place to get the degree.

Finally, I would like to thank my committee members Dr. Massimo Bertino, Dr. Jörg Schmalian, Dr. Carsten Ullrich and Dr. Gerald Wilemski for their help and valuable suggestions.

TABLE OF CONTENTS

Page

PUBLICATION DISSERTATION OPTION iii

ABSTRACT iv

ACKNOWLEDGMENT v

LIST OF ILLUSTRATIONS ix

LIST OF TABLES xi

SECTION

1. INTRODUCTION 1
   - 1.1. CONTINUOUS PHASE TRANSITIONS AND CRITICALITY . . 3
     - 1.1.1. Order parameter. 3
     - 1.1.2. Landau theory. 3
     - 1.1.3. Fluctuations and correlation functions. 7
     - 1.1.4. Breakdown of Landau theory. 8
     - 1.1.5. Landau-Ginzburg-Wilson theory. 9
     - 1.1.6. Universality. 9
     - 1.1.7. Scaling. 10
     - 1.1.8. Dynamical scaling. 12
   - 1.2. QUANTUM PHASE TRANSITIONS 12
     - 1.2.1. Role of quantum mechanics. 13
     - 1.2.2. Statics vs. dynamics. 14
     - 1.2.3. Scaling law. 15
     - 1.2.4. A generic phase diagram. 16
     - 1.2.5. Experimental examples. 18
   - 1.3. QUANTUM PHASE TRANSITIONS OF ITINERANT ELECTRONS 19
     - 1.3.1. Hertz' theory. 19
     - 1.3.2. Hertz' theory revised. 21
     - 1.3.3. Quantum phase transitions and generic scale invariance. . 23
     - 1.3.4. A helimagnetic quantum phase transition of itinerant electrons. 24
     - 1.3.5. Disorder driven quantum phase transition in an exotic superconductor. 27
   - 1.4. PHASE TRANSITIONS IN THE PRESENCE OF DISORDER . 31

1.4.1. Harris criterion. 32
1.4.2. Harris criterion fulfilled. 33
1.4.3. Harris criterion violated. 33
1.4.4. Griffiths phenomena. 35
1.4.5. Smearing of phase transitions induced by correlated disorder. 35
1.4.6. Smeared phase transition in a three-dimensional Ising model with planar defects. 36
1.4.7. Quantum phase transition in a disordered bilayer quantum Heisenberg antiferromagnet. 38
1.5. SUMMARY AND OUTLOOK 40

BIBLIOGRAPHY 42

2. THE QUANTUM PHASE TRANSITION OF ITINERANT HELIMAGNETS (*Phys. Rev. B*, vol. 64, p. 052404, 2001) 49

3. ORDER PARAMETER SYMMETRY AND MODE COUPLING EFFECTS AT DIRTY SUPERCONDUCTING QUANTUM PHASE TRANSITIONS (submitted to *Phys. Rev. B cond-mat/0211519*) 60
I. INTRODUCTION 61
II. LANDAU-GINZBURG-WILSON THEORY 64
A. $p-$wave pairing case 64
B. Anomalous density correlation functions in the $p-$wave channel 66
C. Higher angular momentum channels 70
III. RENORMALIZATION GROUP ANALYSIS 71
IV. CONCLUSIONS 74
APPENDIX A: RENORMALIZED VERTEX 76
APPENDIX B: TWO-POINT LGW VERTEX 78
APPENDIX C: INTERACTION EFFECTS 79
APPENDIX D: 4-POINT VERTICES 82

4. SMEARED PHASE TRANSITION IN A THREE-DIMENSIONAL ISING MODEL WITH PLANAR DEFECTS: MONTE-CARLO SIMULATIONS (submitted to *Phys. Rev. B*, *cond-mat/0311394*) 87
I. INTRODUCTION 88
II. THE MODEL 91
A. 3D Ising model with planar defects 91
B. Results of extremal statistics theory 93
C. Finite-size effects 96
III. NUMERICAL RESULTS 97
A. The method 97

B. Total magnetization and susceptibility 98
C. Finite size effects and sample-to-sample fluctuations 100
D. Local magnetization 104
IV. CONCLUSIONS 106
5. EXOTIC VS. CONVENTIONAL SCALING AND UNIVERSALITY IN A DISORDERED BILAYER QUANTUM HEISENBERG ANTIFERROMAGNET (submitted to *Phys. Rev. Lett.*, *cond-mat/0402352*) 112
VITA 123

LIST OF ILLUSTRATIONS

Figure Page

Section 1.

1.1 Sketch of the phase diagram of water 2

1.2 First order phase transition 4

1.3 Continuous phase transition 5

1.4 Typical phase diagram 16

1.5 Phase diagram of $MnSi$ 24

1.6 Schematic plot of the helical ordering in $MnSi$ 25

1.7 Phase diagram of UGe_2 28

1.8 Schematic plot of a region (Griffiths island) 34

1.9 Logarithm of the total magnetization m 37

1.10 Dimer-diluted $2d$ spin-$\frac{1}{2}$ bilayer quantum Heisenberg antiferromagnet . . 38

1.11 L_τ^{max}/L vs. L for four disorder concentrations 39

Section 3.

1. Contributions to the leading terms of the Gaussian part 66

2. Leading singular contributions to $\chi^{(4)}_{diag}$ 68

3. The leading contribution to the $\chi^{(4)}_{off}$ 69

4. Schematic flow diagram on the critical surface 73

5. Definition of the particle-particle ladder 77

6. Renormalized vertex 78

7. Diagrams arising in the first order perturbation theory 80

8. Renormalized interaction vertex 80

9. Diagrams contributing to the $\chi^{(4)}_{off}$ 83

Section 4.

1. Average magnetization 99

2. Logarithm of the total magnetization m as a function of $|T_c^0 - T|^{-\nu}$ ($\nu = 0.627$) for several impurity concentrations 100

3. Logarithm of the total magnetization m as a function of $|T_c^0 - T|^{-\nu}$ ($\nu = 0.627$) for disorder concentration $p = 0.2$ 101

4. Logarithm of the total magnetization m as a function of $|T_c^0 - T|^{-\nu}$ ($\nu = 0.627$) for $L_\perp = 200$, $L_C = 280$ and $p = 0.2$ 103

5. The probability distribution of sample critical temperature 104

6. Local magnetization 105

Section 5.

1. Phase diagram of the diluted bilayer Heisenberg antiferromagnet 115

2. Upper panel: Binder ratio g_{av} as a function of L_τ 118

3. L_τ^{max}/L vs. L for four different concentrations 119

4. Scaling plot of g_{av} vs. $(T - T_c)x_L$ 119

5. Scaling factor vs. L 120

LIST OF TABLES

Table Page

1.1 Definitions of the commonly used critical exponents. 6

1. INTRODUCTION

It is a common wisdom that matter can exist in different phases. A glass of water placed into a freezer will turn into a solid chunk of ice, i.e., the macroscopic properties of water fundamentally change as the temperature is lowered. Freezing of water is a well known example in the countless series of phenomena generally known as *phase transitions*. Examples of phase transitions range from somewhat exotic transformations of matter in the early stages of the Universe that shaped the night sky as we see it today to the never-ending cycle of water on Earth, essential for the existence of life. It is clear that understanding the mechanisms that drive phase transitions is one of the central tasks of the physical sciences.

Generically, phase transitions can be classified as: *(i)* those that involve *latent heat* and *(ii)* those that do not. The latter are commonly known as *continuous phase transitions* or *critical points*[a]. We'll explain the main characteristics of these two classes of phase transitions using water as an example. In Fig. 1.1, we sketch the phase diagram of water. The boundaries between different phases are represented by solid lines. Crossing each solid line corresponds to a phase transition which involves absorbing or releasing finite amount of latent heat. Note that the line separating the liquid from the gas phase terminates with a critical point (CP). The boundaries of all three phases meet at the *triple point* (TP). The main landmark of first order phase transitions is coexistence of two phases, i.e., when heated, a cube of ice will start melting and the mixture of water and ice will stay at the same temperature ($0°C$) until all ice melts[b]. In contrast, at a critical point the transition between two phases[c] is continuous, i.e., there is no coexistence of two distinct phases and no latent heat is absorbed or released during the transition.

A well known example of a continuous phase transition occurs at the Curie point of, e.g., iron ($T_c = 1043K$). At $T > T_c$, iron is a paramagnet. In the absence of an external magnetic field, there is no magnetization. If a weak magnetic field $\vec{h}$

[a]Phase transitions that involve latent heat are, for historical reasons, referred to as *first order* phase transitions. Continuous phase transitions are also known as *second order* phase transitions.

[b]For the ice-water transition latent heat is $\approx 335kJ/kg$.

[c]E.g., between vapor and liquid water at $T_c \approx 647K$ and $p_c \approx 21.8MPa$.

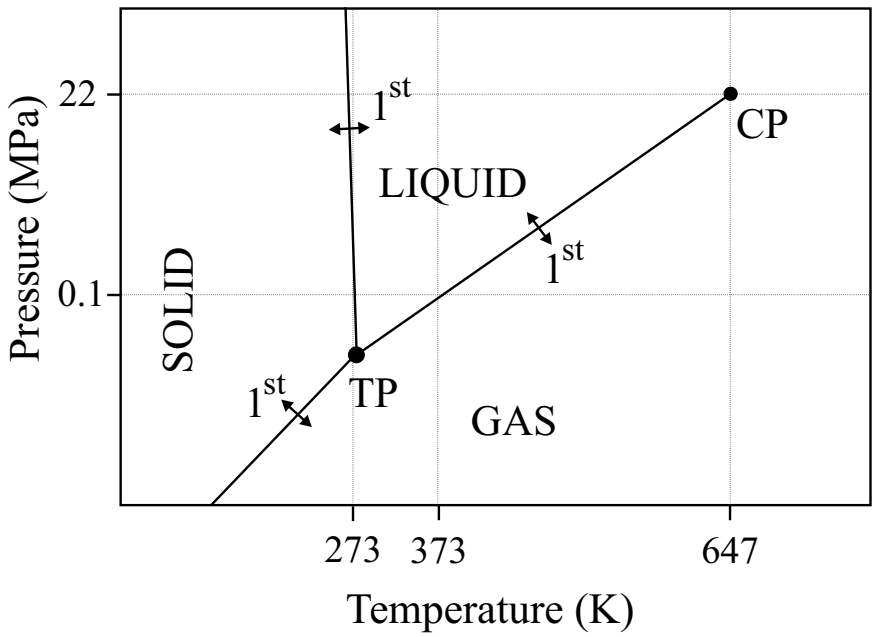

Figure 1.1. Sketch of the phase diagram of water in the pressure–temperature plane. The boundaries between different phases are represented by solid lines. Crossing each solid line corresponds to a phase transition which involves absorbing or releasing finite amount of latent heat (1^{st}). Note that the line separating the liquid from the gas phase terminates with a critical point (CP). Boundaries of all three phases meet at the *triple point* (TP).

is applied, the sample develops a magnetization that grows linearly with the applied field, $\vec{m} \propto \vec{h}$. At $T < T_c$, the situation is drastically different. Even without an external field, the sample develops a macroscopic magnetization. If an external field is applied, the magnetization rapidly aligns with the external field, resulting in a non-linear relation between $\vec{m}$ and $\vec{h}$. Experiments show that the magnitude of the magnetization $\vec{m}$ steadily decreases if T_c is approached from below and eventually vanishes continuously at T_c in contrast to the ice–water transition, where one observes abrupt changes of observables, e.g., a jump in density between water and ice.

The examples discussed so far fit into the broad class of *thermal* or *classical*[d] phase transitions. A property common to all thermal phase transitions is that they

[d]The use of words *thermal* and *classical* as synonyms in the case of phase transitions will be explained in the subsection 1.2.

occur at finite temperatures. The system is often, but not necessarily always[e], driven through a phase transition by tuning the temperature: The rapidly expanding early Universe was quickly cooling down which lead to separation of matter and energy and eventually to the formation of galaxies; a glass of water was cooling down in a freezer, a block of iron was losing magnetization when heated up etc. Recently, a new field has emerged dealing with the transformations of matter that occur at the absolute zero of temperature as a function of some non-thermal external parameter, e.g., pressure, chemical composition, external magnetic field, etc. Such transitions are called *quantum phase transitions*. Although the absolute zero is experimentally not reachable, the effects of such *quantum critical points* are manifest at finite temperatures, as it will be discussed in section 1.2.. Before focusing on these quantum phase transitions we present a brief overview of classical continuous phase transitions.

1.1. CONTINUOUS PHASE TRANSITIONS AND CRITICALITY

A full understanding of continuous phase transitions developed over more than a century, and in this process the important paradigms of scale invariance, universality, and the renormalization group were introduced. Here we summarize major results of the theory of critical phenomena. Detailed and pedagogical introductions to the field are presented in a few excellent texts, e.g., [1–3].

1.1.1. **Order parameter.** The general concept of the *order parameter* was introduced by Landau [4]. The order parameter is a thermodynamic quantity which is zero in one phase (the disordered phase) and nonzero in the other (the ordered phase). Quite often the choice of the order parameter is obvious, e.g., the magnetization in the case of the ferromagnetic phase transition. On the other hand, there are cases where finding an appropriate order parameter is a complicated task itself, e.g., in the disorder driven localization-delocalization transition of non-interacting electrons.

1.1.2. **Landau theory.** Landau [4] proposed a very general theory to describe phase transitions. The main assumption of the theory is that the free energy F is an analytic function of the order parameter m and can be expanded in a power series in m. The stable phase is then determined by the global minimum of F with respect to

[e] At a constant temperature the system can undergo a phase transition as a function of pressure. In the case of water at $T = 100^{\circ}C$, vapor condenses into liquid water via a first order phase transition at $p \approx 100kPa$. This process corresponds to moving along the vertical $T = 100^{\circ}C$ line in Fig. 1.1.

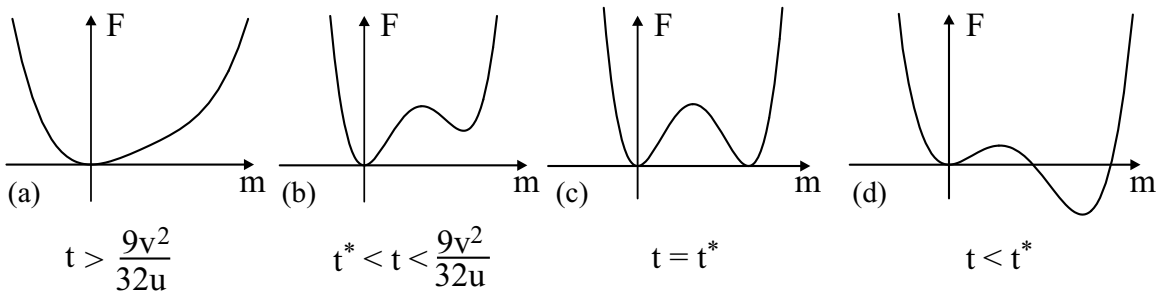

Figure 1.2. First order phase transition. Free energy F, eq. (1.1), as a function of m for four different values of t ($h = 0$). (a) $t > \frac{9v^2}{32u}$, (b) $t^* < t < \frac{9v^2}{32u}$, (c) $t = t^*$, and (d) $t < t^*$.

m. Close to the critical point m is small, and it is sufficient to keep only a few lowest order terms[f] in the expansion,

$$F = tm^2 + vm^3 + um^4 - hm + O(m^5), \tag{1.1}$$

where t, v and u are system parameters and h is the external scalar field conjugate to the order parameter. F is commonly known as the *Landau function* and is equal to the Gibbs free energy only for the value of m which minimizes it. For classical critical points t corresponds to the distance from the critical temperature, i.e., $t = a(T - T_c)$, with a being a constant. Note that $u > 0$, otherwise eq. (1.1) has minimum at $|m| \to \infty$.

Landau theory is remarkably general. In the case of $v \neq 0$, eq. (1.1) describes a first order phase transition. In the absence of the external field h, for $t > \frac{9v^2}{32u}$ there is a single minimum at $m = 0$ (Fig. 1.2a). As t is lowered below $\frac{9v^2}{32u}$ a secondary minimum starts to develop (Fig. 1.2b). At some $t = t^*$, both minima have the same value (Fig. 1.2c). Below t^*, the secondary minimum becomes the global minimum and the value of m which minimizes F jumps *discontinuously* from $m = 0$ to a nonzero value (Fig. 1.2d).

If accidentally or for symmetry reasons $v = 0$, the theory describes a continuous phase transition. For $t > 0$ and $h = 0$, the Landau function F will have a minimum

[f] For simplicity we will discuss a transition with the scalar order parameter.

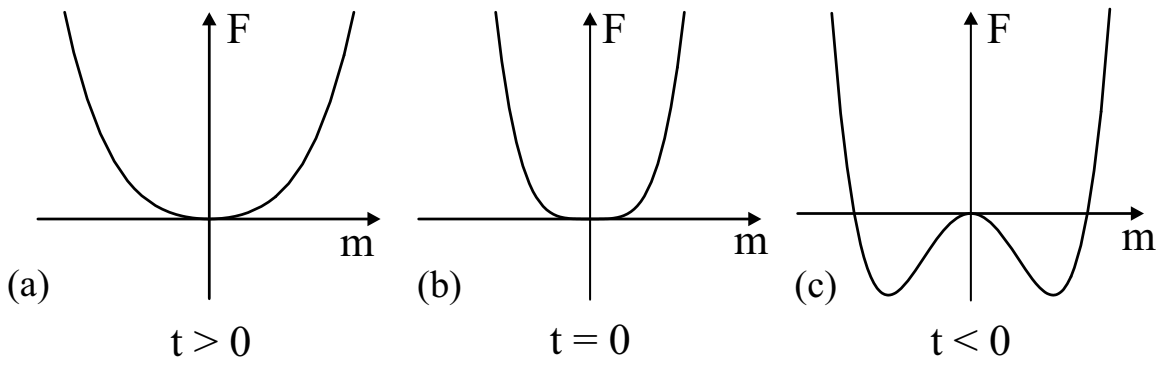

Figure 1.3. Continuous phase transition. Free energy F, eq. (1.1), as a function of m for three different values of t ($h = 0$). (a) $t > 0$, (b) $t = 0$, and (c) $t < 0$.

at $m = 0$ (Fig. 1.3a). As t is lowered below zero, two minima start to emerge (Fig. 1.3b,c) at

$$m = \pm\sqrt{\frac{-t}{2u}} \propto -t^{\frac{1}{2}}. \tag{1.2}$$

Therefore, Landau theory predicts a second-order transition with

$$m \propto (T_c - T)^{\beta}, \tag{1.3}$$

with $\beta = 1/2$ being a *critical exponent*. The critical exponent β controls the temperature dependence of the order parameter in the vicinity of the critical temperature. Similarly, there are other critical exponents which control the behavior of thermodynamic quantities in the vicinity of T_c. In order to determine the other critical exponents we have to allow for a non-zero external field h. From the free energy minimum requirement $\partial F/\partial m = 0$, we derive the equation of state,

$$\frac{\partial F}{\partial m} = h, \tag{1.4}$$

or

$$2a(T - T_c)m + 4um^3 = h, \tag{1.5}$$

Table 1.1. Definitions of the commonly used critical exponents in terms of magnetic phase transitions, m is the order parameter (magnetization) and h is the conjugate field. t denotes the distance from the critical point and d is the space dimensionality.

	exponent	definition	conditions
specific heat	α	$c \propto \lvert t\rvert^{-\alpha}$	$t \to 0, h = 0$
order parameter	β	$m \propto (-t)^{\beta}$	$t \to 0$ from below, $h = 0$
susceptibility	γ	$\chi \propto \lvert t\rvert^{-\gamma}$	$t \to 0, h = 0$
critical isotherm	δ	$h \propto \lvert m\rvert^{\delta}\mathrm{sign}(m)$	$h \to 0, t = 0$
correlation length	ν	$\xi \propto \lvert t\rvert^{-\nu}$	$t \to 0, h = 0$
correlation function	η	$G(r) \propto \lvert r\rvert^{-d+2-\eta}$	$t = 0, h = 0$
dynamical[g]	z	$\xi_\tau \propto \xi^z$	$t \to 0, h = 0$

where we have explicitly written $t = a(T - T_c)$. At $T = T_c$, from eq. (1.5), we get

$$m = \left(\frac{h}{4u}\right)^{\frac{1}{3}}, \tag{1.6}$$

i.e., at the critical temperature the order parameter vanishes as

$$m \propto h^{\delta}, \tag{1.7}$$

with $\delta = 1/3$. If we take the derivative of eq. (1.5) with respect to h and use the definition of the order parameter susceptibility $\chi = \partial m/\partial h$ we get

$$\chi \propto \frac{1}{|t|}, \tag{1.8}$$

or

$$\chi \propto |T - T_c|^{-\gamma}, \tag{1.9}$$

with the susceptibility exponent $\gamma = 1$. For further reference, in Tab. 1.1 we summarize the commonly used critical exponents in terms of magnetic phase transitions.

[g] ξ_τ is the correlation time, to be discussed in 1.1.8.

Note that the Landau theory is *super*universal, i.e., it states that all continuous phase transitions have identical critical exponents.

1.1.3. **Fluctuations and correlation functions.** At a finite temperature the order parameter fluctuates around its equilibrium value. Experiments show that as a critical point is approached the order parameter fluctuations become correlated over large distances. Exactly at the critical point, the *correlation length* (ξ) of these fluctuations diverges. In order to quantify the fluctuations we introduce the local fluctuating order parameter $\phi(\vec{x})$ which is obtained by coarse-graining the microscopic order parameter: Close to the critical point the system contains patches of linear size $\approx \xi$ in which the order parameter is approximately constant. This suggests that we divide the system up into blocks of linear dimension L much larger than the microscopic length scale a_{latt} but smaller than the correlation length ξ. Within each block, the system is approximately uniform, and since $L \gg a_{latt}$, it is sensible to define the local order parameter $\phi(\vec{x})$ within each block centered at $\vec{x}$. The correlations between the order parameter fluctuations are described by *correlation functions*, i.e.,

$$G(\vec{x}_1 - \vec{x}_2) = \langle \phi(\vec{x}_1)\, \phi(\vec{x}_2) \rangle - \langle \phi(\vec{x}_1) \rangle \langle \phi(\vec{x}_2) \rangle. \tag{1.10}$$

Note that we assume a translational invariant system, i.e., $G(\vec{x}_1, \vec{x}_2) = G(\vec{x}_1 - \vec{x}_2)$. The order parameter correlation function is related to the order parameter susceptibility via a *fluctuation-dissipation theorem*,

$$\chi(\vec{x}_1 - \vec{x}_2) = \frac{1}{k_B T} G(\vec{x}_1 - \vec{x}_2) \tag{1.11}$$

(see, e.g., [1,5]). Within the original Landau theory the order parameter fluctuations are completely suppressed. In order to take them into account Landau theory has to be generalized. The Landau function becomes a functional of the fluctuating order parameter $\phi(\vec{x})$,

$$S[\phi(\vec{x})] = \frac{1}{T} \int d^d x \left[t\phi^2(\vec{x}) + c(\nabla \phi(\vec{x}))^2 \right] + u \int d^d x \phi^4(\vec{x}), \tag{1.12}$$

where $\int d^d \vec{x}$ stands for the integral over a d dimensional space. The last expression is known as the *Landau-Ginzburg-Wilson* functional. The new element in eq. (1.12)

is the gradient term in the Gaussian part of S. It penalizes configurations with large differences between the order parameters in adjacent blocks (which are energetically unfavorable). Note that keeping only the first order gradient term is justified solely in the limit of long wavelength fluctuations which is appropriate in the vicinity of a critical point where the physics is controlled by long-wavelength fluctuations.

Landau [6] analyzed the fluctuating theory within the *Gaussian approximation*. The Gaussian approximation assumes that the fluctuations are distributed normally around the average values m. In this approximation the fluctuations are non-interacting, i.e., the ϕ^4 term is neglected. As a consequence, at the critical point the correlation length behaves as

$$\xi \propto t^{-\frac{1}{2}}, \tag{1.13}$$

i.e., it diverges as

$$\xi \propto |T - T_c|^{-\nu}, \tag{1.14}$$

with the correlation length critical exponent $\nu = 1/2$.

1.1.4. **Breakdown of Landau theory.** As we have already seen, Landau theory predicts super-universal rational critical exponents. However, experiments find critical exponents which are in general some irrational numbers significantly different from those predicted by Landau theory. The reason is that the Landau theory does not properly treat the effects of the order parameter fluctuations.[h] The order parameter fluctuations are negligible if their strength is much smaller than the average value of the order parameter, i.e., if

$$E_{fl} = \frac{\int_V d^d\vec{x} G(\vec{x})}{\int_V d^d\vec{x} m^2(\vec{x})} \ll 1, \tag{1.15}$$

where $G(\vec{x})$ is defined in eq.(1.10) and the integral is over a correlation volume $V = \xi^d$. Using eqs. (1.11), (1.8) and (1.13), eq. (1.15) becomes

$$E_{fl} \propto \frac{t^{-1}}{t^{d/2}t} = t^{\frac{d}{2}-2} \ll 1 \qquad (\text{for } t \to 0), \tag{1.16}$$

[h]The Landau theory is an example of a mean-field theory.

which is the *Ginzburg criterion* [7, 8]. The Ginzburg criterion ensures that for all dimensions $d < 4$ the order parameter fluctuations are important at the critical point and the phase transition can not be accurately described by the Landau theory. For $d > 4$ the Landau theory is self-consistent and provides an accurate description of the critical behavior. Therefore $d = d_c^+ = 4$ is called the *upper critical dimension* for the model (1.12). The concept of an upper critical dimension can be generalized to other models, in general it can be shown (see, e.g., [1]) that Landau theory is applicable if

$$d > \frac{2\beta + \gamma}{\nu} \equiv d_c^+. \tag{1.17}$$

1.1.5. **Landau-Ginzburg-Wilson theory.** In order to obtain the correct critical behavior below d_c^+ one has to go beyond the Gaussian approximation, i.e., one has to keep the interactions of the fluctuations (the ϕ^4 term in eq. (1.12)). The solution of the problem was found by Wilson [9, 10] for which he was awarded a Nobel Prize in Physics in 1982. Wilson treated the Landau-Ginzburg-Wilson theory by means of a renormalization group (RG)[i] (see, e.g., [1, 2]). Wilson's RG uses the fact that at a critical point the correlation length diverges and therefore the system effectively looks scale invariant. By integrating out fluctuations on short length scales one generates a succession of effective theories that describe the behavior near the critical point. The critical theory is then a fixed point of the RG transformation. In addition to providing a conceptional framework, Wilson established a controlled method for calculating critical exponents. Two major achievements of the Wilson's theory are the explanation of the *universality* and *scaling*.

1.1.6. **Universality.** Experiments have shown that there are wide classes of intrinsically very different systems which share the same critical exponents.[j] This property is called *universality*. From Wilson's theory it follows that critical exponents depend only on the spatial dimensionality, the symmetry of the order parameter and the symmetry and range of the interactions, but not on the detailed form and magnitude of the interactions. Therefore very different systems can have identical critical behavior. All systems that share the same critical exponents form a *universality*

[i] The lowest order of the RG analysis is exactly the Gaussian approximation.

[j] e.g., experiments found $\beta = 0.327(6)$ for sulphurhexaflouoride and $\beta = 0.321(6)$ for ^3He. Note that also $\beta = 0.326(4)$ for the 3d Ising model.

class. Universality makes continuous phase transitions very attractive for theoretical physics. It is sufficient to find a simple model that represents a universality class and determine its critical properties. Universality then ensures that all systems in that class will share exactly the same critical exponents.

1.1.7. **Scaling.** Scaling has been observed in experiments and summarized by Widom in the *scaling hypothesis* [11]. Within Wilson's theory it is possible to derive the scaling hypothesis from first principles. Widom proposed that close to the critical point the singular part of the free energy density, $f = F/V$, is a function of *one* rather than two arguments[k]:

$$f(t,h) = b^{-d} f(tb^{1/\nu}, hb^{y_h}) = t^{d\nu}\psi(\frac{h}{t^{y_h\nu}}), \tag{1.18}$$

t is the distance from the critical point, h is the external field and b is an arbitrary scaling factor which was set to $b = t^{-\nu}$ in the last expression. $y_h > 0$ is a scaling dimension which at the critical point controls the dependence of the singular part of the free energy on external field h. Parameters with scaling dimension larger than zero, like, h and t, are called *relevant*; parameters with negative scaling dimension are *irrelevant*[l]. If the scaling dimension is zero the parameter is called *marginal*[m]. Note that only relevant variables contribute to the leading singularity in f. Therefore, the others have been suppressed in eq. (1.18).

Using the scaling form of the free energy, it can be shown that not all critical exponents are independent. It is sufficient to determine only two of them and the rest can be determined from the *scaling relations*. For example, from (1.18) the zero field order parameter is

$$m|_{h=0} = -\left(\frac{\partial f}{\partial h}\right)_T = t^{d\nu-\nu y_h}\psi(0) \propto t^{\beta}. \tag{1.19}$$

Therefore,

$$\beta = \nu\,(d - y_h) \tag{1.20}$$

[k]For simplicity we assume a magnetic phase transition

[l]They have been suppressed in eq. (1.18).

[m]Terms *relevant*, *irrelevant* and *marginal* originate in the renormalization group scheme and correspond to the behavior of the parameters under renormalization, i.e., if they respectively increase, decrease or do not change under renormalization.

Further, the zero-field susceptibility is

$$\chi|_{h=0} = -\left(\frac{\partial^2 f}{\partial h^2}\right)_T = t^{d\nu-2\nu y_h} \propto t^{-\gamma}, \tag{1.21}$$

leading to

$$\gamma = -\nu d + 2\nu y_h. \tag{1.22}$$

Finally, the specific heat

$$c_h = -T\left(\frac{\partial^2 f}{\partial T^2}\right)_h = const. \times t^{\nu d-2} \propto t^{-\alpha}, \tag{1.23}$$

and

$$\alpha = 2 - \nu d. \tag{1.24}$$

Combining eqs. (1.20), (1.22) and (1.24) we get Rushbrooke's [12] scaling relation,

$$\alpha + 2\beta + \gamma = 2. \tag{1.25}$$

Expression (1.24) is also known as Josephson's scaling law [13] or *hyperscaling* relation, and it is valid only below the upper critical dimension $d < d_c^+$. Similarly, one can derive Fisher's [14] scaling law,

$$(2 - \eta)\,\nu = \gamma. \tag{1.26}$$

Now we briefly discuss scaling in finite size systems known as *finite size scaling*. Finite size scaling is particularly important for analyzing results of numerical simulations. For a finite size system of linear size L, the inverse length L^{-1} behaves as a relevant variable, i.e.,

$$f(t, h, L^{-1}, A) = b^{-d} f(tb^{1/\nu}, hb^{y_h}, L^{-1}b, Ab^{-|y_A|}), \tag{1.27}$$

where A is an irrelevant variable[n] and $y_A < 0$ is the corresponding irrelevant scale dimension. Now if we can set $b = L$ eq. (1.27) becomes

$$f(t, h, L^{-1}, A) = L^{-d}\phi(tL^{1/\nu}, hL^{y_h}, AL^{-|y_A|}). \tag{1.28}$$

For sufficiently large L, the product AL^{y_A} is small ($y_A < 0$) and $\phi(tL^{1/\nu}, hL^{y_h}, AL^{-|y_A|})$ can be expanded in powers of AL^{y_A} around $AL^{y_A} = 0$,

$$\begin{aligned} \phi(tL^{1/\nu}, hL^{y_h}, AL^{-|y_A|}) &= \phi(tL^{1/\nu}, hL^{y_h}, 0) + \\ &+ \frac{\partial\phi(tL^{1/\nu}, hL^{y_h}, AL^{-|y_A|})}{\partial\left(AL^{-|y_A|}\right)}\Big|_{AL^{-|y_A|}=0} AL^{-|y_A|} + \\ &+ o(\left(AL^{-|y_A|}\right)^2), \end{aligned} \tag{1.29}$$

and we stopped the expansion at the first order. Eq. (1.29) represents a leading irrelevant correction to finite size scaling and is important for the discussion in chapter 5.

1.1.8. **Dynamical scaling.** In the vicinity of a critical point the relaxation toward equilibrium becomes very slow [15,16]. This phenomenon in known as *critical slowing down*. In addition to the diverging correlation length there is a diverging correlation in time ξ_τ. Its divergence is governed by the *dynamical* critical exponent z, i.e., $\xi_\tau \propto \xi^z$.

1.2. QUANTUM PHASE TRANSITIONS

At zero temperature one can trigger fundamental changes in the ground state properties of a system by tuning some non-thermal parameter, e.g., pressure or chemical composition. These changes are driven by quantum rather than thermal fluctuations and known as *quantum phase transitions*. In addition to being of fundamental interest, quantum phase transitions are important because they are believed to underlie a number of interesting low temperature phenomena like high temperature superconductivity, quantum Hall effect, various magnetic phenomena etc. Extensive introductions to quantum phase transitions have recently been given in [17,18].

[n] Leading irrelevant variables control corrections to scaling which are often observed in numerical simulations.

1.2.1. **Role of quantum mechanics.** Before discussing quantum phase transitions in detail we have to address an important question: *Is quantum mechanics necessary to describe the physics in the vicinity of a critical point?*[o]. Following a simple intuitive argument, a quantum mechanical description of a problem is necessary if the typical energy scale of quantum fluctuations $E_c = \hbar\omega_c$ (ω_c is the typical frequency of the fluctuations) is of the same order of magnitude as a typical energy scale of thermal fluctuations ($k_B T$), i.e., if:

$$\hbar\omega_c \gtrsim k_B T. \tag{1.30}$$

In section 1.1.8., we argued that close to a critical point the correlation time ξ_τ of the order parameter fluctuations diverges, i.e.,the typical frequency scale, $\omega_c \propto 1/\xi_\tau$, vanishes as:

$$\omega_c \propto |t|^{\nu z}, \tag{1.31}$$

as the critical point is approached. At any finite temperature, sufficiently close to T_c, the condition in eq. (1.30) will be violated. As the critical point is approached quantum fluctuations become less important and one observes a cross-over to the region dominated by thermal (classical) fluctuations. Therefore, the immediate vicinity of a critical point can be described solely in terms of classical statistical mechanics. The cross-over happens at $|t| < t_x$,

$$t_x \propto T_c^{1/\nu z}. \tag{1.32}$$

Note that eq. (1.32) is valid only below the upper critical dimension. Above d_c^+ the condition (1.32) becomes more complicated as a consequence of the existence of dangerously irrelevant variables[p].

The situation is fundamentally different at $T = 0$. At zero temperature, the system is in its ground state and the thermal fluctuations are completely suppressed. Eq. (1.30) is fulfilled all the way to the *quantum* critical point. Therefore, quantum mechanics is necessary to describe properties of a quantum phase transition.

[o]This should not be mixed with the question of the necessity for a quantum mechanical description of the ordered phases, e.g., the superconducting state is a purely quantum mechanical phenomenon.

[p]A dangerously irrelevant variable w is a variable which is renormalization group irrelevant but in the limit $w \to 0$ the free energy is non-analytic.

Since all experiments are done at often very low but unavoidably finite temperatures it is legitimate to ask if quantum phase transitions are merely an academic problem. It turns out that they are not. According to (1.32), at sufficiently low temperatures the quantum to classical crossover happens extremely close to the critical point. Therefore it is very hard or even impossible to observe the crossover experimentally. We will come back to this question in section 1.2.4. when discussing a generic phase diagram in the vicinity of a quantum critical point (Fig. 1.4).

1.2.2. **Statics vs. dynamics.** The main problem in statistical mechanics is to derive the macroscopic behavior of a system from its microscopic Hamiltonian. This can be done by calculating the partition function:

$$Z = \mathrm{Tr} e^{-H/k_B T}, \tag{1.33}$$

where H is the many-body Hamiltonian and k_B the Boltzmann constant. In the classical case Tr is an integral over the phase space. In the quantum case Tr stands for the trace in Hilbert space.

The partition function of a classical system is:

$$Z = \int d^{3N}p \; d^{3N}q \; e^{-(K(p)+V(q))/k_B T} = \int d^{3N} \; p \; e^{-K(p)/k_B T} \int d^{3N} q \; e^{-V(q)/k_B T}, \tag{1.34}$$

with $K(p)$ being kinetic and $V(q)$ potential terms of the Hamiltonian. For simplicity we assume that the potential depends only on coordinates q. This excludes, e.g., the case of the potential describing a charged particle in an electromagnetic field. The $6N$ dimensional integral in eq. (1.34) factorizes into two independent integrals, one over momenta and the other over coordinates. Therefore dynamics and statics are decoupled and it is possible to solve for one without paying attention to the other.

The situation is distinctly different in the quantum case. The Hamiltonian becomes a quantum mechanical operator, i.e., $\hat{H} = \hat{K}(\hat{p}) + \hat{V}(\hat{q})$. The separation of dynamical and statical terms in the partition function is *not* possible since, in general, $\hat{K}(\hat{p})$ and $\hat{V}(\hat{q})$ do not commute, i.e.,

$$Z = \mathrm{Tr} e^{-\hat{H}/k_B T} = \mathrm{Tr} e^{-(\hat{K}+\hat{V})/k_B T} \neq \mathrm{Tr} e^{-\hat{K}/k_B T} Tr e^{-\hat{V}/k_B T}. \tag{1.35}$$

Statics and dynamics are closely coupled and it is not possible to solve for one without solving for the other. As a consequence, universality classes of quantum phase transitions are generically narrower, e.g., two classical systems which belong to the same classical universality class can have different dynamics. As a result, quantum correspondents of those two systems will inevitably belong to different quantum universality classes.

1.2.3. **Scaling law.** The canonical density operator $e^{-\hat{H}/k_BT}$ in eq. (1.33) can be seen as a time evolution operator in imaginary time τ if we identify:

$$\frac{1}{k_BT} = \tau = -i\frac{\Theta}{\hbar}, \tag{1.36}$$

where Θ is real time. As a consequence the imaginary time acts as an extra dimension. Formally this can be seen from the path integral representation of the partition function (see, e.g., [19]). Thus, the quantum partition function in d dimensions maps onto a classical partition function in $d+1$ dimensions. At finite temperatures $\beta \equiv 1/k_BT < \infty$, and this extra dimension extends only over a finite interval. Sufficiently close to the critical point correlation length in time $\xi_\tau > 1/T$ and thus the extra dimension will not affect the asymptotic critical behavior[q]. It rather produces finite-size effects which will lead to corrections to scaling [20, 21]. At $T = 0$ the extra dimension is infinite and the effective dimensionality of the system is increased. Note that eq. (1.36) together with eq. (1.35) suggests that imaginary time always scales like a length which leads to the dynamical critical exponent $z = 1$ in all cases. That is however true only for a full microscopic Lorentz invariant theory, i.e., the theory in which no degrees of freedom are integrated out. The relation between space and time can change as the high energy degrees of freedom are integrated out and the effective, low energy critical theory can have an arbitrary value for z, as was first noted by Hertz [22]. For scaling purposes, the quantum critical theory in d dimensions is equivalent to a classical critical theory in $d+z$ dimensions. As a result, Landau theory is valid at lower dimensions, $d_c^+\,(quantum) = d_c^+\,(classical) - z$.

[q]This is just another argument showing that the immediate vicinity of a critical point can indeed be described in terms of classical physics only.

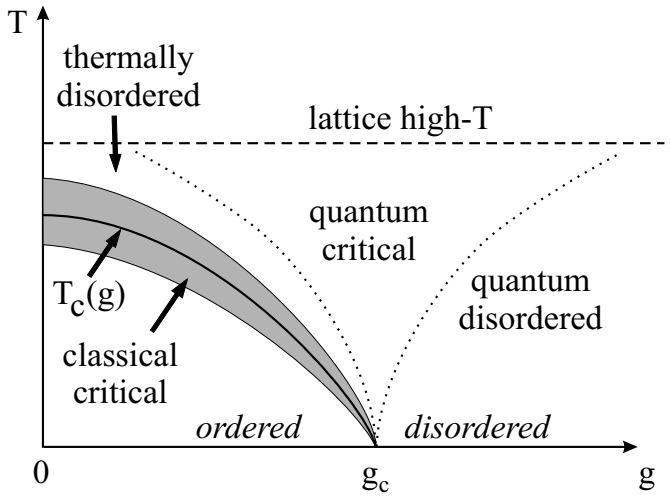

Figure 1.4. Typical phase diagram of a system in the vicinity of a quantum critical point. The phase boundary is indicated by the solid line. It terminates at $g = g_c$, which is a quantum critical point. The region below the solid line and $g < g_c$ is the ordered phase. In the shaded region the physics is dominated by thermal fluctuations (classical description of the phase transition). For $g > g_c$ and low T ("quantum disordered"), the system is in the disordered phase controlled by quantum fluctuations. In the region labeled "thermally disordered" the system is also in a disordered phase, but the physics is dominated by thermal fluctuations. The region between the dotted lines ("quantum critical") residing exactly above the quantum critical point is characterized by an interplay of both quantum and thermal fluctuations. At sufficiently high temperatures ("lattice high-T") the underlying lattice starts to play a role.

In the quantum case the scaling relation for the free energy density, eq. (1.18), has to be modified because temperature is a relevant variable, i.e.,

$$f(t, B, T) = b^{-(d+z)} f(tb^{1/\nu}, Bb^{y_B}, Tb^z). \tag{1.37}$$

1.2.4. **A generic phase diagram.** In Figure 1.4 we show a generic phase diagram of a system in the vicinity of a quantum critical point. T is temperature and g is some tuning parameter, e.g., pressure or external magnetic field. A phase boundary (solid line) terminates at $g = g_c$ which is the quantum critical point. For $g < g_c$ and $T < T_c(g)$, the system is in the ordered phase, i.e., the expectation value

of the order parameter is non-zero. If we raise the temperature, at some $T_c(g < g_c) > 0$, the system will undergo a continuous phase transition to the disordered phase. In Figure 1.4 this region is denoted as "thermally disordered". The dominant fluctuations are classical thermal fluctuations. On the other hand, if we vary g at a fixed low temperature, the system will undergo a phase transition at some $g = g(T) < g_c$. Within a certain distance from the critical point, one can observe the critical behavior, e.g., thermodynamic observables scale as power-laws of the distance from the critical point, etc. That distance denotes the onset of the critical region (for clarity omitted from Fig. 1.4). As we enter the critical region quantum fluctuations will dominate the physics. The quantum fluctuations will be gradually suppressed by the thermal fluctuations as we approach the critical point. At sufficiently low temperatures, the crossover will happen only asymptotically close to the critical point. Only asymptotically close to the $T = 0$ and $g = g_c$, will the critical properties be determined solely by quantum fluctuations. The shaded area represents the region described in terms of classical physics. It becomes narrower as the temperature is lowered. For $g > g_c$, at all temperatures the system will be in the disordered phase. In this "quantum disordered" region the physics is dominated by quantum fluctuations and the system essentially looks as if it is in its quantum disordered ground state at $g > g_c$.

The most intriguing is the region between the dotted lines labeled as "quantum critical". This region is located near the critical value $g \approx g_c$, but somewhat surprisingly at relatively high temperatures. In the quantum critical region the system "looks critical" with respect to g, but it is driven away from criticality by temperature. The system is very incoherent, and quantum and classical fluctuations play comparable roles. The physics in the quantum critical region is controlled by thermal excitations of the quantum critical ground state. The main characteristic of the excitations is that they are not conventional quasiparticle-like. This causes unusual finite temperature properties in the quantum critical region, such as unconventional power laws, non-Fermi liquid behavior etc., as is observed, e.g., in high transition temperature superconducting materials. The description of the quantum critical region is one of the central problems in contemporary condensed matter physics. We end this discussion with a remark about high temperatures. At sufficiently high temperatures,

the typical energy of the thermal fluctuations becomes comparable with the microscopic energy scale. Lattice details become important and all universal properties are lost. Therefore this region is denoted "lattice high-T" (above dashed line). This region is of no interest from the quantum critical point of view.

1.2.5. **Experimental examples.** Now we discuss a few experiments in which quantum phase transitions are observed.

$LiHoF_4$ is an insulator with a magnetic moment residing on each Ho atom. The magnetic moments have Ising symmetry, i.e., they can point parallel or antiparallel to a certain crystalline axis. At $T = 0$ magnetic dipolar interactions force all spins to have the same orientation, and the ground state is a ferromagnet. If placed into a magnetic field perpendicular to the magnetic axis the system starts to tunnel between its two spin states. For sufficiently large magnetic field the tunneling rate will eventually become strong enough to destroy the long-range magnetic order. Such a quantum phase transition has indeed been observed at a magnetic field strength of $H_c \approx 49.3kOe$ [23].

Another quantum phase transition can be found in the heavy fermion material $CeCu_{6-x}Au_x$ [24–27]. For $x > 0.1$ one observes magnetic order. As the dopant x is decreased or the crystal is placed under pressure the magnetic order is destroyed. The ground state becomes a paramagnetic Fermi liquid with rather large effective mass of the quasiparticles.

The phase diagram of the two dimensional electron gas in semiconductor heterostructures is amazingly rich and many quantum phase transitions are observed. The two dimensional electron gas placed in a strong transverse field exhibits the quantum Hall effect (see, e.g., [28–32]). Asymptotically close to the zero temperature one can tune the system through a sequence of distinct thermodynamic phases by suitably adjusting the density of carriers and the transverse magnetic field. Within each phase the longitudinal resistivity vanishes while the Hall resistivity becomes quantized [33]. Also, if the density and the field are chosen such that the lowest Landau level is filled the electron spins are fully polarized in the direction of the field, and the ground state is a ferromagnet. If we now bring two such ferromagnetic layers close to each other [34–37], for large spacing both layers will have their magnetic moments aligned with the field. If the interlayer distance is reduced one observes a substantial

antiferromagnetic exchange between the two layers, so the ground state eventually becomes a spin singlet [38–40].

1.3. QUANTUM PHASE TRANSITIONS OF ITINERANT ELECTRONS

Historically, the investigation of the zero temperature ferromagnetic phase transition in a Fermi liquid [22] was one of the first works to address the problem of quantum phase transitions. Subsequent studies showed that the physics of the quantum ferromagnetic phase transition was far more complicated than it was originally thought, and even today some aspects of this transition are not fully understood. In this section we summarize some of the main results of the theory of quantum phase transitions in Fermi liquids.

Landau [41, 42] argued that the excitation spectrum of interacting fermions will be very similar to that of a non-interacting Fermi gas. The basic excitations are weakly interacting fermionic *quasiparticles* with renormalized parameters, e.g., effective mass. This state is called a *Fermi liquid*. At low temperatures sufficiently strong interactions have the potential to render the Fermi liquid unstable. The system can undergo a phase transition to a state with a broken symmetry, e.g., ferromagnet, superconductor, spin glass, Wigner crystal, etc. Which low-temperature phase will be realized in practice depends on the microscopic details of the system. It is clear that by tuning microscopic parameters at zero temperature one can drive a Fermi liquid through a quantum phase transition. The zero temperature ferromagnetic phase transition of itinerant electrons is an example of such a quantum phase transition.

1.3.1. **Hertz' theory.** Starting from a microscopic Hamiltonian, Hertz [22] derived a Landau-Ginzburg-Wilson theory for the ferromagnetic quantum phase transition of itinerant electrons.

We now sketch the main ideas of Hertz' approach. Following the Landau-Ginzburg-Wilson philosophy, Hertz expressed the free energy only in terms of the local magnetization $\vec{\phi}(\vec{x}, \tau)$, i.e., in terms of the order parameter fluctuations. Technically this can be achieved by decoupling the interaction term in the original microscopic Hamiltonian via a Hubbard-Stratonovich transformation [43, 44] and integrating out the fermionic degrees of freedom. Upon carrying out the described procedure, the

partition function Z takes the form,

$$Z = e^{-\frac{F_0}{T}} \int D[\vec{\phi}] e^{-S[\vec{\phi}]}, \tag{1.38}$$

where F_0 is a regular (non-critical) part of the free energy. The resulting Landau-Ginzburg-Wilson free energy reads

$$\begin{aligned} S[\vec{\phi}] &= \frac{1}{2} \int dxdy \left[\frac{1}{\Gamma} \delta(x-y) - \chi^{(2)}(x-y) \right] \vec{\phi}(x) \vec{\phi}(y) + \\ &+ \sum_{n=3}^{\infty} \frac{(-1)^{n+1}}{n!} \int dx_1 \dots dx_2 \chi^{(n)}_{a_1 \dots a_n}(x_1, \dots, x_n) \phi^{a_1}(x_1) \dots \phi^{a_n}(x_n), \end{aligned} \tag{1.39}$$

where Γ is the exchange interaction strength and we used a four-vector notation $x = (\vec{x}, \tau)$ and $\int dx = \int_V dx \int_0^{1/k_B T} d\tau$. The physical information about the original microscopic system is encoded in the coefficients $\chi^{(n)}$ of eq. (1.39), which are the connected $n-$point spin density correlation functions of a conventional Fermi liquid. Close to the quantum critical point the physics is dominated by fluctuations correlated over long distances in space and over long times. The properties of the long-range fluctuations are determined by the behavior of $\chi^{(2)}(\vec{q}, \omega)$ in the limit of $\vec{q}, \omega \to 0$, where $\chi^{(2)}(\vec{q}, \omega)$ is a Fourier transform of $\chi^{(2)}(x-y)$ and $\vec{q}$, and ω are the wave vector and the Matsubara frequency, respectively. In the limit of small $\vec{q}$ and ω, $\chi^{(2)}(\vec{q}, \omega)$ takes the form (see, e.g., [45])

$$\chi^{(2)}(\vec{q}, \omega) = \chi_0^{(2)}(\vec{q}) \left[1 - c_\omega \frac{|\omega|}{|\vec{q}|} + \dots \right], \tag{1.40}$$

where $\chi_0^{(2)}(\vec{q})$ is the static spin susceptibility and $c_\omega > 0$ is a constant. The crucial step is to properly calculate $\chi_0^{(2)}(\vec{q})$. For a long time it was assumed that $\chi_0^{(2)}(\vec{q})$ was an analytic function of $|\vec{q}|^2$. In his original work Hertz used this assumption and cited the well known free electron result for $\chi_0^{(2)}(\vec{q})$ (see, e.g., [45])

$$\chi_0^{(2)}(\vec{q}) = N_F \left[1 - \frac{1}{3} \left(\frac{|\vec{q}|}{2k_F} \right)^2 + \dots \right], \tag{1.41}$$

where N_F is the density of states at the Fermi energy and k_F is the Fermi momentum. Inserting (1.40) together with (1.41) into (1.39) completes Hertz' derivation of the

Landau-Ginzburg-Wilson free energy. The resulting expression reads

$$S\left[\phi\right]=\frac{1}{2}\sum_{\vec{q},\omega}\left(t_0+|\vec{q}|^2+\frac{|\omega|}{|\vec{q}|}\right)|\phi\left(\vec{q},\omega\right)|^2+u\sum_{\{\vec{q}\}}\phi^4\left(\{\vec{q}\}\right), \tag{1.42}$$

where $t_0=\frac{1}{\Gamma}-\chi_0^{(2)}(\vec{q}=0)$ and $u\propto\chi^{(4)}(\vec{q}\to 0,\omega\to 0)$ is a constant[r]. Note that we have suppressed the prefactors in the first term of eq. (1.42) and written the second term symbolically.

Hertz analyzed the theory (1.42) by means of renormalization group methods which were a direct generalization of Wilson's treatment of classical transitions. From eq. (1.42) it follows $\omega\sim|\vec{q}|^3$, i.e., the dynamical critical exponent $z=3$ and Hertz concluded that in all physical dimensions $d>d_c^+=4-z=1$ the quantum magnetic transition was mean-field like. Hertz also analyzed the quantum to classical crossover at finite temperatures and found the corresponding cross-over exponent $z/2$. While it was later found [46] that Hertz' description of the finite temperature phenomena close to the quantum critical point was incomplete, it was generally believed that the main qualitative results of his model at zero temperature apply to real itinerant ferromagnets as well.

1.3.2. **Hertz' theory revised.** Sachdev [47] pointed out that in an academic, but still interesting case of dimensions below one, Hertz' results violate an exact exponent equality. Hertz' theory has been revised by Vojta, Belitz, Narayanan, and Kirkpatrick [48]. The authors of Ref. [48] have shown that the quantum ferromagnetic transition has much more complicated properties than predicted by Hertz. The reason behind this is the coupling of the magnetization to additional non-critical *soft* modes present in the electronic system at zero temperature. In a clean electronic system at zero temperature, particle-hole excitations at the Fermi surface are gapless or soft, i.e., they have infinite lifetime. If these soft excitations couple sufficiently strongly to the order parameter fluctuations they can generate an effective long-range interaction of the latter. This long-range interaction may produce significant effects on the transition itself changing it from a continuous transition with mean-field exponents to either a continuous transition with non mean-field exponents or to a first

[r]Hertz showed that for free electrons to the leading order in small $\vec{q}$ and ω connected $4-$point spin density correlation function $\chi^{(4)}(\vec{q},\omega)$ is indeed a constant.

order transition. The different transition scenarios resulting from the mode-coupling effects have been discussed in Ref. [49].

Technically, the mode-coupling leads to coefficients of eq. (1.39) which are singular for $\vec{q}, \omega \to 0$, resulting in an intractable non-local field theory. This renders the Landau-Ginzburg-Wilson approach impractical. Specifically, Belitz, Kirkpatrick, and Vojta have shown that the static spin susceptibility of a Fermi liquid $\chi_0^{(2)}(\vec{q})$, introduced in eq. (1.40), is a non-analytic function of $|\vec{q}|$. To second order, perturbation theory in the interaction strengths leads to [50]

$$\chi^{(2)}(\vec{q}) = N_F \left(1 + c_d |\vec{q}|^{d-1}\right) (\text{for } d < 3), \tag{1.43}$$

while in $d = 3$ the non-analytic term becomes $\propto |\vec{q}|^2 \log(1/|\vec{q}|)$. Inserting Eqs. (1.43) and (1.40) into eq. (1.39) leads to the

$$S[\phi] = \frac{1}{2} \sum_{\vec{q},\omega} \left(t_0 + |\vec{q}|^{d-1} + |\vec{q}|^2 + \frac{|\omega|}{|\vec{q}|} \right) |\phi(\vec{q}, \omega)|^2, \tag{1.44}$$

for the Gaussian part of the Landau-Ginzburg-Wilson free energy. The resulting expression is non-analytic in $|\vec{q}|$ which is a consequence of the long-range interaction of the spin fluctuations generated by the mode-coupling. Note that for the same physical reason, in general, the higher coefficients $\chi^{(n)}$ $(n \geq 4)$ in eq. (1.39) diverge for $\vec{q}, \omega \to 0$. Consequently, the free energy functional (1.39) is mathematically ill-defined. Therefore, a proper description of a quantum phase transition in the presence of strong coupling of the order parameter fluctuations to the non-critical soft modes calls for a more elaborate approach. Such treatment requires keeping track of all gapless degrees of freedom and couplings between them and leads to a rather involved coupled field theory. Recently, such a coupled field theory has been developed which provides a full description of the soft modes of an itinerant electronic systems in the presence of quenched disorder [51] and partially describes clean systems [52]. Based on that theory it has been shown that the quantum ferromagnetic transition in the presence of quenched disorder is not mean-field like [53–55], in contrast to the predictions of Hertz' theory [22].

1.3.3. **Quantum phase transitions and generic scale invariance.** The mode-coupling effects discussed above are a specific example of the influence of generic scale invariance on quantum phase transitions. Let us now give a broader idea of this effect. Typically, correlation functions of fluctuations decay exponentially for large distances in space or time, i.e., fluctuations far apart are weakly correlated. There is a typical length scale, correlation length ξ, associated with the decay and the correlations are called *short range*. As discussed in section 1.1., at a critical point the order parameter fluctuations become *long range*, i.e., the correlation length diverges and the correlation functions decay as power laws in space and time. Such correlation functions are scale invariant, i.e., a scale change in space and/or time can be compensated by multiplying the correlation function by a simple scale factor.

Scale invariance can also be observed in the entire regions of the phase diagram, rather than only at the critical points. This phenomenon is usually referred to as *generic scale invariance*. Generic scale invariance can be generated by spontaneous breaking of a global symmetry, gauge symmetries and conservation laws (for details see, e.g., [56–59]).

These generic soft modes can be present in both classical and quantum systems. In the vicinity of a critical point they can couple to the order parameter fluctuations and non-trivially affect the critical behavior, as already noted for the quantum ferromagnetic transition. In the classical case the mode-coupling effects are in general much weaker and often influence only the dynamics, e.g., the critical behavior of transport coefficients [60]. The situation in the quantum case is more drastic because of two reasons. *(i)* There are more soft modes at zero temperature than at $T > 0$. In a Fermi liquid, for example, there are particle-hole excitations which are gapless at $T = 0$ but acquire mass for $T > 0$. *(ii)* Also, previously we discussed that quantum mechanically statics and dynamics are coupled. Effects which would classically influence only dynamics quantum mechanically manifest themselves in the statics as well. Recently, a general criterion was established [61] for the mode coupling effects to influence quantum phase transitions in itinerant electronic systems with homogeneous order parameter. Based on symmetry considerations it was shown that order

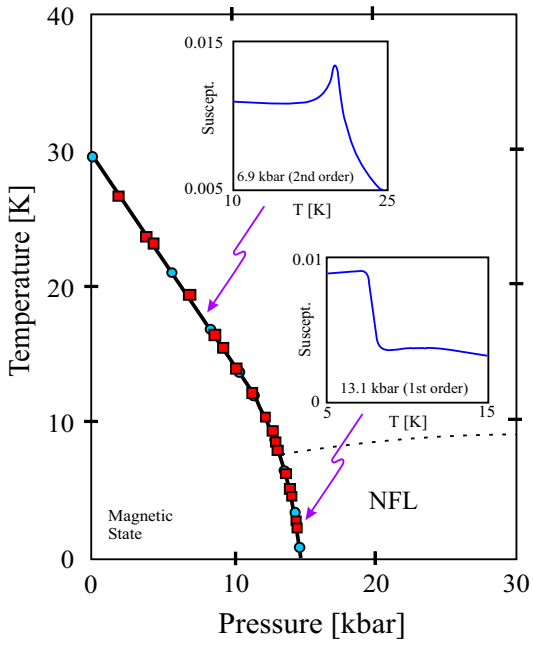

Figure 1.5. Phase diagram of $MnSi$. For higher temperatures the magnetic transition is continuous. As the temperature is lowered the transition changes to first order. Dashed line denotes the onset of non-Fermi liquid behavior. Inset: The behavior of the susceptibility close to the transition (after Ref. [62])

parameters with the particle-particle (Cooper) and spin-triplet particle-hole symmetry are generically affected by mode coupling effects while order parameters in the particle-hole spin-singlet channel do allow for a local Landau-Ginzburg-Wilson theory.

1.3.4. **A helimagnetic quantum phase transition of itinerant electrons.** We now give a summary of the first project of this dissertation. Perhaps the most extensively studied weak (low transition temperature) itinerant-electron magnet is $MnSi$. $MnSi$ belongs to the group of nearly or weakly ferromagnetic materials. This group consists of transition metals and their compounds such as $MnSi$, $ZrZn_2$, $TiBe_2$, Ni_3Al, YCo_2 and UGe_2. At ambient pressure $MnSi$ is a paramagnet for temperatures larger than $T_c = 29.5K$ [63]. Below T_c it orders magnetically. By applying hydrostatic pressure one can reduce the transition temperature $T_c(p)$, which subsequently reaches $T_c(p_c) = 0$ at $p_c = 14.6kbar$. For $p > p_c$, $MnSi$ is paramagnetic at all temperatures. Therefore one can tune $MnSi$ through a magnetic quantum phase

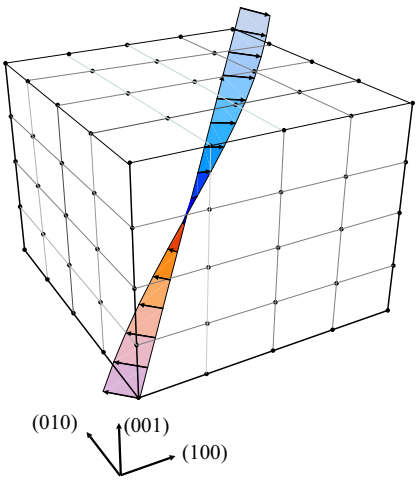

Figure 1.6. Schematic plot of the helical ordering in $MnSi$. Long-wavelength spin spiral forms along (111) direction of the crystal.

transition by varying the pressure [62, 64]. One of the most notable properties of the magnetic phase transition in $MnSi$ is that it changes from continuous to first order as temperature is decreased (Fig. 1.5). The insets of Fig. 1.5 show the susceptibility data close to the transition at low pressure, i.e., comparatively high transition temperature (upper inset) and high pressure, i.e., low transition temperature (lower inset). In the former case one observes a prominent peak reminiscent of the singularity expected at a continuous phase transitions while in the latter case, the susceptibility has a step suggesting a first order transition. The physical reason for the change in the type of the phase transition is the previously discussed coupling of the non-critical soft modes to the order parameter fluctuations, as argued in [49, 65].

$MnSi$ has a cubic $B20$ structure with lattice spacing $a = 4.56$Å. The $B20$ structure lacks an inversion symmetry and weak spin-orbit interaction assumes a Dzyaloshinsky-Moriya form [66], whose action is $\int \vec{S} \cdot (\nabla \times \vec{S}) d\vec{x}$. Therefore [67, 68], the ordered state is not exactly ferromagnetic, but a long-wavelength (≈ 175Å) helical spin spiral. The spin spiral is locked along the $\vec{K} = \langle 111 \rangle$ direction of the crystal with $\vec{S} \perp \vec{Q}$ [67–70] (Fig. 1.6). The spiral order can be suppressed by a homogeneous magnetic field $B \approx 0.6T$ leading to ferromagnetic order. To understand $MnSi$ it is important to investigate the quantum phase transition between the paramagnetic

state and a state with helical ordering. The details of that analysis are given in the attached paper (chapter 2.). Here we briefly summarize main results and discuss the applicability of our theory to the $MnSi$ in the light of recent experiments.

The order parameter for the helimagnetic quantum phase transition has eight components, four different orientations of the spiral, i.e., $\vec{K} = \langle 1,1,1\rangle$, $\langle -1,-1,1\rangle$, $\langle -1,1,-1\rangle$ and $\langle 1,-1,-1\rangle$ with two directions (left or right) for each orientation. Expanding the free energy of the system in terms of fluctuations around one of the spirals leads to a Landau-Ginzburg-Wilson action similar to eq. (1.44). The main difference compared to (1.44) is that the $|\vec{q}| = 0$ singularity is protected and instead a term $\propto |\vec{K}|^2 \log(1/|\vec{K}|)$ arises. As a result the coefficients $\chi^{(n)}$ in eq. (1.39) are finite and the Landau-Ginzburg-Wilson approach is applicable. Physically, the mode-coupling induced long-range interaction is cut-off by the spiral order. The resulting Landau-Ginzburg-Wilson theory is analyzed by conventional renormalization group methods [22]. It is found that the quantum critical behavior is mean-field like with dynamical exponent $z = 2$. In order to distinguish possible phase transition scenarios one needs to keep track of the physics at finite length scales. In addition to the magnetic correlation length, the system is characterized by two non-trivial length scales, i.e., the length scale of the spiral ℓ_S and the nucleation length scale ℓ_N associated with the first order transitions in itinerant quantum ferromagnets [49, 65]. If $\ell_S \ll \ell_N$, i.e., the Dzyaloshinski instability is much stronger than the effective long-range interaction produced by electronic correlations, the system crosses over from a ferromagnet to a helimagnet before the self-generated effective long-range interaction becomes sufficiently strong to induce a first order transition. The helimagnetic quantum phase transition is therefore continuous with mean-field critical exponents. In contrast, if $\ell_N \ll \ell_S$, i.e., the Dzyaloshinski instability is much weaker than the electronic correlations, the system undergoes a first-order transition which is analogous to the ferromagnetic transition. In $MnSi$ the wave-length of the spin spiral is rather large ($\ell_S \approx 175$Å), in contrast to the nucleation length ℓ_N is of the order of the microscopic scale[s] (≈ 5Å). Therefore $\ell_N \ll \ell_S$, and one expects a first-order

[s]This can be seen as follows: Assume that the nucleation length was much larger than the microscopic length scale: as the transition is approached the correlation length ξ of the order parameter fluctuations increases producing an increase of the magnetic susceptibility χ. Only when ξ reaches ℓ_N does one observe a sudden drop of χ which corresponds to the first order transition.

transition identical to the quantum ferromagnetic transition which has been observed in earlier experiments [64].

Since this work was published in 2001 new experiments [71, 72] have been performed. They found exotic non-Fermi liquid behavior for temperatures below $\approx 6K$ over a large pressure range above $p_c = 14.6kbar$ (the region below the dashed line denoted as "NFL" on Fig. 1.5). The resistivity shows $\rho \propto T^{3/2}$ dependence in contrast to the behavior of a conventional Fermi liquid. For a conventional Fermi liquid it has been shown that at the magnetic quantum critical point the resistivity depends on temperature as $\rho \propto T^{5/3}$ [73]. Away from the critical point the temperature dependence of the resistivity should be $\rho \propto T^2$ on both sides of the transition. Since in the experiments $\rho \propto T^{3/2}$ behavior prevails even for pressures two times the critical pressure and, thus, far from the critical point, it is clear that the low temperature disordered phase in $MnSi$ is not a conventional paramagnetic Fermi liquid. There have been attempts to explain this unconventional behavior [74], which have recently been supported by neutron diffraction measurements [75]. The authors of Ref. [75] have found that spin spirals survive above p_c but the direction of the helix is unlocked leading to an unusual pattern with partial long-range order. At present, the mechanisms that lead to the non-Fermi liquid behavior and the first order transition observed at low temperatures in $MnSi$ are not fully understood.

1.3.5. **Disorder driven quantum phase transition in an exotic superconductor.** We now give a summary of the second project of this dissertation. Before we proceed with the discussion we note that the results of this project are valid in the limit of weak disorder. In general, strong disorder can non-trivially affect phase transitions as will be discussed in section 1.4.

Even a century after its discovery superconductivity is still one of the central topics of experimental and theoretical research in condensed matter physics. In the heart of its underlying microscopic mechanism is an effective attractive interaction of electrons which overwhelms the Coulomb repulsion and allows electrons to form bound pairs. In the standard model of superconductivity due to Bardeen, Cooper

Low-temperature measurements on $MnSi$ (see lower inset in Fig. 1.5) show a jump of susceptibility at the transition temperature with no signs of increase in χ on either sides of the transition. This suggests that the nucleation length is indeed of the order of the microscopic scale.

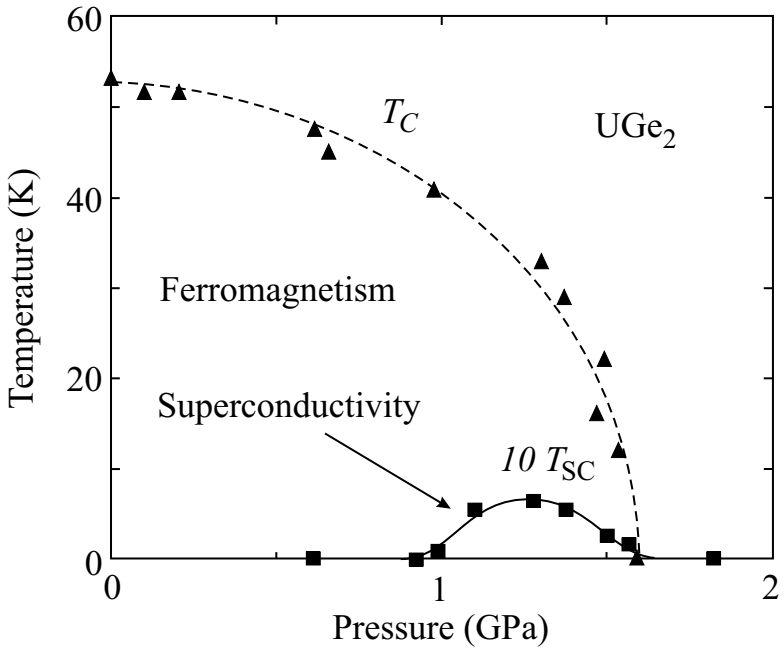

Figure 1.7. Phase diagram of UGe_2. A superconducting phase has been observed inside the ferromagnetic phase (after Ref. [83])

and Schrieffer (BCS) the attractive electron-electron interaction arises from the deformations of the underlying crystalline lattice [76], i.e., the exchange of phonons. The BCS picture is believed to account for the majority of known superconductors. However, there is a growing number of metallic compounds, including high-Tc superconductors, in which superconductivity appears to be anomalous or *exotic* and the pairing mechanism is controversial. Alternative models for electron pairing have been proposed that rely on the dynamical effects of the electrons themselves. Somewhat paradoxically, an effective attractive interaction between pairs of electrons, or more precisely of the fermionic quasiparticles close to the Fermi surface, can arise from the correlation effects of a system of electrons whose bare interaction is repulsive. In general, the effective quasiparticle interaction can have both signs. Specifically, magnetic fluctuations lead to attraction for electrons in the triplet state, but to repulsion for electrons in the singlet state. This can lead to spin-triplet, magnetically mediated superconductivity (see, e.g., [77]). We note that this mechanism is analogous to that leading to superfluidity in ^3He [78–82].

Recently, superconductivity has been observed on the border of ferromagnetism in a pure system, UGe_2 [83]. The same phenomenon has soon after been observed in $ZrZn_2$ [84] and $URhGe$ [85]. UGe_2 is a transition metal compound with orthorhombic structure and full inversion symmetry that undergoes a ferromagnetic transition at $T_c = 53K$ at ambient pressure. The transition temperature monotonously decreases with pressure and reaches zero at $p_c \approx 1.6GPa$ (Fig. 1.7). Therefore, like $MnSi$, UGe_2 can be tuned through a ferromagnetic quantum phases transition by applying hydrostatic pressure. The superconductivity is observed in a narrow range of pressures slightly below p_c for temperatures below $\approx 1K$. Unlike other uranium compounds which have highly localized $5f$ levels, the $5f$ electrons in UGe_2 are more itinerant and essentially behave like the $3d$ electrons in the traditional itinerant-electron ferromagnets such as Fe or Co. It is believed that both superconductivity and ferromagnetism originate in these itinerant $5f$ electrons. Therefore, is likely that the ferromagnetic superconductivity observed in UGe_2 is a result of the pairing mechanism discussed in previous paragraph.

It is interesting that superconductivity is observed only inside the ferromagnetic phase while it is completely absent above p_c (for all experimentally available temperatures) in contrast to earlier theoretical work [77] which predicted that the superconducting transition temperature should be roughly as high in the paramagnetic state as it is in the ferromagnetic one. Recently, a generic mechanism has been proposed to account for the enhancement of the superconducting transition temperature inside the ferromagnetic state [86]. The authors of Ref. [86] argued that the critical temperature for spin-triplet, magnetically mediated superconductivity is generically much higher in a ferromagnetic phase than in a paramagnetic one, due to an indirect coupling of the superconductivity to transverse magnetic fluctuations, i.e., spin waves. However, UGe_2 has uniaxial anisotropy, therefore this coupling is reduced and it is unclear whether it can explain the exclusively ferromagnetic superconductivity in this metal. An alternative explanation of the enhancement of the superconducting transition temperature in the ferromagnetic state of UGe_2 is based on its unusual two peak paramagnetic density of states [87].

Let us now ask how disorder, i.e., non-magnetic impurities influence superconductivity. According to Anderson's theorem [88], conventional BCS superconductivity

will not be affected by weak non-magnetic random impurities. This theorem is based on the observation that non-magnetic impurities can not break time reversal symmetry. Each state can still be paired with its time reversed state, therefore rendering $s-$wave superconductivity insensitive to their presence. The situation is rather different in the case of exotic superconductors when Cooper pairs are in formed in higher angular momentum channels. For example, as discussed above, magnetic fluctuations lead to attraction in the spin-triplet channel. Due to the Pauli exclusion principle the orbital angular momentum state of a spin-triplet Cooper pair has to be odd, i.e., in the simplest case a $p-$wave. Therefore, the superconducting gap is not isotropic but has $p-$wave symmetry with nodes corresponding to the nodes of a $p-$wave function. In the case of Cooper pairs with non-zero orbital angular momentum Anderson's theorem ceases to be valid. Impurity scattering mixes gap and node regions of the Fermi surface and Cooper pairs are destroyed when the mean free path[t] reaches the pair coherence length. Therefore, exotic superconductivity can easily be destroyed even by small amounts of disorder. Note that this is consistent with the experiments in UGe_2, which have found ferromagnetic superconductivity only in samples of exceptional purity [83–85].

It is thus important to investigate effects of disorder on exotic superconductivity, or more specifically to deduce properties of the disorder–driven quantum phase transition between an exotic superconductor and a normal metal. For the case of $d-$wave paring in $2d$ this has been done in Ref. [89]. We extend this analysis to pairing in an arbitrary angular momentum channel and discuss the important question of mode couping effects in analogy to section 1.3.3.. A detailed analysis is given in the attached paper (chapter 3.). Here we summarize the main results.

We have derived a Landau-Ginzburg-Wilson theory for the quantum phase transition between a metal and an exotic superconductor. The Landau-Ginzburg-Wilson theory for this transition proved to be equivalent (up to logarithmic corrections in the Gaussian part in the case of p-wave pairing) to the extensively studied Landau-Ginzburg-Wilson theory of the dirty itinerant quantum antiferromagnetic phase transition [90–94]. A renormalization group analysis of the Landau-Ginzburg-Wilson theory yielded runaway flow toward large disorder. As a result, the asymptotic fate of the

[t] I.e., the average distance between random impurities.

quantum phase transition is unknown. However, we were able derive a Ginzburg-type criterion for the importance of the disorder fluctuations. For weak bare disorder, as is realized in many experimental systems, the true asymptotic behavior is observed only exponentially close to the quantum critical point. It is preempted by a wide region with mean-field behavior (and logarithmic corrections for p-wave pairing). This result is also important from a general mode-coupling point of view. It is known [95] that mode coupling effects drastically affect a quantum phase transition between a dirty metal and a conventional, $s-$wave superconductor. We have shown that mode coupling effects are present in all angular momentum channels, but they are increasingly suppressed in higher angular momentum channels. This suppression can be understood as follows: In the presence of non-magnetic quenched disorder, the dominant electronic soft modes are those that involve fluctuations of the number density, spin density, or anomalous density in the zero angular momentum channel while the corresponding densities in higher angular momentum channels are not soft. Since the different angular momentum modes are orthogonal at zero wavenumber, the coupling between a finite angular momentum order parameter and the zero angular momentum soft modes is not strong enough to produce significant effects such as those observed in the $s-$wave channel.

1.4. PHASE TRANSITIONS IN THE PRESENCE OF DISORDER

Phase transitions in the presence of disorder remain one of the central and only partially solved problems in statistical physics. As we mentioned at the beginning of section 1.3.5., disorder can non-trivially affect critical behavior. In this section we discuss the main properties of phase transitions in the presence of disorder, paying particular attention to strong non-perturbative effects. Here we briefly summarize the main effects of quenched disorder on continuous phase transitions.

Originally it was believed that even weak disorder would destroy any critical point. According to that scenario the disordered system would divide itself up into regions that would independently, at different temperatures, undergo the transition. The transition would be smeared over an interval of temperatures and there would be no sharp singularities in thermodynamic observables [96]. However, it was soon found

that phase transitions generically remain sharp in the presence of weak, short-range correlated disorder.

1.4.1. **Harris criterion.** Harris derived [97] a simple but powerful criterion for the disorder to affect a phase transition. Here we reproduce the derivation because of its beauty and extreme simplicity. Consider a system on a lattice with random quenched impurities of concentration p. The pure system undergoes a continuous phase transition at a temperature T_c^0. In the presence of disorder the system will undergo a phase transition at some $T_c(p) < T_c^0$. The effects of disorder may be described by a position dependent local transition temperature $T_c(\vec{x})$. We define

$$\delta T_c(\vec{x}) = T_c(\vec{x}) - T_c(p) \tag{1.45}$$

as the local deviation from the critical temperature $T_c(p)$ and assume that $\delta T_c(\vec{x})$ is a Gaussian random function. The average value $\Delta T_c(p) = 1/L^d \int_{L^d} d\vec{x} \delta T_c(\vec{x})$ of $\delta T_c(\vec{x})$ over a region of linear dimension L much greater than the lattice spacing will be governed by the central limit theorem, i.e.,

$$\Delta T_c(p) \propto L^{-\frac{d}{2}}, \tag{1.46}$$

where d is the dimensionality. If we require that the universal properties, e.g., critical exponents of the clean transition are unchanged, the fluctuations $\Delta T_c(p)$ of the average local transition temperature $\langle T_c(\vec{x}) \rangle_{\xi^d}$ between correlation volumes ξ^d must be smaller than global distance from critical point, i.e.,

$$\Delta T_c(p) < t, \tag{1.47}$$

where

$$t \propto |T - T_c(p)| \propto \xi^{-\frac{1}{\nu}} \tag{1.48}$$

is the distance from the critical point, and ν is the correlation length critical exponent of the clean system. Combining eqs. (1.45), (1.46) and (1.47) we get

$$\xi^{-\frac{d}{2}} < \xi^{-\frac{1}{\nu}}, \tag{1.49}$$

or, the Harris criterion

$$\nu > \frac{2}{d}. \tag{1.50}$$

Therefore, the disorder will not affect a phase transition if the correlation length critical exponent ν fulfills inequality (1.50). We note that non-universal quantities like critical temperature are in general changed by the disorder.

In what follows we discuss possible phase transition scenarios if the Harris criterion is fulfilled or if it is violated.

1.4.2. **Harris criterion fulfilled.** If the Harris criterion is fulfilled the universal properties, e.g., universality class, critical exponents, etc. of the phase transition are not affected by disorder. As the critical point is approached the system asymptotically becomes homogeneous at large length scales, i.e., it averages out disorder and its critical properties are identical to those of a clean system. The system is called *self-averaging*. An example for this case is the $3d$ site diluted Heisenberg model. The clean critical exponent $\nu = 0.698$ [98] fulfills the Harris criterion and the critical behavior of the diluted system is identical to the one of the clean $3d$ Heisenberg model. In the renormalization group language, the critical behavior of the system is governed by a zero disorder fixed point.

1.4.3. **Harris criterion violated.** This case is much more interesting. Violation of the Harris criterion leads to three possible scenarios: *(i)* a conventional finite-disorder critical point with power-law scaling and new critical exponents which fulfill the Harris criterion, *(ii)* an infinite-randomness phase transition or *(iii)* destruction of sharp phase transitions, i.e., the transition is smeared over a range of temperatures.

(i) Finite-disorder critical point: Under renormalization the disorder strength tends to a constant. The system is inhomogeneous on all length scales and the critical behavior is changed. At the critical point, thermodynamic observables exhibit conventional power-law scaling but with modified critical exponents that fulfill the Harris criterion [99]. In the limit of infinite sample size, thermodynamic observables do not have single average values, but they are randomly distributed with probability distributions of a universal finite width [100, 101], i.e., thermodynamic observables are sample dependent. The system is *not* self-averaging. An example is the $3d$ site diluted Ising model. The clean $\nu = 0.627(2)$ (see, e.g., [3]) does not fulfill the Harris

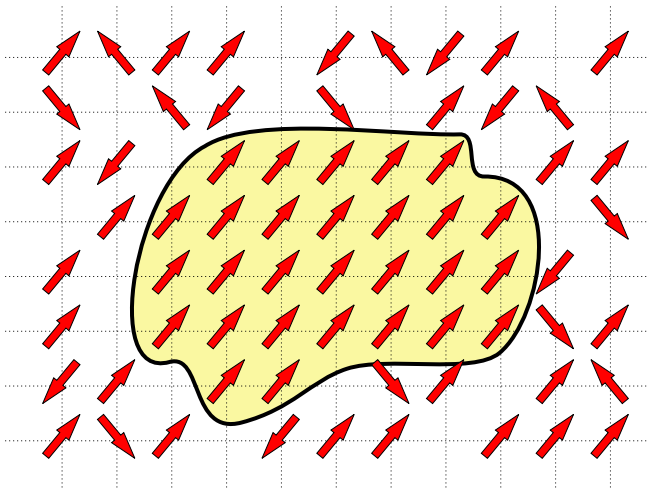

Figure 1.8. Schematic plot of a region (Griffiths island) devoid of impurities (circled shaded area).

criterion. Therefore, the critical behavior of the disordered model is different from that of the clean $3d$ Ising model, with the new value of $\nu = 0.682(2)$ [101] that fulfills the Harris criterion.

(ii) Infinite-randomness critical point: Disorder effects are more drastic than in *(i)* but the phase transition remains sharp. The relative magnitude of the inhomogeneities increases without limit under renormalization, i.e., the system is increasingly inhomogeneous on larger length scales. The probability distribution of thermodynamic variables becomes very broad (even on a logarithmic scale) with the width increasing with the system size. In the vicinity of an infinite-randomness critical point one observes activated rather than conventional power-law scaling, i.e., the relation between the correlation time ξ_τ and the correlation length ξ is exponential: $\log \xi_\tau \propto \xi^\mu$. A classical example of an infinite-randomness critical point occurs in the McCoy-Wu model [102, 103]. The random quantum Ising models in $1d$ [104–107] and $2d$ [108, 109] are the best known examples of quantum systems having infinite-randomness quantum critical points.

(iii) If the disorder is sufficiently correlated it can destroy the sharp phase transition and smear it over an interval of temperatures. We'll return to this interesting case in more detail below.

1.4.4. **Griffiths phenomena.** Griffiths phenomena are nonperturbative effects produced by rare disorder fluctuations in the vicinity of a critical point. In general, disorder will decrease the critical temperature T_c from its clean value T_c^0. For temperatures $T_c < T < T_c^0$ the system will globally be in the disordered phase. Nevertheless, in an infinitely large system, it is possible to find, with an exponentially small but finite probability, arbitrary large regions devoid of impurities (Fig. 1.8). These rare regions or *Griffiths islands* are locally ordered and have very slow dynamics because to flip them requires changing the order parameter over a large volume. Griffiths [110] showed that due to these rare regions the free energy is non-analytic everywhere in the region $T_c < T < T_c^0$. This region is known as *Griffiths phase* or *Griffiths region* [111]. However, the singularity of the free energy is only essential [110, 112], and in the classical case its effects on the thermodynamic observables are very weak. In contrast, the consequence for the dynamics are much more severe with the rare regions dominating the behavior for long times [111, 113–119].

1.4.5. **Smearing of phase transitions induced by correlated disorder.** Often, the disorder in real materials is not point like but spatially extended. Grain boundaries, dislocations and disordered layers are just a few examples of disorder that can extend over a sizable region. Such extended disorder can be modeled as perfectly *correlated* in d_C dimensions and uncorrelated in the remaining $d_\perp = d - d_C$ dimensions. Quenched impurities are time independent and therefore perfectly correlated in time direction. Thus, in the quantum case even spatially point–like disorder is always correlated in, at least, $d_C = 1$ dimension. It thus to be expected that the disorder effects will be more drastic in the quantum than in the classical case.

It is generally accepted that correlated disorder produces stronger effects on critical behavior, but it has been controversial if it can destroy the sharp phase transition. Early studies [120] based on a single expansion in $\epsilon = 4 - d$ did not produce a critical fixed point. This was interpreted as a smeared transition or a first order one [121, 122]. An improved analysis which included an additional expansion in the number d_C of correlated dimensions found a critical point with conventional power-law scaling [90, 123, 124]. Further support for the sharp transition scenario came from Monte-Carlo simulations of a $3d$ Ising model with planar defects [125].

However, all perturbative renormalization group studies miss the effects of rare regions and Griffiths phenomena. These effects have been extensively studied in the McCoy-Wu model [102, 103], a disordered $2d$ Ising model in which the disorder is perfectly correlated in one dimension and uncorrelated in the other. The transition in this model was originally thought to be smeared. It was later found that it was sharp but of infinite-randomness type [104–106]. Similar behavior has been found in several random quantum models which are related to classical models with linear defects [107–109, 126]. Therefore, it was believed that the phase transitions generically remain sharp even in the presence of extended disorder.

However it has recently been shown that this belief in not true in general [127, 128]. If the disorder is correlated in a sufficient number of dimensions, the Griffiths islands become infinite in these dimensions and true static long-range order can develop on them. As a result, the order parameter is very inhomogeneous in space close to the clean critical temperature, and it develops an exponential dependence on the temperature. Different regions order independently as the temperature is lowered and there is no unique critical temperature for the whole system. The phase transition is smeared over a range of temperatures.

1.4.6. **Smeared phase transition in a three-dimensional Ising model with planar defects.** Now we give a summary of the third project of this dissertation. Originally, the proposed mechanism for smearing [127, 128] of a phase transition had been tested on a mean-field model. It is therefore important to check if a phase transition in a realistic model will also be smeared in the presence of the correlated disorder. To this end we have performed large-scale Monte-Carlo simulations of a 3d Ising model with short-ranged, nearest neighbor interactions and planar defects[u], introduced via correlated bond disorder. The details of this analysis are presented in the attached paper (chapter 4.). Here we summarize the main results. We have found that the phase transition is indeed not sharp, but rather smeared over a range of temperatures by the presence of the extended defects. As a result, the magnetization develops an exponential tail toward the disordered phase.

[u]Note that $d_C = 2$ is the lowest dimension in which the Ising model orders. Therefore, in order to observe smearing the disorder has to be correlated in at least two dimensions.

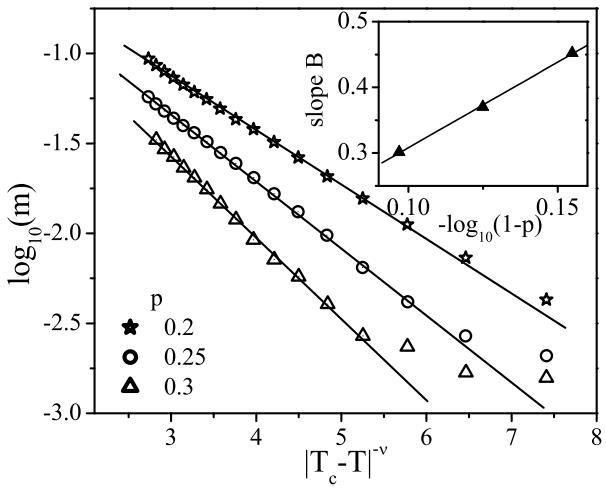

Figure 1.9. Logarithm of the total magnetization m as a function of $|T_c^0 - T|^{-\nu}$ ($\nu = 0.627$) for several impurity concentrations $p = 0.2$, 0.25, 0.3. Inset: Decay slope B as a function of $-\ln(1-p)$.

In Fig. 1.9 we show the logarithm of the total magnetization *vs.* the distance from the clean critical point, $|T - T_c^0|^{-\nu}$ (for the clean $3d$ Ising model $\nu \approx 0.627$) for three different disorder concentrations ($p = 0.2$, 0.25 and 0.3). For all three concentrations the total magnetization follows the predicted [128] exponential law, $m \propto \exp\left(-Bt^{-d\nu}\right)$. The slope $B \propto -\ln(1-p)$ is shown in the inset of Fig. 1.9. The numerical results are in good agreement with the theoretical predictions of Refs. [127, 128].

Notice that long-range interactions increase the tendency toward smearing. If the interaction in the direction in which the disorder is correlated falls off as $1/r^2$ or slower, even linear defects can lead to smearing, because a $1d$ Ising model with $1/r^2$ interaction has an ordered phase.

We end our discussion with the brief remark about smearing of quantum phase transitions in disordered itinerant electronic systems. As previously discussed each quantum phase transition can be mapped to a classical phase transition in higher dimension, with imaginary time acting as additional dimension. For dirty itinerant ferromagnets the effective interaction between the spin fluctuations in the imaginary

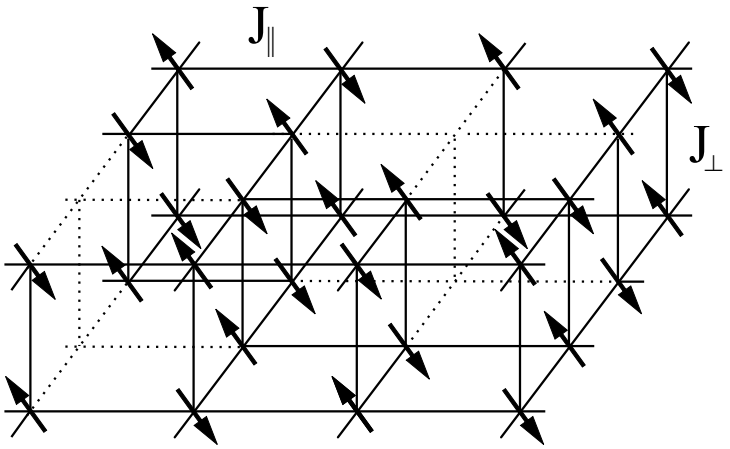

Figure 1.10. Dimer-diluted $2d$ spin-$\frac{1}{2}$ bilayer quantum Heisenberg antiferromagnet: Quantum spins (arrows) reside on the two parallel square lattices. The spins in each plane interact with the coupling strength $J_{\parallel}$. Interplane coupling is $J_{\perp}$. Dilution is done by removing dimers.

time direction falls off as $1/\tau^2$, and the disorder is correlated in this direction [22]. Therefore, the dirty itinerant ferromagnetic transition is smeared even for point like impurities [127].

1.4.7. **Quantum phase transition in a disordered bilayer quantum Heisenberg antiferromagnet.** Here we discuss the main results of the fourth project of this dissertation. As we have already discussed, disorder generically has stronger effects on quantum phase transitions. At a quantum critical point space and time are coupled, and since quenched impurities are time independent they are necessary perfectly correlated in time. Prominent consequences are the infinite-randomness critical points in $1d$ random spin chains [126,129,130] and in $1d$ [105–107] and $2d$ [108, 109] random quantum Ising models. In itinerant electronic systems disorder effects can be even more dramatic. For Ising symmetry, quenched disorder completely destroys the sharp quantum phase transition by smearing, as discussed in the previous section. Further unconventional phenomena include non-universal, continuously varying critical exponents, observed in the Griffiths region associated with a quantum phase transition [104–106, 108–110] or at certain impurity quantum

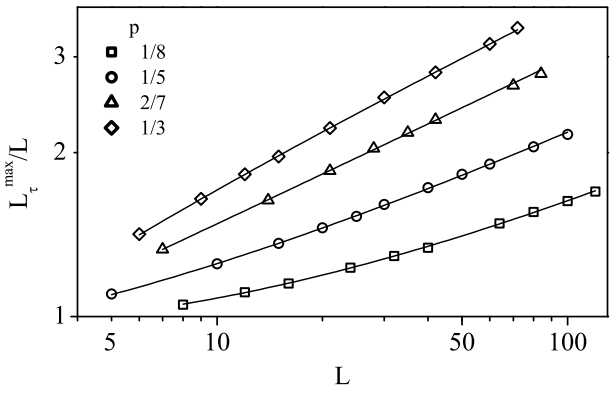

Figure 1.11. L_τ^{max}/L vs. L for four disorder concentrations $p = 1/8$, $1/5$, $2/7$ and $1/3$. Solid lines: Fit to $L_\tau^{max} = aL^z(1 + bL^{-\omega})$ with $z = 1.310(6)$ and $\omega = 0.48(3)$.

phase transitions (e.g., [131]). These results lead to a general belief that all quantum phase transitions in the presence of disorder are unconventional.

In the paper presented in chapter 5., we have shown that this belief is not true in general. We have performed large scale Monte-Carlo simulations of a dimer-diluted spin-$\frac{1}{2}$ bilayer quantum Heisenberg antiferromagnet (Fig. 1.10). The spins in each square-lattice plane interact with an exchange energy $J_\parallel$, and the interplane coupling energy is $J_\perp$. For $J_\perp \gg J_\parallel$, neighboring spins from the two layers form singlets, and the ground state is paramagnetic. In contrast, for $J_\parallel \gg J_\perp$ the system develops Néel order. Both phases are separated by a quantum phase transition at $J_\perp/J_\parallel \approx 2.525$.

We have found that this model has a conventional quantum critical point with power-law scaling. Moreover, the critical exponents are universal, i.e., dilution-independent, but only after accounting for strong corrections to scaling characterized by an irrelevant exponent $\omega \approx 0.48$ (see Fig. 1.11). The asymptotic dynamical and correlation length exponents are $z = 1.310(6)$ and $\nu = 1.16(3)$. We have also calculated the exponents β and γ. However, the corrections to scaling for magnetization and susceptibility are very strong, leading to larger errors for β and γ. We have found $\beta/\nu = 0.56(5)$ and $\gamma/\nu = 2.15(10)$. These exponents fulfill the hyperscaling relation $2\beta+\gamma = (d+z)\nu$ (see section 1.1.7.) which is a strong argument for our results being

asymptotic rather than effective. Details of this analysis are presented in the attached paper (chapter 5.).

Finally, we comment on experiments. If chemical doping replaces magnetic by non-magnetic ions in a 2d antiferromagnet, e.g., Cu by Zn in $YBa_2Cu_3O_6$, the case of site rather than dimer dilution is realized. The most promising way to effectively achieve bond dilution is the introduction of strong antiferromagnetic interdimer bonds at random locations. Thus we propose to study magnetic transitions in bond-disordered systems; those transitions can be expected to be in the same universality class as the one discussed here. One candidate material – albeit $3d$ – is $(Tl, K)\,CuCl_3$ under pressure; interesting quasi-$2d$ compounds are $SrCu_2(BO_3)_2$ or $BaCuSi_2O_6$, where suitable dopants remain to be found.

1.5. SUMMARY AND OUTLOOK

In this chapter we gave a general introduction to classical and quantum phase transitions (sections 1.1. and 1.2.). In section 1.3. we discussed the main aspects of the mode-coupling effects on the quantum phase transitions of itinerant electrons. We have also summarized the main results of the first two projects of this dissertation (chapters 2. and 3.).

In section 1.4. we discussed the strong non-perturbative disorder effects on phase transitions. We summarized the main results of the other two projects of this dissertation (chapters 4. and 5.)

The results presented in this dissertation are far from final and complete. Although in the past decade our understanding of the magnetic quantum phase transition has become significantly deeper it is still not complete. Despite recent developments, the complete description of the quantum magnetic phase transition in clean systems is at present unknown. Our study of the mode coupling effects in higher angular momentum channels in disordered systems is based on low order perturbation theory. Although our conclusions are likely to be correct to all orders in the perturbation theory it is impossible to prove it within our approach. A more general theory should be developed. Smearing of the phase transitions in the presence of disorder is closely related to the dimensionality of the disorder and order parameter symmetry. It would be interesting to check the theoretical predictions on the models with

continuous, e.g., Heisenberg symmetry. If the dimensionality of the disorder is such that the rare regions are on the verge of ordering, i.e., at the lower critical dimension, the disorder effects can be non-trivial. They will not be strong enough to destroy the transition but may lead to the non-trivial effects, e.g., an infinite-randomness phase transition. Such a situation is met in the $3d$ Heisenberg model with planar defects, which is the topic of work currently in progress.

BIBLIOGRAPHY

[1] N. Goldenfeld, *Lectures on Phase Transitions and the Renormalization Group*. Reading, Massachusetts: Addison-Wesley Publishing Company, first ed., 1992.

[2] S. K. Ma, *Modern Theory of Critical Phenomena*. Cambridge, Massachusetts: Perseus publishing, first ed., 2000.

[3] A. J. F. J. J. Binney, N. J. Dorwick and M. E. J. Newman, *The Theory of Critical Phenomena - an introduction to the renormalization group*. Oxford, United Kingdom: Oxford University Preess, first ed., 1992.

[4] L. D. Landau *Phys. Z. Sowjetunion*, vol. 11, p. 26, 1937.

[5] D. Forster, *Hydrodynamic Fluctuations, Broken Symmetry, and Correlation Functions*. Reading, MA: Benjamin, 1975.

[6] L. D. Landau and E. M. Lifshitz, *Statistical Physics Part 1*. Oxford, United Kingdom: Butterworth Heinemann, first ed., 1980.

[7] A. P. Levanyuk *Sov. Phys. JETP*, vol. 36, p. 571, 1959.

[8] V. L. Ginzburg *Sov. Phys. Sol. State.*, vol. 2, p. 1824, 1960.

[9] K. G. Wilson *Phys. Rev. B*, vol. 4, p. 3174, 1971.

[10] K. G. Wilson *Phys. Rev. B*, vol. 4, p. 3184, 1971.

[11] B. Widom *J. Chem. Phys.*, vol. 43, p. 3892, 1965.

[12] G. S. Rushbrooke *J. Chem. Phys.*, vol. 39, p. 842, 1963.

[13] B. D. Josephson *Proc. Phys. Soc.*, vol. 92, pp. 269–276, 1967.

[14] M. E. Fisher *Phys. Rev.*, vol. 180, p. 594, 1969.

[15] L. van Hove *Phys. Rev.*, vol. 95, p. 1374, 1954.

[16] L. D. Landau and I. M. Khalatnikov *Dokl. Akad. Nauk. SSSR*, vol. 96, p. 469, 1954.

[17] S. Sachdev, *Quantum Phase Transitions*. Cambridge, United Kingdom: Cambridge University Press, first ed., 1999.

[18] S. L. Sondhi, S. M. Girvin, J. P. Carini, and D. Shahar *Rev. Mod. Phys.*, vol. 69, p. 315, 1997.

[19] J. W. Negele and H. Orland, *Quantum many-particle systems*. New York: Addison-Wesley, 1988.

[20] M. N. Barber in *Phase Transitions and Critical Phenomena* (C. Domb and J. L. Lebowitz, eds.), New York: Academic, 1983.

[21] J. Cardy, *Scaling and Renormalization in Statistical Physics.* Cambridge, United Kingdom: Cambridge University Preess, 1996.

[22] J. Hertz *Phys. Rev. B*, vol. 14, p. 1165, 1976.

[23] D. Bitko, T. F. Rosenbaum, and G. Aeppli *Phys. Rev. Lett.*, vol. 77, p. 940, 1996.

[24] A. Rosch, A. Schröder, O. Stockert, and H. von Löhneysen *Phys. Rev. Lett.*, vol. 79, p. 159, 1997.

[25] A. Schröder, G. Aeppeli, E. Bucher, R. Ramazashvili, and P. Coleman *Phys. Rev. Lett.*, vol. 80, p. 5623, 1998.

[26] O. Stockert, H. von Löhneysen, A. Rosch, N. Pyka, and M. Loewenhaupt *Phys. Rev. Lett.*, vol. 80, p. 5627, 1998.

[27] H. von Löhneysen and *et al. Eur. Phys. J. B*, vol. 5, p. 447, 1998.

[28] A. H. MacDonald, ed., *Quantum Hall Effect: A Perspective*, Kluwer, Boston, 1989.

[29] R. E. Prangle and S. M. Girvin, eds., *The Quantum Hall Effect*, Springer, New York, 1990.

[30] M. Stone, ed., *The Quantum Hall Effect*, World Scientific, Singapore, 1992.

[31] T. Chakraborty and P. Pietiläinen, "The quantum hall effects: Integral and fractional," in *Springer Series in Solid State Sciences* **85**, New York: Springer, 1995.

[32] S. DasSarma and A. Pinczuk, eds., *Perspectives in Quantum Hall Effects: Novel Quantum Liquids in Low Dimensional Semiconductor Structures*, Wiley, New York, 1996.

[33] D. C. Tsui *Physics B*, vol. 164, p. 59, 1990.

[34] A. Pinczuk and *et al. Phys. Rev. Lett.*, vol. 68, p. 3623, 1992.

[35] V. Pellegrini and *et al. Phys. Rev. Lett.*, vol. 78, p. 310, 1997.

[36] V. Pellegrini and *et al. Science*, vol. 281, p. 799, 1998.

[37] A. Sawada and *et al. Phys. Rev. Lett.*, vol. 80, p. 4534, 1998.

[38] L. Zheng, R. J. Radtke, and S. DasSarma *Phys. Rev. Lett.*, vol. 78, p. 2453, 1997.

[39] S. DasSarma, S. Sachdev, and L. Zheng *Phys. Rev. Lett.*, vol. 79, p. 917, 1997.

[40] S. DasSarma, S. Sachdev, and L. Zheng *Phys. Rev. B*, vol. 58, p. 4672, 1998.

[41] L. D. Landau *Zh. Eksp. Teor. Fiz.*, vol. 30, p. 1058, 1956.

[42] L. D. Landau *Zh. Eksp. Teor. Fiz.*, vol. 32, p. 59, 1957.

[43] J. Hubbard *Phys. Rev Lett.*, vol. 3, p. 77, 1956.

[44] R. L. Stratonovich *Dokl. Akad. Nauk SSSR*, vol. 115, p. 1907, 1957.

[45] G. D. Mahan, *Many-particle physics*. New York: Kluwer Academic/Plenum Publishers, 3d ed., 2000.

[46] A. J. Millis *Phys. Rev. B*, vol. 48, p. 7183, 1993.

[47] S. Sachdev *Z. Phys. B*, vol. 94, p. 469, 1994.

[48] T. Vojta, D. Belitz, R. Narayanan, and T. R. Kirkpatrick *Europhys. Lett.*, vol. 36, p. 191, 1996.

[49] D. Belitz, T. R. Kirkpatrick, and T. Vojta *Phys. Rev. Lett.*, vol. 82, p. 4707, 1999.

[50] D. Belitz, T. R. Kirkpatrick, and T. Vojta *Phys. Rev. B*, vol. 55, p. 9452, 1997.

[51] D. Belitz and T. R. Kirkpatrick *Phys. Rev. B*, vol. 56, p. 6513, 1997.

[52] D. Belitz and T. R. Kirkpatrick *Phys. Rev. B*, vol. 67, p. 024419, 2003.

[53] D. Belitz and T. R. Kirkpatrick *Phys. Rev. B*, vol. 53, p. 14364, 1996.

[54] D. Belitz, T. R. Kirkpatrick, M. T. Mercaldo, and S. L. Sessions *Phys. Rev. B*, vol. 63, p. 174427, 2001.

[55] D. Belitz, T. R. Kirkpatrick, M. T. Mercaldo, and S. L. Sessions *Phys. Rev. B*, vol. 63, p. 174428, 2001.

[56] D. Belitz, T. R. Kirkpatrick, and T. Vojta *to appear in Rev. Mod. Phys.*, 2004.

[57] J. R. Dorfman, T. R. Kirkpatrick, and J. V. Sengers *Ann. Rev. Phys. Chem. A*, vol. 45, p. 213, 1994.

[58] B. M. Law and J. C. Nieuwoudt *Phys. Rev. A*, vol. 40, p. 3880, 1989.

[59] S. Nagel *Rev. Mod. Phys.*, vol. 64, p. 321, 1992.

[60] P. C. Hohenberg and B. I. Halperin *Rev. Mod. Phys.*, vol. 49, p. 435, 1977.

[61] D. Belitz, T. R. Kirkpatrick, and T. Vojta *Phys. Rev. B*, vol. 65, p. 165112, 2002.

[62] C. Pfleiderer, G. J. McMullan, and G. G. Lonzarich *Physica B*, vol. 206&207, p. 847, 1995.

[63] D. Bloch, J. Voiron, V. Jaccarino, and J. H. Wernick *Phys. Lett.*, vol. 51, p. 259, 1975.

[64] C. Pfleiderer, G. J. McMullan, S. R. Julian, and G. G. Lonzarich *Phys. Rev. B*, vol. 55, p. 8330, 1997.

[65] T. Vojta, D. Belitz, R. Narayanan, and T. R. Kirkpatrick *Ann. Phys. (Leipzig)*, vol. 8, p. 593, 1999.

[66] I. E. Dzyaloshinsky *J. Exp. Theor. Phys.*, vol. 46, p. 1420, 1964.

[67] P. Bak and M. H. Jensen *J. Phys. C*, vol. 13, p. L881, 1980.

[68] O. Nakanishi, A. Yanase, A. Hasegawa, and M. Kataoka *Solid State Commun.*, vol. 35, p. 995, 1980.

[69] Y. Ishikawa and M. Arai *J. Phys. Soc. Jpn.*, vol. 53, p. 2726, 1984.

[70] B. Lebech in *Recent Advances in Magnetism of Transition Metal Compounds* (A. Kotani and N. Suzuki, eds.), Singapore: World Scientific, 1993.

[71] C. Pfleiderer, S. R. Julian, and G. G. Lonzarich *Nature*, vol. 414, p. 427, 2001.

[72] N. Doiron-Layraud, I. R. Walker, L. Taillefer, M. J. Steiner, S. R. Julian, and G. G. Lonzarich *Nature*, vol. 425, p. 595, 2003.

[73] J. Mahton *Proc. R. Soc. A*, vol. 306, p. 355, 1968.

[74] J. Schmalian and M. Turlakov *cond-mat/0310186*, 2003.

[75] C. Pfleiderer, D. Reznik, L. Pintschovius, H. v. Löhneysen, M. Garst, and A. Rosch *Nature*, vol. 427, p. 227, 2004.

[76] J. Bardeen, L. N. Cooper, and J. R. Schrieffer *Phys. Rev.*, vol. 108, p. 1175, 1957.

[77] D. Fay and J. Appel *Phys. Rev. B*, vol. 22, p. 3173, 1980.

[78] K. A. Brueckner, T. Soda, P. W. Anderson, and P. Morel *Phys. Rev.*, vol. 118, p. 1442, 1960.

[79] S. Nakajima *Prog. Theor. Phys.*, vol. 50, p. 1101, 1973.

[80] W. F. Brinkman, J. W. Serene, and P. W. Anderson *Phys. Rev. A*, vol. 10, p. 2386, 1974.

[81] A. J. Leggett *Rev. Mod. Phys.*, vol. 47, p. 331, 1975.

[82] R. Levin and O. T. Valls *Phys. Rev. B*, vol. 17, p. 191, 1978.

[83] S. S. Saxena and *et al. Nature*, vol. 406, p. 587, 2000.

[84] C. Pfleiderer and *et al. Nature*, vol. 412, p. 58, 2001.

[85] D. Aoki and *et al. Nature*, vol. 413, p. 613, 2001.

[86] T. R. Kirkpatrick, D. Belitz, T. Vojta, and R. Narayanan *Phys. Rev. Lett.*, vol. 87, p. 127003, 2001.

[87] K. G. Sandeman, G. G. Lonzarich, and A. J. Schofield *Phys. Rev. Lett.*, vol. 90, p. 167005, 2003.

[88] P. W. Anderson *J. Phys. Chem. Solids*, vol. 11, p. 26, 1959.

[89] I. Herbut *Phys. Rev. Lett.*, vol. 85, p. 1532, 2000.

[90] D. Boyanovsky and J. L. Cardy *Phys. Rev. B*, vol. 26, p. 154, 1982.

[91] T. R. Kirkpatrick and D. Belitz *Phys. Rev. Lett.*, vol. 76, p. 2571, 1996.

[92] T. R. Kirkpatrick and D. Belitz *Phys. Rev. Lett.*, vol. 78, p. 1197, 1997.

[93] R. Narayanan, T. Vojta, D. Belitz, and T. R. Kirkpatrick *Phys. Rev. Lett.*, vol. 82, p. 5132, 1999.

[94] R. Narayanan, T. Vojta, D. Belitz, and T. R. Kirkpatrick *Phys. Rev. B*, vol. 60, p. 10150, 1999.

[95] T. R. Kirkpatrick and D. Belitz *Phys. Rev. Lett.*, vol. 79, p. 3042, 1997.

[96] G. Grinstein, *Fundamental Problems in Statistical Mechanics VI.* New York: Elsevier, 1985.

[97] A. B. Harris *J. Phys. C*, vol. 7, p. 1671, 1974.

[98] C. Holm and W. Janke *Phys. Rev. B*, vol. 48, p. 936, 1993.

[99] J. Chayes, L. Chayes, D. S. Fisher, and T. Spencer *Phys. Rev. Lett.*, vol. 57, p. 2999, 1986.

[100] A. Aharony and A. B. Harris *Phys. Rev. Lett.*, vol. 77, p. 3700, 1996.

[101] S. Wiseman and E. Domany *Phys. Rev. Lett.*, vol. 81, p. 22, 1998.

[102] B. M. McCoy and T. T. Wu *Phys. Rev.*, vol. 176, p. 631, 1968.

[103] B. M. McCoy and T. T. Wu *Phys. Rev.*, vol. 188, p. 982, 1969.

[104] B. M. McCoy *Phys. Rev. Lett.*, vol. 23, p. 383, 1969.

[105] D. S. Fisher *Phys. Rev. Lett.*, vol. 69, p. 534, 1992.

[106] D. S. Fisher *Phys. Rev. B*, vol. 51, p. 6411, 1995.

[107] A. P. Young and H. Rieger *Phys. Rev. B*, vol. 53, p. 8486, 1996.

[108] C. Pich, A. P. Young, H. Rieger, and N. Kawashima *Phys. Rev. Lett.*, vol. 81, p. 5916, 1998.

[109] O. Motrunich, S.-C. Mau, D. A. Huse, and D. S. Fisher *Phys. Rev. B*, vol. 61, p. 1160, 2000.

[110] R. B. Griffiths *Phys. Rev. Lett.*, vol. 23, p. 17, 1969.

[111] M. Randeria, J. Sethna, and R. G. Palmer *Phys. Rev. Lett.*, vol. 54, p. 1321, 1985.

[112] A. J. Bray and D. Huifang *Phys. Rev. B*, vol. 40, p. 6980, 1989.

[113] D. Dhar in *Stochastic Processes: Formalism and Applications* (D. S. Argawal and S. Dattagapta, eds.), Berlin: Springer, 1985.

[114] D. Dhar, M. Randeria, and J. P. Sethna *Europhys. Lett.*, vol. 5, p. 485, 1988.

[115] A. J. Bray *Phys. Rev. Lett.*, vol. 60, p. 720, 1988.

[116] A. J. Bray and G. J. Rodgers *Phys. Rev. B*, vol. 38, p. 9252, 1988.

[117] A. J. Bray *Phys. Rev. Lett.*, vol. 59, p. 586, 1987.

[118] S. Cesi, C. Maes, and F. Martinelli *Commun. Math. Phys.*, vol. 189, p. 135, 1997.

[119] S. Cesi, C. Maes, and F. Martinelli *Commun. Math. Phys.*, vol. 189, p. 323, 1997.

[120] T. C. Lubensky *Phys. Rev. B*, vol. 11, p. 3573, 1975.

[121] J. Rudnick *Phys. Rev. B*, vol. 18, p. 1406, 1978.

[122] D. Andelman and A. Aharony *Phys. Rev. B*, vol. 31, p. 4305, 1985.

[123] S. N. Dorogovtsev *Fiz. Tverd. Tela (Leningrad)*, vol. 22, p. 321, 1980.

[124] L. DeCesare *Phys. Rev. B*, vol. 49, p. 11742, 1994.

[125] J. C. Lee and R. L. Gibbs *Phys. Rev. B*, vol. 45, p. 2217, 1992.

[126] D. S. Fisher *Phys. Rev. B*, vol. 50, p. 3799, 1994.

[127] T. Vojta *Phys. Rev. Lett.*, vol. 90, p. 107202, 2003.

[128] T. Vojta *J. Phys. A*, vol. 36, p. 10291, 2003.

[129] S. K. Ma, C. Dasgupta, and C.-K. Hu *Phys. Rev. Lett.*, vol. 43, p. 1434, 1979.

[130] R. N. Bhatt and P. A. Lee *Phys. Rev. Lett.*, vol. 48, p. 344, 1982.

[131] A. Georges and A. M. Sengupta *Phys. Rev. Lett.*, vol. 74, p. 2808, 1995.

2. THE QUANTUM PHASE TRANSITION OF ITINERANT HELIMAGNETS

Thomas Vojta[1,2] and Rastko Sknepnek[1]

[1] *Institut für Physik, Technische Universität Chemnitz, D-09107 Chemnitz, Germany*

[2] *Theoretical Physics, University of Oxford, Oxford OX1 3NP, UK*

Abstract

We investigate the quantum phase transition of itinerant electrons from a paramagnet to a state which displays long-period helical structures due to a Dzyaloshinskii instability of the ferromagnetic state. In particular, we study how the self-generated effective long-range interaction recently identified in itinerant quantum ferromagnets is cut-off by the helical ordering. We find that for a sufficiently strong Dzyaloshinskii instability the helimagnetic quantum phase transition is of second order with mean-field exponents. In contrast, for a weak Dzyaloshinskii instability the transition is analogous to that in itinerant quantum ferromagnets, i.e. it is of first order, as has been observed in MnSi.

Quantum phase transitions are phase transitions that occur at zero temperature as a function of some non-thermal control parameter like pressure, magnetic field, or chemical composition. While the usual finite-temperature phase transitions are driven by thermal fluctuations, zero-temperature quantum phase transitions are driven by quantum fluctuations which are a consequence of Heisenberg's uncertainty principle. Quantum phase transitions have attracted considerable attention in recent years, in particular since they are believed to be at the heart of some of the most exciting discoveries in modern condensed matter physics, such as the localization problem, the quantum Hall effects, various magnetic phenomena, and high-temperature superconductivity.[1–5]

One of the most obvious examples of a quantum phase transition is the transition from a paramagnetic to a ferromagnetic metal that occurs as a function of the exchange coupling between the electron spins. In a pioneering paper this transition was studied by Hertz[6] who generalized Wilson's renormalization group to quantum phase transitions. The finite temperature properties were later discussed by Millis.[7] Building on these results the theory of the ferromagnetic quantum phase transition has recently been worked out in much detail. It was shown that in a zero-temperature correlated itinerant electron system additional non-critical soft modes couple to the order parameter. This effect produces a (self-generated) effective long-range interaction between the spin fluctuations, even if the microscopic exchange interaction is short-ranged.[8] In a clean system the resulting ferromagnetic quantum phase transition is generically of first order.[9]

The experimentally best studied example of such a transition is probably provided by the pressure-tuned transition in MnSi.[10,11] MnSi belongs to the class of nearly or weakly ferromagnetic metals. These materials are characterized by strongly enhanced spin fluctuations. Thus, their ground state is close to a ferromagnetic instability which makes them good candidates for actually reaching the ferromagnetic quantum phase transition experimentally. At ambient pressure MnSi is paramagnetic for temperatures larger than $T_c = 30\,\mathrm{K}$. Below T_c it orders magnetically. The phase transition temperature can be reduced by applying pressure, and at about 14 kBar the magnetic phase vanishes altogether. Thus, at 14 kBar MnSi undergoes a magnetic quantum

phase transition. The properties of this transition are in semi-quantitative agreement with the theoretical predictions[9], in particular, the quantum phase transition is of first order while the thermal transition at higher temperatures is of second order.[12]

However, the magnetic order in MnSi is not exactly ferromagnetic but a long-wavelength (190 Å) helical spin spiral along the (111) direction of the crystal. The ordering wavelength depends only weakly on the temperature, but a homogeneous magnetic field of about 0.6 T suppresses the spiral and leads to ferromagnetic order. The helical structure is a consequence of the so-called Dzyaloshinskii mechanism,[13,14] an instability of the ferromagnetic state with respect to small 'relativistic' spin-lattice or spin-spin interactions. The helical ordering in MnSi immediately leads to the question, to what extent the properties of the quantum phase transition in MnSi are generic for itinerant quantum ferromagnets or whether the agreement between the experiments and the ferromagnetic theory is accidental.

In this paper we therefore study how the long-period helimagnetism caused by a Dzyaloshinskii instability influences the properties of the quantum phase transition of an itinerant magnet. Our starting point is the effective action for the spin degrees of freedom in a three-dimensional itinerant quantum magnet. This action can be derived from a microscopic model of interacting electrons.[8] In terms of the magnetization $\mathbf{M}$ the action reads

$$\begin{aligned} S_{\rm FM}[\mathbf{M}] \;=\; & \frac{1}{2}\int dxdy\, \mathbf{M}(x)\,\Gamma_0(x-y)\,\mathbf{M}(y) \\ & - \sum_{n=3}^{\infty} \frac{(-1)^n}{n!} \int dx_1 \ldots dx_n\; \chi^{(n)}(x_1,\ldots,x_n)\,\times \\ & \qquad\qquad \times \mathbf{M}(x_1)\ldots\mathbf{M}(x_n)\;. \end{aligned} \tag{1}$$

We have used a 4-vector notation with $x = (\mathbf{r}, \tau)$ comprising a real space vector $\mathbf{r}$ and imaginary time τ. Analogously, $\int dx = \int d\mathbf{r} \int_0^{1/T} d\tau$, where T is the temperature. The bare Gaussian vertex Γ_0 is proportional to $(1 - J\chi^{(2)})$ where J is the spin-triplet (exchange) interaction amplitude and $\chi^{(2)}$ is the spin susceptibility of a reference system which is a Fermi liquid (precisely, it is the original electron system with the bare spin-triplet interaction taken out). For the purpose of this paper we can consider the Fourier transform $\Gamma_0(\mathbf{k}, \omega)$ of the Gaussian vertex in the limit of long-wavelengths and low frequencies, $|\mathbf{k}| \ll k_F$ and $\omega \ll \epsilon_F$, since we are interested in spiral states

whose wavelength is large compared to the Fermi wave length and in long-wave length low-frequency fluctuations around such states. In this limit Γ_0 is given by[8]

$$\Gamma_0(\mathbf{k},\omega) = t_0 + B_1 k^2 + C_3 k^2 \log(1/k) + C_\omega \frac{|\omega|}{k} \ . \tag{2}$$

The third term in $\Gamma_0(\mathbf{k},\omega)$ merits particular attention. It represents an effective long-range interaction induced by the coupling between the magnetization and additional non-critical soft modes in a zero-temperature electronic system. Generically, this interaction is repulsive, i.e $C_3 < 0$, but rather weak, $|C_3| \ll B_1$, since it is caused by electronic correlations. In the ordered phase the magnetization M cuts off the logarithmic singularity, and the term qualitatively takes the form $C_3 M^4 \log(1/M)$ which leads to a first-order phase transition.[9] The nucleation length scale $\ell_{\rm Nucl}$ associated with this transition is given by the length at which the B_1 and C_3 terms in the Gaussian vertex (2) are equal and opposite, i.e. $\log(\ell_{\rm Nucl}) \sim B_1/|C_3|$. The coefficients $\chi^{(n)}$ of the higher order terms in eq. (2) are proportional to the higher spin density correlation functions of the reference system. Because of the same mode coupling effects that lead to the non-analytic C_3 term in the Gaussian action they are in general not finite in the limit of zero frequencies and wave numbers. For $\mathbf{p} \to 0$ they behave like $\chi^{(n)} \sim v^{(n)} |\mathbf{p}|^{4-n}$.

We now add a new term, the helical or Dzyaloshinskii term,[13,14] to the effective action (2):

$$S[\mathbf{M}] = S_{\rm FM}[\mathbf{M}] + D \int dx \, \mathbf{M}(x) \cdot \mathrm{curl}\, \mathbf{M}(x) \ . \tag{3}$$

This term will cause an instability of the ferromagnetic state. Physically, it may be caused by relativistic interactions between spins of the form $\mathbf{S}_i \times \mathbf{S}_j$. Therefore, it will generically be small compared to the other Gaussian terms, with the possible exception of the long-range C_3 term. The Dzyaloshinskii term defines a new length scale $\ell_{\rm Spiral}$ which is the length at which the Dzyaloshinskii term and the conventional gradient (B_1) term in the action are of the same strength, $\ell_{\rm Spiral} \sim B_1/|D|$.

Clearly, the qualitative properties of the helimagnetic quantum phase transition crucially depend on the ratio of the two length scales $\ell_{\rm Spiral}$ and $\ell_{\rm Nucl}$. Let us first discuss the two possible scenarios qualitatively: In the case $\ell_{\rm Spiral} \ll \ell_{\rm Nucl}$, i.e. for a strong Dzyaloshinskii instability or weak electronic correlations the growing magnetic

correlation length first reaches $\ell_{\rm Spiral}$ when approaching the quantum phase transition. Therefore the system crosses over from ferromagnetic to helimagnetic behavior *before* the self-generated effective long-range interaction becomes sufficiently strong to induce a first-order transition. The dominant fluctuations close to the quantum phase transition are therefore of spiral character. In the opposite case, $\ell_{\rm Spiral} \gg \ell_{\rm Nucl}$, i.e. a weak Dzyaloshinskii instability or strong electronic correlations, the magnetic correlation length first reaches $\ell_{\rm Nucl}$, and the system undergoes a first-order phase transition. In this case, the dominant fluctuations close to the quantum phase transition are of ferromagnetic nature even though the ordered state is a spiral. Therefore the properties of the transition are completely analogous to that of the ferromagnetic quantum phase transition.

After this qualitative discussion we now analyze the action (3) in more detail. In order to determine the character of the ordered state we begin with a saddle point-level investigation of the Gaussian term of the action. In the presence of the Dzyaloshinskii term, the Gaussian action is minimized by a state $\mathbf{M}(x)$ which is periodic in space but homogeneous in imaginary time:

$$\mathbf{M}(\mathbf{r},\tau) = \mathbf{A}_{\mathbf{k}} e^{i\mathbf{k}\cdot\mathbf{r}} + \mathbf{A}_{\mathbf{k}}^{*} e^{-i\mathbf{k}\cdot\mathbf{r}} \ . \tag{4}$$

Here $\mathbf{A}_{\mathbf{k}} = \mathbf{a}_{\mathbf{k}} + i\mathbf{b}_{\mathbf{k}}$ is a complex vector. Inserting this ansatz into the action (3) we obtain

$$\begin{aligned} S^{\rm SP}(\mathbf{k}) \ &= \ \left[t_0 + B_1 k^2 + C_3 k^2 \log(1/k)\right] |\mathbf{A}_{\mathbf{k}}|^2 \\ &\quad + iD\, \mathbf{k}\cdot(\mathbf{A}_{\mathbf{k}} \times \mathbf{A}_{\mathbf{k}}^{*}) + O(|\mathbf{A}_{\mathbf{k}}|^4) \ . \end{aligned} \tag{5}$$

The Gaussian part of $S^{\rm SP}(\mathbf{k})$ is minimized for $|\mathbf{a}_{\mathbf{k}}| = |\mathbf{b}_{\mathbf{k}}|$ and $\mathbf{a}_{\mathbf{k}} \perp \mathbf{b}_{\mathbf{k}}$. The sign of D determines the handedness of the resulting spin spiral. For $D > 0$ the minimum action is achieved for $\mathbf{k}$ antiparallel to $\mathbf{a}_{\mathbf{k}} \times \mathbf{b}_{\mathbf{k}}$, this is a right-handed spiral. In contrast, for $D < 0$ the vector $\mathbf{k}$ must be parallel to $\mathbf{a}_{\mathbf{k}} \times \mathbf{b}_{\mathbf{k}}$, leading to a left-handed spiral. Taking all these conditions into account the saddle-point action reads

$$\begin{aligned} S^{\rm SP}(\mathbf{k}) \ &= \ \left[t_0 + B_1 k^2 + C_3 k^2 \log(1/k) - 2|D|k\right] |\mathbf{A}_{\mathbf{k}}|^2 \\ &\quad + O(|\mathbf{A}_{\mathbf{k}}|^4) \ . \end{aligned} \tag{6}$$

The term in brackets is minimized by the ordering wave vector $\mathbf{K}$. Since in general $|D| \ll B_1$ the ordering wavevector will be small. The direction of $\mathbf{K}$ cannot be determined from our rotational invariant Gaussian vertex (2). It will be fixed by additional (weak) anisotropic terms in the model. In MnSi the spiral wavevector is known to be parallel to the (111) or equivalent crystal directions.[10,11,15] In the following we will focus on this case, a generalization to other directions is straightforward. There are four equivalent ordering wave vectors $\mathbf{K}_j$, *viz.* $K\,(1,1,1)/\sqrt{3}$, $K\,(-1,-1,1)/\sqrt{3}$, $K\,(-1,1,-1)/\sqrt{3}$, and $K\,(1,-1,-1)/\sqrt{3}$. For each wave vector $\mathbf{K}_j$ there are two equivalent directions in the plane orthogonal to $\mathbf{K}_j$. Together this defines 8 equivalent spirals, i.e. the order parameter has eight components, $\psi_j, \bar{\psi}_j$, $(j = 1 \ldots 4)$.[14] We now consider slow fluctuations of the order parameter by writing the magnetization as

$$\begin{aligned}\mathbf{M}(\mathbf{r},\tau) = \sum_{j=1}^{4} \quad & \Big\{\psi_j(\mathbf{r},\tau)\left[\mathbf{A}_{\mathbf{K}_j} e^{i\mathbf{K}_j\cdot\mathbf{r}} + \mathbf{A}^*_{\mathbf{K}_j} e^{-i\mathbf{K}_j\cdot\mathbf{r}}\right] \\ & + \bar{\psi}_j(\mathbf{r},\tau)\left[-i\mathbf{A}_{\mathbf{K}_j} e^{i\mathbf{K}_j\cdot\mathbf{r}} + i\mathbf{A}^*_{\mathbf{K}_j} e^{-i\mathbf{K}_j\cdot\mathbf{r}}\right]\Big\}\,,\end{aligned} \tag{7}$$

where $\mathbf{A}_{\mathbf{K}_j} = \mathbf{a}_{\mathbf{K}_j} + i\mathbf{b}_{\mathbf{K}_j}$ with $|\mathbf{a}_{\mathbf{K}_j}| = |\mathbf{b}_{\mathbf{K}_j}| = 1$, $\mathbf{a}_{\mathbf{K}_j} \perp \mathbf{b}_{\mathbf{K}_j}$, and $\mathbf{K}_j$ parallel or antiparallel to $\mathbf{a}_{\mathbf{K}_j} \times \mathbf{b}_{\mathbf{K}_j}$ depending on the sign of D. The order parameter fields $\psi_j(\mathbf{r},\tau)$ and $\bar{\psi}_j(\mathbf{r},\tau)$ are slowly varying in space and imaginary time, in particular, they are only slowly varying over the wavelength of the spiral. Inserting the order parameter representation (7) into the action (3) leads to the desired order parameter field theory for the itinerant quantum helimagnet.

In the non-magnetic phase the leading terms in an expansion of the Landau-Ginzburg-Wilson free energy functional Φ in powers of momenta and frequencies of the order parameter field are given by

$$\begin{aligned}\Phi[\psi_j,\bar{\psi}_j] \;=\; & \frac{1}{2}\sum_{\mathbf{q},\omega,j}\left[|\psi_j(\mathbf{q},\omega)|^2 + |\bar{\psi}_j(\mathbf{q},\omega)|^2\right]\times \\ & \times\left[t + B_1 q^2 + C_3\,K^2\log\left(\frac{1}{K}\right) + \right. \\ & \left. + \tilde{B}_1 q^2\log(1/K) + C_\omega\frac{|\omega|}{K} + O(q^3,\omega q^2)\right] \\ & +\; O(\psi^4,\bar{\psi}^4)\;.\end{aligned} \tag{8}$$

As a consequence of the spiral magnetic ordering the non-analyticities in the Gaussian vertex (2) are cut-off at the ordering wave vector $\mathbf{K}$. For clarity we have written the resulting K-dependent terms explicitly in (8). In the rest of the paper they will be absorbed into renormalizations of the parameters t, B_1, and C_ω. The spiral ordering cuts off not only the non-analyticities in the Gaussian vertex but also the singularities in the higher-order terms. In contrast to the ferromagnetic case (2) the coefficients of all higher-order terms in (8) are finite in the limit $\mathbf{q}, \omega \to 0$.

We now analyze the order-parameter field theory (8) at mean-field level. As discussed after eq. (2), in the magnetic phase the long-range interaction (the logarithmic term) will be cut off not only by K but also by $|\psi|$.[9] Qualitatively, the resulting term takes the form $-C_3\,\psi^4\,\ln(\psi^2+K^2)$. Consequently, the mean-field free energy in the magnetic phase reads

$$F \;\sim\; t\,\psi^2 - C_3\,\psi^4\,\log(\psi^2+K^2) + \tilde{u}\,\psi^4 + O(\psi^6)\;. \tag{9}$$

At mean-field level the order of the transition is determined by the sign of the coefficient u of the ψ^4 term. Expanding the logarithm in (9) we find $u = \tilde{u} - 2C_3 \log K$. Thus, for large K and small C_3 the mean-field free energy displays a continuous transition with conventional mean field critical exponents (this is the first scenario mentioned above), in the opposite case a first-order transition analogous to that in itinerant ferromagnets[9] (the second scenario discussed above). There is a quantum tricritical point at $|K| = \exp(-\tilde{u}/2|C_3|)$ which separates the two regimes. The tricritical behavior is also conventional mean-field like.

What remains to be done is to check the stability of the mean-field theory (9) with respect to quantum fluctuations. In the case of the first-order scenario this was done in Ref. 9. To do the same for the continuous-transition scenario we keep only the most relevant terms (in the renormalization group sense) in (8) and suppress unessential constants. The resulting Landau-Ginzburg-Wilson functional Φ can be written as

$$\begin{aligned}\Phi[\psi_j,\bar{\psi}_j] \;=\; & \frac{1}{2}\sum_{\mathbf{q},\omega,j}(t+q^2+|\omega|)\left[|\psi_j(\mathbf{q},\omega)|^2+|\bar{\psi}_j(\mathbf{q},\omega)|^2\right] \\ & +\; u\int dx\left\{\sum_j[\psi_j^2(x)+\bar{\psi}_j^2(x)]\right\}^2\end{aligned}$$

$$+ \ \lambda \int dx \sum_j [\psi_j^2(x) + \bar{\psi}_j^2(x)]^2 \ . \tag{10}$$

Here the u term is the conventional isotropic 4th order term, while the λ term represents a cubic anisotropy connected with the discrete 4-fold degeneracy of the action with respect to the direction of the spiral wave vector $\mathbf{K}$. One might worry whether additional relevant contributions to (10) arise from the anisotropic terms in the action necessary to fix the directions of the spirals, as discussed after (6). However, once the rotational symmetry is broken by the discrete set of spiral directions additional anisotropic terms in the action do not produce new contributions to (10). An explicit calculation shows that they only renormalize the coefficients u and λ.

We proceed by analyzing the Landau-Ginzburg-Wilson free energy functional (10) by conventional renormalization group methods for quantum phase transitions.[6] At tree-level the Gaussian fixed point is defined by the requirement that the coefficients of the q^2 and $|\omega|$ terms in the Gaussian vertex do not change under renormalization. Therefore, the dynamical exponent is $z = 2$. The other critical exponents which can be read off the Gaussian vertex take their mean-field values: $\nu = 1/2$, $\gamma = 1$, and $\eta = 0$. Defining the scale dimension of a length to be $[L] = -1$, we find the scale dimension of the fields at the Gaussian fixed point to be $[\psi] = [\bar{\psi}] = (d+z-2)/2 = 3/2$ (d is the spatial dimensionality)

The properties of the Gaussian fixed point in our model are identical to those of a conventional itinerant antiferromagnet. This is not surprising since the structure of the Gaussian vertex of the Landau-Ginzburg-Wilson functional (10) is identical to that derived by Hertz[6] for itinerant antiferromagnets. The only difference is the number of order parameter components.

In order to check the stability of the Gaussian fixed point we calculate the scale dimensions of the coefficients of the quartic terms, u and λ. They turn out to be $[u] = [\lambda] = d+z-4[\psi] = 4-d-z$. In our case, $d = 3$, $z = 2$ this means $[u] = [\lambda] = -1$. The quartic terms are irrelevant at the Gaussian fixed point which is therefore stable. This is again analogous to a conventional itinerant quantum antiferromagnet, the more complicated order parameter component structure does not play any role at the Gaussian fixed point. Consequently, the mean-field theory (9) of the helimagnetic

quantum phase transition is indeed stable, and the quantum-critical point, if any, is characterized by the usual mean-field exponents and a dynamic exponent of $z = 2$.

In the final section of the paper we relate our findings to the experiments on the quantum phase transition in the prototypical itinerant helimagnet, MnSi.[10,11] Our study has revealed that the properties of the helimagnetic quantum phase transition crucially depend on the ratio of two length scales, *viz.* the wave length ℓ_{Spiral} of the spiral and the nucleation length ℓ_{Nucl} associated with the first-order transition in the corresponding itinerant quantum ferromagnet. In MnSi the wave length of the spiral is rather large, approximately 190 Å. In contrast, the experimental data for the magnetic susceptibility suggest that the nucleation length of the first order transition is small (of the order of the microscopic scales). This can be seen from the fact that no susceptibility increase is observed close to the quantum phase transition, instead the susceptibility close to the transition is approximately a step function. (If the first order transition would occur at some large length scale the susceptibility should increase when approaching the transition until the magnetic correlation length reaches this scale.)

Therefore, the nucleation length scale is much shorter than the spiral wave length, and our theory predicts a first-order transition, in agreement with the experiments. According to our theory the properties of the quantum phase transition in MnSi are identical to that of the quantum *ferro*magnetic transition and MnSi is indeed a prototypical example for this transition.

In summary, we have studied the quantum phase transition of itinerant electrons from a paramagnet to a state which displays long-period helical structures due to a Dzyaloshinskii instability of the ferromagnetic state. We found that depending on the relative strengths of the helical (Dzyaloshinskii) term and the correlation-induced self-generated long range interaction two different phase transition scenarios are possible. If the self-generated long-range interaction is stronger than the helical term the transition is of first-order with the same properties as the quantum ferromagnetic transition. This is the situation encountered in MnSi. In contrast, if the helical term is stronger the transition is a continuous one with mean-field critical exponents and a

dynamical exponent of $z = 2$. The two regimes are separated by a quantum tricritical point.

We gratefully acknowledge helpful discussions with S. Bekhechi, D. Belitz, T.R. Kirkpatrick and R. Narayanan. This work was supported in part by the DFG under grant No. Vo659/2 and Vo659/3 and by the NSF under grant No. DMR–98–70597. Part of this work was performed at the Aspen Center for Physics.

---

[1] S.L. Sondhi, S.M. Girvin, J.P. Carini, and D. Shahar, Rev. Mod. Phys. **69**, 315 (1997).

[2] S.-C. Zhang, Science **275**, 1089 (1997).

[3] T.R. Kirkpatrick and D. Belitz, in *Electron Correlations in the Solid State*, edited by N.H. March, Imperial College Press, London (1999).

[4] S. Sachdev, *Quantum Phase Transitions*, Cambridge University Press, Cambridge (2000).

[5] T. Vojta, Ann. Phys. (Leipzig) **9**, 403 (2000).

[6] J. Hertz, Phys. Rev. B **14**, 1165 (1976).

[7] A.J. Millis, Phys. Rev. B **48**, 7183 (1993).

[8] T. Vojta, D. Belitz, R. Narayanan, and T.R. Kirkpatrick, Z. Phys. B **103**, 451 (1997); D. Belitz, T.R. Kirkpatrick, and T. Vojta, Phys. Rev. B 55, 9452 (1997).

[9] D. Belitz, T.R. Kirkpatrick and T. Vojta, Phys. Rev. Lett **82**, 4707 (1999); T. Vojta, D. Belitz, T.R. Kirkpatrick, and R. Narayanan, Ann. Phys. (Leipzig) **8**, 593 (1999).

[10] C. Pfleiderer, G.J. McMullan, and G.G. Lonzarich, Physica B **206 & 207**, 847 (1995).

[11] C. Pfleiderer, G.J. McMullan, S.R. Julian, and G.G. Lonzarich, Phys. Rev. B **55**, 8330 (1997); and references therein.

[12] There are experimental[15] and theoretical[14] indications for the thermal transition at higher temperatures actually being weakly (fluctuation-driven) first order. However, the quantum phase transition is a much stronger first order transition.

[13] I.E. Dzyaloshinskii, J. Exp. Theor. Phys. **46**, 1420 (1964) [Sov. Phys. – JETP **19**, 960 (1964)].

[14] P. Bak and M.H. Jensen, J. Phys. C **13**, L881 (1980).

[15] Y. Ishikawa, K. Tajima, D. Bloch, and M. Roth, Solid State Commun. **19**, 525 (1976);

Y. Ishikawa, T. Komatsubara, and D. Bloch, Physica **86**–**88B**, 401 (1977)

[16] Technically, the spiral wave vector plays the same role as a finite temperature in protecting the singularity (see Ref. 9) but the physics is different. At a finite temperature the interaction range becomes finite since the temperature gives the fermionic particle-hole excitations a mass. In the case of helical ordering, however, the order parameter fluctuations beyond the spiral length scale cease to couple to the soft particle-hole excitations at $\mathbf{k} = 0$.

3. ORDER PARAMETER SYMMETRY AND MODE COUPLING EFFECTS AT DIRTY SUPERCONDUCTING QUANTUM PHASE TRANSITIONS

Rastko Sknepnek and Thomas Vojta

Department of Physics, University of Missouri - Rolla, Rolla, MO, 65409, USA

Rajesh Narayanan

Institut für Nanotechnologie, Forschungszentrum Karlsruhe, 76021 Karlsruhe, Germany and

Max-Planck-Institut für Physik komplexer Systeme, Nöthnitzer Straße, 01187 Dresden, Germany

Abstract

We derive an order-parameter field theory for a quantum phase transition between a disordered metal and an exotic (non-s-wave) superconductor. Mode coupling effects between the order parameter and other fermionic soft modes lead to an effective long-range interaction between the anomalous density fluctuations which is reflected in singularities in the free energy functional. However, this long-range interaction is not strong enough to suppress disorder fluctuations. The asymptotic critical region is characterized by run-away flow to large disorder. For weak coupling, this asymptotic region is very narrow. It is preempted by a wide crossover regime with mean-field critical behavior and, in the p-wave case, logarithmic corrections to scaling in all dimensions. These results are discussed from a general mode-coupling point of view and in relation to recent experiments.

I. INTRODUCTION

During the past two and a half decades considerable effort has been devoted to understanding the physics underlying quantum phase transitions, still leaving them one of the most intriguing problems in condensed matter physics.[1–3] Quantum phase transitions are fundamental changes in the macroscopic properties of matter occurring at zero temperature as functions of some external parameters. In addition to being of fundamental interest, quantum phase transitions are important because they are believed to underlie a number of interesting low-temperature phenomena, in particular various forms of exotic superconductivity.[4–6]

In a seminal paper,[1] Hertz introduced a general scheme for the theoretical treatment of quantum phase transitions in itinerant electronic systems. The basic idea of his approach is to integrate out all microscopic degrees of freedom and to derive a Landau-Ginzburg-Wilson (LGW) theory entirely in terms of the order parameter fluctuations. Within this scheme, all microscopic details of the system are encoded in vertices of the LGW theory which are given by the appropriate correlation functions of a Fermi liquid. Hertz applied this scheme to the ferromagnetic and antiferromagnetic quantum phase transitions of itinerant electrons. He showed that a quantum phase transition in d dimensions is essentially equivalent to a classical phase transition in $d + z$ dimensions (z is the dynamical critical exponent). Therefore the upper critical dimension d_c^+ for most quantum phase transitions is reduced below $d = 3$. Hertz then concluded that most quantum phase transitions are not very interesting from a critical phenomena point of view since their critical behavior in the physically relevant dimensions is mean-field like.

However, in recent years, it has become clear that for many quantum phase transitions in itinerant electronic systems there are problems with Hertz' scheme because besides the order parameter fluctuations, which are soft (gapless) at the critical point, there are additional non-critical fermionic soft modes present in the system. These additional soft modes exist not only at the critical point but also in the bulk phases. They are related to the existence of conservation laws and/or broken symmetries and constitute examples of generic scale invariance.[7] If the coupling between the order pa-

rameter and these additional soft modes is sufficiently strong it generates an effective long-range interaction between the order parameter fluctuations. This is reflected in a non-analytic wave-number dependence of the order parameter susceptibilities, i.e., non-analytic vertices of the LGW theory of the corresponding quantum phase transition. Generically, such a non-localities in the LGW theory will lead to non-mean-field critical behavior of the quantum phase transition.

The precise influence of the mode-coupling effects on a quantum phase transition depends on the structure of the additional soft modes and their coupling to the order parameter. One of the most prominent examples is the ferromagnetic quantum phase transition of itinerant electrons. In the disordered phase (i.e., a paramagnetic Fermi liquid) the mode-coupling leads to a non-analyticity in the static magnetic susceptibility of the form $|\mathbf{q}|^{d-1}$ for clean electrons[8–10] and an even stronger singularity of the form $|\mathbf{q}|^{d-2}$ for diffusive electrons.[11] This effect is analogous to the well known Altshuler-Aronov interaction correction to the conductivity of diffusive electrons.[12] As a result, the clean ferromagnetic quantum phase transition can either be of second order with non-mean-field exponents or even of first order.[13,14] For dirty electrons, the transition is generically second order but with highly unusual exponents which can nonetheless be determined exactly.[11,15] Even stronger singularities were found for the quantum phase transition between a dirty metal and a conventional (s-wave) superconductor.[16] Here the mode-coupling effects lead to a critical point with exponential rather than the conventional power-law scaling, e.g., the correlation length behaves as $\xi \sim e^{1/|t|}$, where t is distance from the quantum critical point.

In order to find out which quantum phase transitions are actually influenced by the mode-coupling effects discussed above, a general criterion was established[17] for quantum phase transitions in itinerant electronic systems with homogeneous ($\mathbf{q} = 0$)[18] order parameters. Based on symmetry considerations it was shown that order parameters in the particle-particle (Cooper) and spin-triplet particle-hole channels are generically affected by mode coupling effects while order parameters in the particle-hole spin-singlet channel do allow for a local LGW theory. This criterion relies on the observation that a source field for an order parameter in the particle-particle or spin-triplet particle-hole channel will break a symmetry of the system forcing the

corresponding soft modes to acquire a mass. Therefore, the corresponding correlation functions become non-analytic functions of the source field. In contrast, a source term in the particle-hole spin-singlet channel is equivalent to a change in chemical potential and leaves soft mode structure of the system intact, resulting in an analytic expressions for reference ensemble correlations functions.

All of the examples mentioned above are quantum phase transitions with zero angular momentum order parameter. The effect of mode-coupling on order-parameters with finite angular momentum are much less understood. Herbut[19] studied the d-wave superconducting quantum phase transition in two dimensions within Hertz' scheme (which is equivalent to Gorkov's mean-field theory). He found that the typical Cooper channel (BCS) logarithmic singularities are demoted to irrelevant terms by the d-wave symmetry. This raises the important general question: How does a finite order parameter angular momentum influence the coupling between order parameter and additional fermionic soft modes?

In this Paper, we study this question for quantum phase transitions between a metal and an exotic superconductor in the presence of non-magnetic quenched disorder. These transitions are of particular experimental importance since various superconducting states with p-wave, d-wave and maybe higher symmetries have been observed in recent years and their quantum phase transitions are experimentally accessible[4–6] in principle. Experiments recently performed on the weakly ferromagnetic compounds UGe_2[5] and $ZrZn_2$[6] revealed the existence of a superconducting phase within the ferromagnetic phase at temperatures below 1K. It is believed[5] that both superconductivity and ferromagnetism arise from the same electrons, suggesting that the superconducting state is of spin-triplet (p-wave) type. One of the good candidates for the mechanism of superconductivity is p-wave triplet pairing mediated by magnetic fluctuations produced by a nearby magnetic quantum critical point,[20] although this is still not a settled issue. The onset of the phenomenon has proven to be very sensitive to the presence of non-magnetic disorder, making it observable only in highly pure samples. This fact also points to a non-s-wave order parameter. In $ZrZn_2$ the superconducting quantum phase transition as a function of disorder has already been observed.[6]

The paper is organized as follows. In Section II we derive the LGW free energy functional starting from a microscopic model of interacting disordered electrons. Subsections II A and II B are devoted to the case of p-wave pairing symmetry, higher angular momenta L are considered in subsection II C. In Section III, we investigate the resulting LGW theory by means of the renormalization group and determine the critical behavior. In Section IV we analyze our findings from a general mode-coupling point of view, we discuss differences between paramagnetic and ferromagnetic as well as clean and dirty systems, and we briefly mention possible experiments. Technical details of the calculation are presented in appendices.

II. LANDAU-GINZBURG-WILSON THEORY

A. p-wave pairing case

In this section, we derive an effective LGW theory for the disorder-driven quantum phase transition between a paramagnetic metal and an exotic superconductor with p-wave triplet pairing. Our starting point is a microscopic action for interacting electrons in $d > 2$ dimensions and subject to a static, single-particle random potential $V(\mathbf{x})$. For simplicity we assume a Gaussian distributed potential with $[V(\mathbf{x}_1)V(\mathbf{x}_2)]_{dis} = W\delta(\mathbf{x}_1 - \mathbf{x}_2)$, with W being measure of disorder strength. The partition function Z can be written as a functional integral over Grassmann variables $\psi, \bar{\psi}$:

$$Z = \int D[\bar{\psi}, \psi] e^{S[\bar{\psi},\psi]} \ . \tag{1}$$

We decompose the action $S = S_p + S_0$ into the p-wave interaction part S_p and a reference system S_0 which comprises the single-particle part, the random potential and S_{int} (the interaction in all channels other than the p-wave channel):

$$S_0 = \int dx \sum_\sigma \bar{\psi}_\sigma(x)[\partial_\tau + \frac{\nabla^2}{2m} + \mu]\psi_\sigma(x) + \tag{2}$$

$$+ \int dx \sum_\sigma \bar{\psi}_\sigma(x) V(\mathbf{x}) \psi_\sigma(x) + S_{int}, \tag{3}$$

$$S_p = \sum_{\{\sigma\}} \frac{\Gamma_t^{\{\sigma\}}}{2} \int dx \bar{\mathbf{n}}_{\sigma\sigma'}(x) \cdot \mathbf{n}_{\sigma_1\sigma_1'}(x) \ . \tag{4}$$

We use a $(d+1)$-vector notation, with $x = (\mathbf{x}, \tau)$, $k = (\mathbf{k}, \Omega)$, $\int dx = \int_V d^d x \int_0^\beta d\tau$ and $\sum_k = \sum_{\mathbf{k}} T \sum_\Omega$, $\mathbf{x}$ is a real space coordinate, τ imaginary time, $\mathbf{k}$ momentum vector and Ω Matsubara frequency. $\mathbf{n}_{\sigma\sigma'}(x)$ is the p-wave anomalous density whose Fourier transform in terms of the fermion fields is given by

$$\mathbf{n}_{\sigma\sigma'}(q) = \sum_k \hat{\mathbf{e}}_{\mathbf{k}} \; \psi_\sigma(k + q/2)\psi_{\sigma'}(k - q/2), \tag{5}$$

with $\hat{\mathbf{e}}_{\mathbf{k}} = \mathbf{k}/|\mathbf{k}|$, σ, σ' being spin indices and $\cdot$ denoting scalar product in the orbital space. Due to the Pauli principle the spin state of the Cooper pair has to be a triplet, i. e. $\sigma\sigma' \in \{(\uparrow\uparrow), (\downarrow\downarrow), 1/\sqrt{2}(\uparrow\downarrow + \downarrow\uparrow)\}$. Which combination of the three possible triplet components is actually realized depends on the system under consideration. The reference ensemble S_0 describes interacting electrons in the presence of non-magnetic quenched disorder and no bare interaction in the p-wave Cooper channel. (A non-vanishing interaction in this channel will be generated in perturbation theory.) S_0 thus describes a general system of disordered interacting electrons with the only restriction being that it must not undergo a phase transition in the parameter region we are interested in.

A standard procedure[1] is used to derive a LGW order-parameter field theory. We decouple the interaction term using a Hubbard-Stratonovich transformation[21,22] introducing a complex field $\mathbf{\Delta}_{\sigma\sigma'}(x)$ which plays the role of an order parameter. Quenched disorder is averaged out using the replica trick,[23] and fermionic degrees are then integrated out, leading to an expression for the critical part of the partition function only in terms of order-parameter field:

$$Z = \int \mathrm{D}[\mathbf{\Delta}] \; e^{-\Phi[\mathbf{\Delta}]} \; . \tag{6}$$

Since our emphasis is on the mode-coupling effects, and in order to avoid unnecessary complications in notation, we restrict our analysis to a certain spin component ($\sigma\sigma' = (\uparrow\uparrow)$) of the order parameter. The LGW free energy $\Phi[\mathbf{\Delta}]$ is expanded in powers of

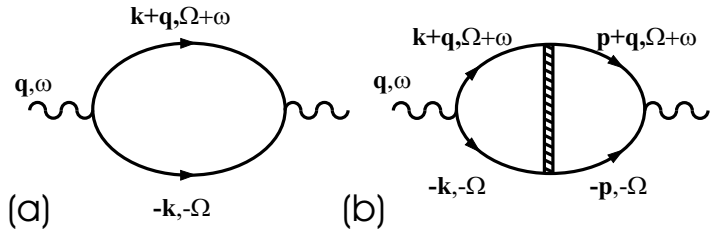

FIG. 1: Contributions to the leading terms of the Gaussian part of the LGW functional. (a) provides a constant ($\sim N_F$) and the frequency dependence, $|\omega|\tau$, while (b) gives the leading momentum dependence, $|\mathbf{q}|^2 \log(1/|\mathbf{q}|)$.

the order parameter $\mathbf{\Delta} \equiv \mathbf{\Delta}_{\uparrow\uparrow}$. Up to quartic order it reads:

$$\begin{aligned}\Phi[\mathbf{\Delta}] \;=\; & \sum_{q,\alpha} \bar{\mathbf{\Delta}}^{\alpha}(q)(1-\Gamma_t \chi^{(2)}(q))\mathbf{\Delta}^{\alpha}(q) \\ & - \sum_{\substack{q_1 \cdots q_3 \\ \alpha,\beta}} \Gamma_t^2 \chi^{(4)}_{\alpha\beta}(q_1,q_2,q_3)\bar{\mathbf{\Delta}}^{\alpha}(q_1)\mathbf{\Delta}^{\alpha}(q_2) \\ & \times\; \bar{\mathbf{\Delta}}^{\beta}(q_3)\mathbf{\Delta}^{\beta}(q_1+q_3-q_2) + O(\Delta^6), \end{aligned} \tag{7}$$

where $\Gamma_t^{\uparrow\uparrow} \equiv \Gamma_t$. Here α, β are replica indexes. The coefficients of the LGW functional are determined by the 2-point and 4-point anomalous density correlation functions of the reference system S_0 which can be written as $\chi^{(2)} = \langle \bar{n}^{\alpha} n^{\alpha} \rangle_0$ and $\chi^{(4)}_{\alpha\beta} = \langle \bar{n}^{\alpha} \bar{n}^{\beta} n^{\beta} n^{\alpha} \rangle_0$ (with the spin and component indices suppressed).

B. Anomalous density correlation functions in the p-wave channel

In this subsection we use diagrammatic perturbation theory in disorder and interactions of the reference ensemble S_0 to calculate $\chi^{(2)}$ and $\chi^{(4)}$, concentrating on the leading behavior for weak disorder. Thus, we neglect all diagrams with crossed impurity lines, i.e., all weak localization effects, which become important only at higher impurity concentrations. This is certainly justified for the ferromagnetic superconductors[5,6] where the superconducting quantum phase transition occurs at very small disorder.

We start our analysis by examining the 2-point correlation function, $\chi^{(2)} = \langle \bar{n}^{\alpha} n^{\alpha} \rangle_0$. The leading contributions are obtained from the diagrams shown in Fig. 1 (details of the calculation of these diagrams are given in Appendix B). Here, the

external vertices represent anomalous p-wave densities, the solid lines are fermionic propagators in Born approximation,

$$G_\sigma^{-1}(\mathbf{k},\omega) = i\omega - \epsilon_{\mathbf{k},\sigma} + \mu + (i/2\tau)\mathrm{sgn}(\omega), \tag{8}$$

where $\epsilon_{\mathbf{k},\sigma}$ is the dispersion relation and τ is the scattering time. The double line represents a particle-particle impurity ladder (Appendix A):

$$W_R(\mathbf{q},\Omega,\omega) = W \begin{cases} 1 & \text{if } \Omega(\Omega+\omega) < 0 \\ \frac{1}{|2\Omega+\omega|\tau+\ell^2|\mathbf{q}|^2/d} & \text{if } \Omega(\Omega+\omega) > 0 \end{cases} \tag{9}$$

$\ell = k_F\tau/m$ is the elastic mean free path and $W = 1/(2\pi N_F\tau)$ with N_F being the density of states at the Fermi level. The calculation of the diagrams in Fig. 1 for $|\mathbf{q}| = \omega = 0$ leads to $\chi^{(2)} = (N_F/3)\ln(2\epsilon_F\tau)$. The well-known logarithmic Cooper channel (BCS) singularities are cut-off by the disorder, reflecting the suppression of exotic superconductivity by non-magnetic scatterers in analogy to the suppression of s-wave superconductivity by magnetic impurities.[24,25] [We note that, in contrast, s-wave superconductivity is not influenced by weak non-magnetic scatterers, as is signified by Anderson's theorem.[26]] However, a closer investigation of diagram 1b) for finite $|\mathbf{q}|$ reveals that a non-analyticity of the form $|\mathbf{q}|^2\ln(1/|\mathbf{q}|)$ survives. Thus, the p-wave symmetry has demoted the BCS singularity to quadratic order in $|\mathbf{q}|$ because each of the renormalized external vertices picks up an extra power of $|\mathbf{q}|$.[27]

In addition to the BCS logarithms $\chi^{(2)}$ contains non-analyticities similar to that in the itinerant ferromagnet. They are caused by the leading corrections to scaling at the dirty Fermi liquid fixed point[28] and can be viewed as particle-particle analogs of the well known Altshuler-Aronov corrections to density of states and conductivity.[12] For s-wave order parameters these singularities (which only arise for interacting electrons) are of the form $|\mathbf{q}|^{d-2}$.[28] For p-wave order parameters, an inspection of the corresponding contributions (details see Appendix C) reveals that they are suppressed by a factor $|\mathbf{q}|^2$ by the same mechanism as the BCS logarithms. [Note that an analogous suppression occurs in the particle-hole channel, as can be seen from a power counting analysis of the Altshuler-Aronov correction to the conductivity: $\delta\sigma = \delta\langle jj\rangle/\omega \sim \omega^{(d-2)/2} \sim |\mathbf{q}|^{d-2}$. Thus, the correction to current-current correlation function $\langle jj\rangle$, which is proportional to the p-wave density, behaves as $\delta\langle jj\rangle \sim |\mathbf{q}|^d$.

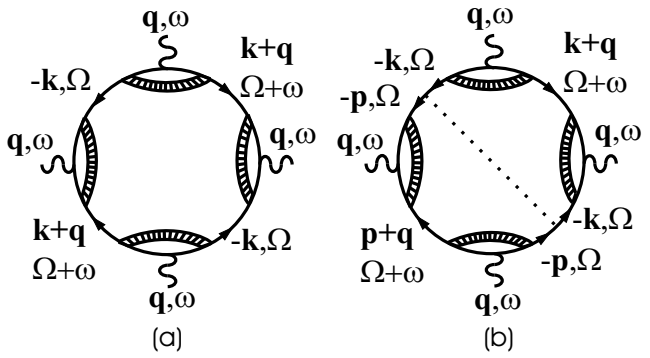

FIG. 2: Leading singular contributions to $\chi^{(4)}_{diag}$. After expansion in small q, the leading order terms of (a) and (b) cancel. (see Appendix D for details)

This means it has picked up an additional factor $|\mathbf{q}|^2$ compared to the zero angular momentum channel.]

As a result of these considerations we find that the leading singularities in $\chi^{(2)}$ are the Cooper channel logarithms. For $(|\mathbf{q}|, \omega) \to 0$, the leading behavior of $\chi^{(2)}$ is given by:

$$\chi^{(2)}_{ij}(\mathbf{q},\omega) = \frac{N_F}{3}[\ln(2\epsilon_F\tau) - |\omega|\tau - \frac{\ell^2|\mathbf{q}|^2}{10}]\delta_{ij} + \\ + \frac{N_F}{3} q_i q_j \ell^2 [-\frac{1}{5} + \frac{1}{3}\ln(\frac{\ell^2|\mathbf{q}|^2}{3})]. \tag{10}$$

where i, j are the order parameter component indices. The anisotropic $\mathbf{q}$-dependence in the last term reflects the spatial anisotropy of the p-wave order parameter.

We now turn our attention to the 4-point correlation function, $\chi^{(4)}$which can be split into a replica-diagonal part and a replica-off-diagonal part, $\chi^{(4)}_{\alpha\beta} = \delta_{\alpha\beta}\chi^{(4)}_{diag} + \chi^{(4)}_{off}$. A detailed discussion of our calculation is given in the Appendix D. We find that the leading contributions to $\chi^{(4)}_{diag}$ in the long-wavelength, low-frequency limit are coming from the diagrams shown in Fig. 2. While each of the two diagrams individually diverges for $(\mathbf{q}, \omega) \to 0$, their leading singularities cancel, and the remaining contribution is finite and proportional to $N_F\tau^2$. The leading contribution to the replica-off-diagonal part of $\chi^{(4)}$ is produced by the diagram shown on the Fig. 3. Note that also in this case there are several diagrams which individually diverge for $(\mathbf{q}, \omega) \to 0$.

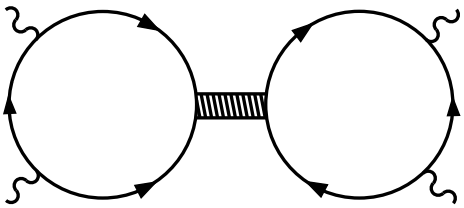

FIG. 3: The leading contribution to the $\chi^{(4)}_{off}$. (see Appendix D for details)

However, these divergences cancel each other. Thus, we finally obtain:

$$\chi^{(4)}_{diag} \;=\; A_d \; N_F \tau^2 \; F_d(\mathbf{q}_i, \omega_i) \;, \tag{11}$$

$$\chi^{(4)}_{off} \;=\; A_o \; (N_F^2/k_F^3) \; F_o(\mathbf{q}_i, \omega_i) \;, \tag{12}$$

where F_d and F_o are dimensionless functions with values between 0 and 1 and A_d and A_o are dimensionless prefactors of order one.

The results (11) and (12) have been obtained from low order perturbation theory. Within perturbation theory, it is non-trivial to prove the leading non-analyticity to all orders. Therefore we follow the guidance of the corresponding results for the s-wave case which have been rigorously established using Q-field-theory and renormalization group arguments.[28] (Corresponding rigorous results for finite angular momentum modes do not yet exist.) Indeed, simply correcting the s-wave results from Ref. 16 for the q-dependence of the renormalized vertex (see appendix A) leads to $\chi^{2n} \sim |\mathbf{q}|^{4-2n}$ in agreement with (11) and (12). Note that the singularity becomes stronger in the higher order anomalous density correlation functions, in agreement with general mode-coupling arguments.[17,29]

Inserting eqs. (10)-(12) into Eq. (7) we obtain the LGW functional up to quartic

order in Δ,

$$\begin{aligned}\Phi &= \sum_{\substack{q,\alpha\\ i}} \Delta^{*\alpha i}(q)(t+|\omega|+c_2|\mathbf{q}|^2)\Delta^{\alpha i}(q) \\ &+ \sum_{\substack{q,\alpha\\ ij}} \Delta^{*\alpha i}(q) c_l q_i q_j [-\frac{1}{5}+\frac{1}{3}\ln(\frac{1}{\ell^2|\mathbf{q}|^2})]\Delta^{\alpha j}(q) \\ &+ U\sum_{\alpha}\int d\mathbf{r}d\tau\ |\Delta^{\alpha}(\mathbf{r},\tau)|^4 \\ &- V\sum_{\alpha\beta}\int d\mathbf{r}d\tau d\tau'\ |\Delta^{\alpha}(\mathbf{r},\tau)|^2|\Delta^{\beta}(\mathbf{r},\tau')|^2\ . \end{aligned} \tag{13}$$

Here we have scaled the order parameter with $(\Gamma_t N_F \tau)^{1/2}$ and replaced the quartic coefficients by numbers which is sufficient for power counting purposes. The coefficients are:

$$t \sim \frac{1}{\tau}[\frac{1}{\tilde{\Gamma}} - \ln(2\epsilon_F\tau)], \tag{14a}$$

$$c_2 \sim c_l \sim \frac{\ell^2}{\tau}, \tag{14b}$$

$$U \sim \frac{1}{N_F}, \tag{14c}$$

$$V \sim \frac{1}{k_F^3\tau^2}, \tag{14d}$$

with $\tilde{\Gamma} = \Gamma_t N_F$ being a dimensionless measure of the interaction strength. The parameter t represents distance from the quantum critical point. Generically, $U > 0$, which leads to a second order transition.[30] This completes the derivation of the LGW theory.

C. Higher angular momentum channels

In this subsection we generalize the findings from the preceding subsections to pairings in higher angular momentum (L) channels. For angular momentum $L > 0$, the renormalized anomalous density vertex is proportional to $|\mathbf{q}|^L$ (see appendix A). The leading non-analyticity in the static anomalous density susceptibility $\chi_L^{(2)}(\mathbf{q})$ is given by the BCS logarithms in diagram 1b. They take the form

$$\delta\chi_L^{(2)}(\mathbf{q}) = \delta\langle\bar{n}_L^M(q)n_L^M(q)\rangle \sim |\mathbf{q}|^{2L}\log(1/|\mathbf{q}|), \tag{15}$$

i.e., they are suppressed by a factor $|\mathbf{q}|^{2L}$ compared to the s-wave case. Here $n_L^M(q) = \sum_k Y_L^M(\hat{\mathbf{e}}_\mathbf{k})\psi_\sigma(k+q/2)\psi_{\sigma'}(k-q/2)$ is a component of the anomalous density for angular momentum L. Note that for $L > 1$ the BCS logarithm is subleading compared to the regular $|\mathbf{q}|^2$ term coming from diagram 1a) while in the p-wave case the BCS logarithm provides the leading wave-number dependence in the LGW functional. The same mechanism also suppresses the interaction induced mode-coupling singularities related to corrections to scaling at the dirty Fermi liquid fixed point. An explicit calculation outlined in Appendix C shows that these mode coupling singularities behave at most like $|\mathbf{q}|^{2L}|\mathbf{q}|^{d-2}$ (d is the spatial dimensionality). Therefore they are sub-leading compared to the BCS logarithms for all $d > 2$. We now turn to the 4-point anomalous density correlation function $\chi_L^{(4)}$. Because of the momentum dependence of the renormalized anomalous density vertex, $\chi_L^{(4)}$ picks up an extra power of $|\mathbf{q}|^{4L}$ compared to the s-wave case. More generally, any $2n$-point anomalous density correlation function $\chi^{(2n)}$ picks up an extra power of $|\mathbf{q}|^{2nL}$ compared to the s-wave case, i.e. $\chi^{(2n)} \sim |\mathbf{q}|^{4+(2L-4)n}$. Therefore their singular contributions are demoted to sub-leading order and do not play a role for the critical behavior.

As a result, the leading terms in the LGW functional for d-wave and higher order parameter angular momentum take the same form (13) as in the p-wave case except for the missing logarithmic wavenumber dependence in the Gaussian part.[19] In summary, the analysis shows that mode-coupling singularities in principle arise for all order parameter angular momenta, but they are increasingly suppressed in higher angular momentum channels. For $L \geq 2$ they cease to influence the leading behavior for small $\mathbf{q}$ and ω.

III. RENORMALIZATION GROUP ANALYSIS

In this section we analyze the LGW theory, eqs. (13) and (14), by means of the renormalization group. There is a Gaussian fixed point with mean-field static exponents $\nu = 1/2$, $\gamma = 1$, $\eta = 0$, and a dynamical exponent of $z = 2$. In the p-wave case there are logarithmic corrections to the mean-field behavior in all dimensions. In order to check the stability of the Gaussian fixed point we investigate the impor-

tance of quantum and disorder fluctuations. The scale dimensions of U and V at the Gaussian fixed point can be calculated by power counting. We obtain $[U] = 2 - d$ and $[V] = 4 - d$. Thus, the conventional fluctuation term (the U term) is renormalization group irrelevant for $d > 2$, but the disorder term (the replica-off-diagonal quartic V term) is relevant for $d < 4$. In three dimensions the Gaussian fixed point is unstable with respect to the disorder term, and thus the calculation of loops is necessary to determine the asymptotic critical behavior. This includes the possibility of replica-symmetry breaking in the replica-off-diagonal quartic term.

Rather than carrying out this program explicitly, we use the analogy between our transition and the disordered itinerant antiferromagnetic quantum phase transition to discuss the asymptotic critical behavior: Except for the logarithmic corrections, the LGW theory, eq. (13) is identical to that of a disordered itinerant antiferromagnet. This transition has been investigated in great detail in recent years.[31–33] By taking into account rare disorder fluctuations it was found that there is no critical fixed point in the perturbative region of parameter space, and the asymptotic critical behavior is characterized by run-away flow toward large disorder (Fig. 4) rendering the perturbation expansion unjustified. The physical implications of this runaway flow are not fully understood so far. Possible scenarios include a non-perturbative fixed point with conventional (power-law) scaling, an infinite randomness fixed point (relative magnitude of inhomogeneities increases without limit under coarse graining), resulting in activated scaling, or a complete destruction of a sharp phase transition. Thus, from the analogy with the quantum phase transition in itinerant antiferromagnets we conclude that the asymptotic critical behavior of our theory is unconventional, and, at present, unknown.

However, in many relevant experimental systems the bare disorder is actually very small. Thus, one may ask at what length scale disorder effects start to play a role. The crossover scale between the Gaussian and the asymptotic critical behavior can be determined from the condition that the renormalized dimensionless disorder coupling constant

$$V_R = \frac{V}{\sqrt{t c_2^3}} \approx 1. \tag{16}$$

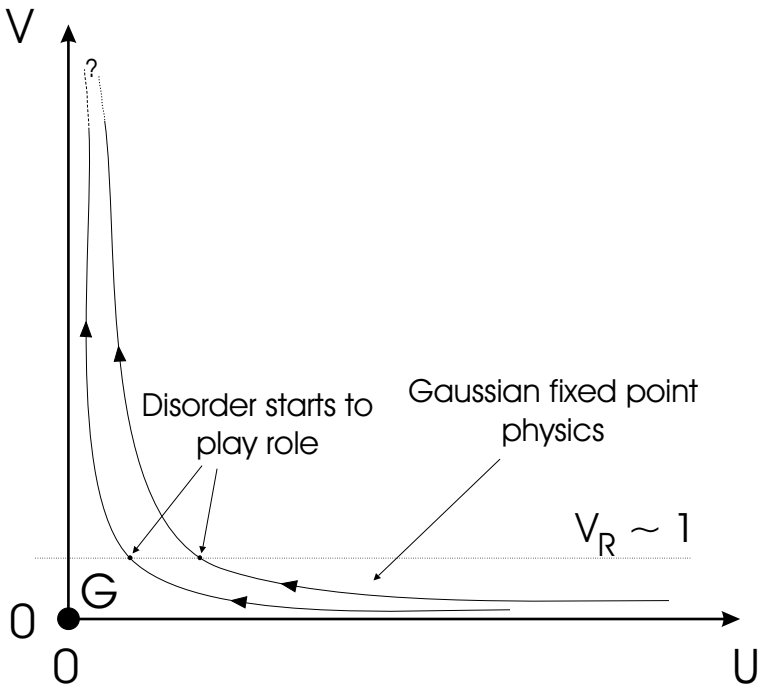

FIG. 4: Schematic flow diagram on the critical surface. The Gaussian fixed point (G) is unstable; the renormalization flow goes toward large values of the disorder V. For weak bare disorder, the flow stays close to the $U-$axis until it almost reaches the Gaussian fixed point before crossing over (black dots) to the asymptotic destination. The dashed line separates the region described by the Gaussian fixed point physics from the strong disorder region.

Now, the quantum phase transition occurs at $t = 0$ in eq. (14a) which leads to

$$\frac{1}{\tilde{\Gamma}_c} = \ln(2\epsilon_F \tau), \tag{17}$$

with $\tilde{\Gamma}_c$ being the dimensionless critical coupling. Thus, the quantum phase transition occurs at an exponentially small bare disorder strength which implies that $V_R \sim 1$ requires an exponentially large length scale. By expressing eqs. (14a), (14b) and (14d) in terms of $\tilde{\Gamma}$ and $\tilde{\Gamma}_c$ and inserting the obtained expressions into eq. (16) we find a Ginzburg type criterion:

$$\frac{|\tilde{\Gamma} - \tilde{\Gamma}_c|}{\tilde{\Gamma}_c} < \tilde{\Gamma}_c^3 \ \exp\left[-\frac{1}{\tilde{\Gamma}_c}\right] \ . \tag{18}$$

Therefore, disorder effects become important only inside an exponentially narrow region surrounding $\tilde{\Gamma}_c$. This asymptotic critical region is preempted by a wide Gaussian

crossover region (region below dashed dashed line on Fig. 4) with mean-field critical behavior. For p-wave symmetry there are logarithmic correction to the power-law scaling whose the $|\mathbf{q}|$ dependence reflects the underlying p-wave symmetry of the order parameter.

IV. CONCLUSIONS

In this paper we have studied the quantum phase transition from a dirty metal to an exotic superconductor. We have started from a microscopic action of disordered interacting electrons. We have derived the Landau-Ginzburg-Wilson theory for this quantum phase transition which proved to be equivalent (up to logarithmic corrections in the Gaussian part in the case of p-wave pairing) to the extensively studied LGW theory of the dirty itinerant quantum antiferromagnetic phase transition. A renormalization group analysis of the LGW theory yielded runaway flow toward large disorder. As a result, the asymptotic fate of the quantum phase transition is unknown. However, we could derive a Ginzburg-type criterion for the importance of the disorder fluctuations. For weak bare disorder, as is realized in many experimental systems, the true asymptotic behavior is observed only exponentially close to the quantum critical point. It is preempted by a wide region with mean-field behavior (and logarithmic corrections for p-wave pairing). In this last section we want to analyze our results from a general mode-coupling point of view and also discuss experiments.

In deriving the LGW functional we have paid particular attention to the coupling between the order parameter and additional soft modes. We have shown that mode coupling effects are indeed present in all angular momentum channels, but they are increasingly suppressed in higher angular momentum channels: In the static order parameter susceptibility the singular terms pick up an extra power of $|\mathbf{q}|^{2L}$. This suppression can be understood as follows: In the presence of non-magnetic quenched disorder, the dominant electronic soft modes are those that involve fluctuations of the number density, spin density, or anomalous density in the zero angular momentum channel[28] while the corresponding densities in higher angular momentum channels are not soft. Since the different angular momentum modes are orthogonal at zero

wavenumber, the coupling between a finite angular momentum order parameter and the zero angular momentum soft modes must involve powers of the wave number $|\mathbf{q}|$.

These arguments suggest a very general difference between the mode-coupling effects in clean and in dirty electronic systems. While the only soft modes in the dirty case are in the zero angular momentum channel, in a clean system the charge, spin, and anomalous density fluctuations in all angular momentum channels are soft (corresponding to an infinite number of Fermi liquid parameters). Therefore, one expects the mode coupling singularities in a clean system *not* to be suppressed by a higher order parameter angular momentum. This is known to be true for the Cooper channel logarithmic singularities which do not pick up an extra $|\mathbf{q}|^{2L}$ in clean electronic systems. A systematic investigation of this question will be published elsewhere.[34]

The explicit calculations in this paper were for a superconducting quantum phase transition in a paramagnetic system. We now discuss to what extend the results change if the transition happens in a ferromagnetic system. Let us assume the magnetization being in z direction. Obviously, not all possible order parameter components are equivalent. Specifically, the symmetric triplet $1/\sqrt{2}(\uparrow\downarrow + \downarrow\uparrow)$ (for p or f-wave pairing) as well as the singlet $1/\sqrt{2}(\uparrow\downarrow - \downarrow\uparrow)$ (for s and d-wave pairing) are suppressed because the exchange gap cuts off the Cooper-channel singularities. In contrast, for equal spin pairing ($\uparrow\uparrow$ and $\downarrow\downarrow$), the leading behavior is the same as discussed in Sections II and III of this paper.

Now we turn our attention to the possible experimental verification of our theory. A possible candidate for a study of the p-wave superconducting quantum phase transition are the recently discovered ferromagnetic superconductors UGe_2[5] or $ZrZn_2$.[6] For these systems, a likely mechanism for superconductivity is p-wave triplet pairing mediated by magnetic fluctuations due to the vicinity to a magnetic quantum critical point,[20] although this has not yet been established beyond doubt. In $ZrZn_2$ the vanishing of superconductivity as a function of disorder has actually already been observed.[6] A systematic study of this transition would therefore be very interesting.[35]

Acknowledgments

We thank D. Belitz, I. Herbut, T. R. Kirkpatrick, and S. Sessions for helpful discussions. We acknowledge support from the German Research Foundation and from the University of Missouri Research Board. Parts of this work have been performed at the University of Oxford (England) and at the Aspen Center for Physics.

APPENDIX A: RENORMALIZED VERTEX

In this Appendix we derive the expression for the particle-particle ladder $W_R(\mathbf{q}, \Omega, \omega)$ in $3d$ in the small $\mathbf{q}, \omega$ limit. We then use this result to calculate the renormalized anomalous density vertex. The particle-particle ladder is defined by the diagrammatic equation shown on Fig. 5. Each Green's function pair and the corresponding impurity line contribute

$$L(\mathbf{q}, \Omega, \omega) = W \sum_{\mathbf{k}} G(\mathbf{k}+\mathbf{q}, \Omega+\omega) G(-\mathbf{k}, -\Omega), \tag{A1}$$

where Green's function G is given by eq. (8) (spin indices are suppressed). After a straightforward calculation we get:

$$L(\mathbf{q}, \Omega, \omega) = \frac{W}{\pi} \frac{m^2}{|\mathbf{q}|} \Theta(\Omega(\Omega+\omega)) \arctan \frac{\ell|\mathbf{q}|}{|2\Omega+\omega|\tau+1}, \tag{A2}$$

with $\Theta(x)$ being Heavyside step function. Inserting this into the equation for the ladder in Fig. 5 leads to:

$$W_R(\mathbf{q}, \Omega, \omega) = \frac{W}{1 - \frac{W}{\pi} \frac{m^2}{|\mathbf{q}|} \Theta(\Omega(\Omega+\omega)) \arctan \frac{\ell|\mathbf{q}|}{|2\Omega+\omega|\tau+1}}. \tag{A3}$$

Expanding eq. (A3) in small $\mathbf{q}$ and ω completes the derivation of eq. (9).

Now we turn our attention to the calculation of the renormalized anomalous density vertex for arbitrary angular momentum L (Fig. 6). In the parametrization shown in the figure, the vertex becomes:

$$\Gamma_L^M(\mathbf{q}, \Omega, \omega) = \sum_{\mathbf{k}} Y_L^M(\hat{\mathbf{e}}_{\mathbf{k}}) W_R G(\mathbf{k}+\mathbf{q}, \Omega+\omega) G(-\mathbf{k}, -\Omega) \ . \tag{A4}$$

We have chosen a coordinate system in which the quantization axis of the orbital part of the order parameter is $\hat{\mathbf{e}}_\Delta = \hat{\mathbf{e}}_z$. In this coordinate system, the directions

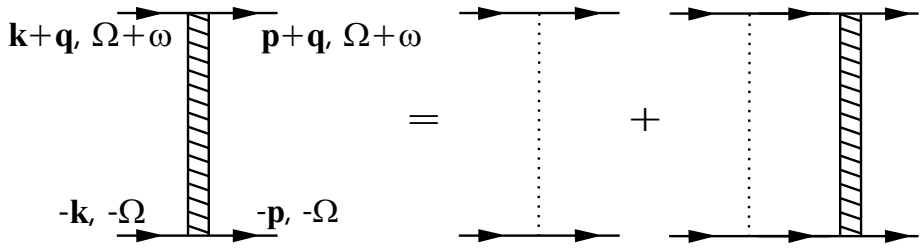

FIG. 5: Definition of the particle-particle ladder.

of the unit vectors $\hat{\mathbf{e}}_\mathbf{k}$ and $\hat{\mathbf{e}}_\mathbf{q}$ are given by the angles θ, ϕ and α, β, respectively. $Y_L^M(\hat{\mathbf{e}}_\mathbf{k}) = Y_L^M(\theta, \phi)$ is a spherical harmonic. In the subsequent calculation we assume $\mathbf{q}$ and ω are small and use eq. (9) for the ladder W_R. An expansion of $G(\mathbf{k}+\mathbf{q}, \Omega+\omega)$ in powers of $\mathbf{q}$ gives:

$$G(\mathbf{k}+\mathbf{q}, \Omega+\omega) = \sum_{L=0}^{\infty} (-1)^L (k_F|\mathbf{q}|)^L \cos^L(\chi) G^{L+1}(\mathbf{k}, \Omega), \tag{A5}$$

with χ being angle between $\mathbf{k}$ and $\mathbf{q}$. Further we can write

$$\cos^L(\chi) = \frac{2^L (L!)^2}{(2L)!} P_L(\cos(\chi)) + \sum_{N=0}^{L-1} A_N P_N(\cos(\chi)), \tag{A6}$$

where P_L and P_N are Legendre polynomials and A_N are, for current analysis, unimportant constants. We now use

$$P_L(\cos(\chi)) = \frac{4\pi}{2L+1} \sum_{M'=-L}^{L} \bar{Y}_L^{M'}(\theta, \phi) Y_L^{M'}(\alpha, \beta) \tag{A7}$$

and insert the expansion (A5) it into eq. (A4). Due to the orthogonality of the spherical harmonics with different L, only the first term in (A6) contributes:

$$\begin{aligned}
&\Gamma_L^M(\mathbf{q}, \Omega, \omega) = \\
&W_R \frac{2^L (L!)^2}{(2L)!} \sum_{L'=0}^{\infty} (-1)^{L'} \frac{4\pi}{2L'+1} (k_F|\mathbf{q}|)^{L'} \times \\
&\sum_{M'} \int\int d\phi \sin\theta d\theta Y_L^M(\theta, \phi) \bar{Y}_{L'}^{M'}(\theta, \phi) Y_{L'}^{M'}(\alpha, \beta) \times \\
&\int_0^\infty k^2 dk G^{L'+1}(|\mathbf{k}|, \Omega+\omega) G(-|\mathbf{k}|, -\Omega).
\end{aligned} \tag{A8}$$

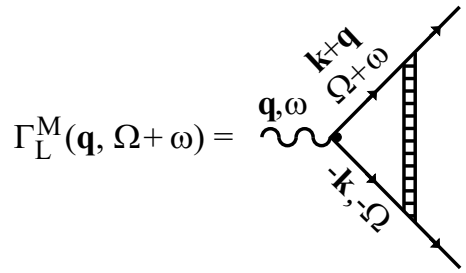

FIG. 6: Renormalized vertex.

After using the orthogonality relation of the spherical harmonics and calculating the remaining k integral we get final expression for the renormalized vertex:

$$\Gamma^M_L(\mathbf{q}, \Omega, \omega) = \frac{2^L (L!)^2}{(2L)!} \frac{(-\imath|\mathbf{q}|\ell)^L}{2L+1} Y^M_L(\hat{\mathbf{e}}_\mathbf{q}) W_R(\mathbf{q}, \Omega, \omega). \tag{A9}$$

APPENDIX B: TWO-POINT LGW VERTEX

In this Appendix we sketch the derivation of the expression (10) for anomalous density susceptibility $\chi^{(2)}$ in $3d$. In a suitable parametrization and for p-wave pairing, diagram Fig. 1a can be written as

$$D^a_{ij}(\mathbf{q}, \omega) = T \sum_{\mathbf{k}, \Omega} Y^i_1(\hat{\mathbf{e}}_\mathbf{k}) Y^j_1(\hat{\mathbf{e}}_\mathbf{k}) G(\mathbf{k}+\mathbf{q}, \Omega+\omega) G(-\mathbf{k}, -\Omega), \tag{B1}$$

with i, j being the order parameter component indices and $\mathbf{q}, \omega$ the external momentum and frequency. A straightforward calculation leads to:

$$D^a_{ij} = \frac{N_F}{3} \left[\log(2\epsilon_F \tau) - |\omega|\tau - \frac{1}{10} \ell^2 |\mathbf{q}|^2 \right] \delta_{ij} - \frac{N_F}{15} \ell^2 q_i q_j. \tag{B2}$$

$\ell = k_F \tau / m$ is elastic mean free path and N_F the density of states at the Fermi level.

The diagram in Fig. 1b in the parametrization shown, reads:

$$\begin{aligned} D^b_{ij} \quad &= \sum_{\substack{\mathbf{k}, \mathbf{p} \\ \Omega}} Y^i_1(\hat{\mathbf{e}}_\mathbf{k}) G(\mathbf{k}+\mathbf{q}, \Omega+\omega) G(-\mathbf{k}, -\Omega) \times \\ &\quad W_R(\mathbf{q}, \Omega, \omega) Y^j_1(\hat{\mathbf{e}}_\mathbf{p}) G(\mathbf{p}+\mathbf{q}, \Omega+\omega) G(-\mathbf{p}, -\Omega), \end{aligned} \tag{B3}$$

with W_R the particle-particle ladder, eq. (9). It is immediately clear that the sums over $\mathbf{k}$ and $\mathbf{p}$ are independent. After carrying out the momentum and frequency sums,

and expanding the final results in small $\mathbf{q}, \omega$ one gets:

$$D^b_{ij} = \frac{N_F}{9}\ell^2 q_i q_j \log(\omega\tau + \frac{\ell^2|\mathbf{q}|^2}{3}). \tag{B4}$$

Adding eqs. (B2) and (B4) completes derivation of eq. (10). For general angular momentum L, a straightforward generalization of this calculation using the renormalized anomalous density vertex (A9) shows that the BCS logarithm in D^b picks up an extra factor $|\mathbf{q}|^{2L}$ compared to the s-wave case.

APPENDIX C: INTERACTION EFFECTS

In this Appendix we analyze the leading corrections to $\chi^{(2)}$ due to the interactions S_{int} in the reference ensemble S_0. They can be understood as corrections to scaling at the dirty Fermi liquid fixed point[28] and are particle-particle analogs of the well known Altshuler-Aronov corrections to density of states and conductivity.[12] We first consider a paramagnetic reference ensemble, differences for a ferromagnetic reference ensemble will be discussed subsequently.

To first order in the interactions, the relevant diagrams are those in Fig. 7 and their counterparts with bare external vertices. We denote these diagrams by $a^{(r)} \dots e^{(r)}$ and $a^{(b)} \dots e^{(b)}$, respectively. The wiggly line represents the interaction which is assumed to be short ranged and can thus be approximated by a number $\Gamma_{\sigma\sigma'}$ (where σ, σ' denote the spin at the two ends of the interaction line). The renormalized interaction vertex is shown in Fig. 8. Note that the impurity ladder in this figure is a particle-hole ladder given by familiar expression:

$$\tilde{W}_R(\mathbf{Q}, \epsilon) = W \begin{cases} 1 & \text{if } \Omega(\Omega+\epsilon) > 0 \\ \frac{1}{|\epsilon|\tau + \ell^2|\mathbf{Q}|^2/d} & \text{if } \Omega(\Omega+\epsilon) < 0 \end{cases}, \tag{C1}$$

with $d = 3$ in the case of interest of this discussion. The contributions to $\chi^{(2)}$ of the diagrams $a^{(r)} \dots e^{(r)}$ and $a^{(b)} \dots e^{(b)}$ can be further subdivided according to the signs of the external and internal frequencies, using the notation $a^{(b)}_{++}$ for the contribution to diagram $a^{(b)}$ coming from $\Omega > 0$ and $\Omega + \omega > 0$.

Particular attention has to be paid to the contributions $a^{(b)}$, $b^{(b)}$ and $c^{(b)}$. In these contributions the spherical harmonics in the two external vertices are not independent.

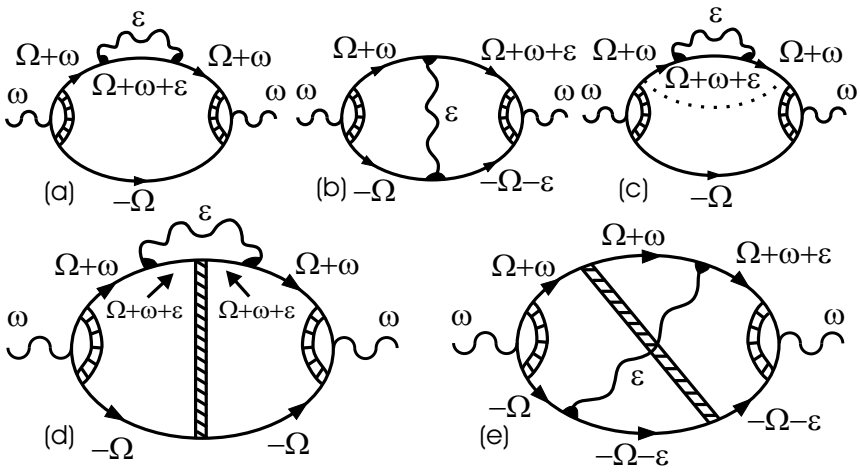

FIG. 7: Diagrams arising in the first order perturbation theory in interaction of the reference ensemble S_0, and produce non-analytic, $|\mathbf{q}|^{2L}|\mathbf{q}|^{d-2}$, term, which is a consequence of the mode-coupling effects.

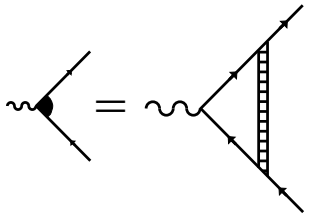

FIG. 8: Renormalized interaction vertex, the impurity ladder is a particle-hole ladder.

Consequently, the mechanism shown in appendix A by which the angular integrations produce extra factors of $|\mathbf{q}|$ is not operative here. Therefore, the contributions $a^{(b)}$, $b^{(b)}$ and $c^{(b)}$ can potentially produce stronger terms than $|\mathbf{q}|^{2L}|\mathbf{q}|^{d-2}$. However, it turns out that these contributions do not produce any non-analytic terms and only contribute to the regular terms. Here we sketch the corresponding calculation for $a^{(b)}_{++}$. In the shown parametrization we obtain:

$$a^{(b)}_{++} = \sum_{\substack{\mathbf{k},\Omega \\ \mathbf{Q},\epsilon}} \Gamma^2_{\sigma\sigma} \tilde{W}_R(\mathbf{Q},\epsilon)^2 G^2(\mathbf{k}+\mathbf{q},\Omega+\omega) \times G(\mathbf{k}+\mathbf{Q}+\mathbf{q},\Omega+\omega+\epsilon) G(-\mathbf{k},-\Omega) \; . \tag{C2}$$

If we now expand $G(\mathbf{k}+\mathbf{q},\Omega+\omega)$ and $G(\mathbf{k}+\mathbf{Q}+\mathbf{q},\Omega+\omega+\epsilon)$ in powers of $|\mathbf{q}|$ (see also Eq. (A5)) and calculate remaining integrals we readily see that all coefficients

in such an expansion are finite, and therefore the expansion itself is valid. Thus, the term $a^{(b)}_{++}$ is analytic.

Let us now look at the remaining contributions. The leading singularities are produced by the contributions with the highest number of active (i.e., retarded-advanced) ladders which is four. These are $a^{(r)}_{++}$ to $e^{(r)}_{++}$ and $a^{(r)}_{--}$ to $e^{(r)}_{--}$. Using the abbreviation

$$f_{\sigma\sigma'}(\epsilon) = \Gamma_{\sigma\sigma'} \int \frac{d^3\mathbf{Q}}{(2\pi)^3} \tilde{W}_R^2 = \int \frac{d^3\mathbf{Q}}{(2\pi)^3} \frac{\Gamma_{\sigma\sigma'}}{(|\epsilon|\tau + \ell^2|\mathbf{Q}|^2/3)^2}, \tag{C3}$$

for zero external frequency, the term $a^{(r)}_{++}$ can be written as

$$a^{(r)}_{++} = \int_{\omega=0}^{\infty} d\Omega \int_{\Omega}^{1/\tau} d\epsilon f_{\sigma\sigma}(\epsilon) \Gamma_L^M(\mathbf{q}, \Omega, \omega)^2 \sum_{\mathbf{k}} G_+^2 G_-^2, \tag{C4}$$

Note that to leading order, the $|\mathbf{q}|$ and $|\mathbf{Q}|$ dependencies in the Born approximation Green's functions can be neglected since k-integrals over these Green's functions have finite values proportional to powers of τ for $|\mathbf{Q}|$,$|\mathbf{q}| = 0$. Therefore in further we'll suppress all arguments of the Green's function and use notation $G_{+(-)}$ depending on the sign of the frequency.

A direct evaluation of the integrals shows that $a^{(r)}_{++}$ behaves like $|\mathbf{q}|^{(2L)}|\mathbf{q}|^{d-4}$. Analogously, it can be shown that all of the terms $a^{(r)}_{++}$-$e^{(r)}_{--}$ have the same q dependence. However, their leading singularities identically cancel among each other. The remaining singularity is at most $|\mathbf{q}|^{2L}|\mathbf{q}|^{d-2}$. This cancellation remains correct if we permit $\Gamma_{\uparrow\uparrow} \neq \Gamma_{\uparrow\downarrow}$ since the corresponding contributions cancel separately. To show this cancellation we note that for $\omega = 0$ the $(++)$ and $(--)$ components of each diagram are identical. They can be written as (note the different spin structures):

$$a^{(r)} = \int_0^{\infty} d\Omega \int_{\Omega}^{1/\tau} d\epsilon f_{\sigma\sigma}(\epsilon) \Gamma_L^M(\mathbf{q}, \Omega, \omega)^2 P, \tag{C5a}$$

$$b^{(r)} = \int_0^{\infty} d\Omega \int_{\Omega}^{1/\tau} d\epsilon f_{\sigma\sigma'}(\epsilon) \Gamma_L^M(\mathbf{q}, \Omega, \omega)^2 R, \tag{C5b}$$

$$c^{(r)} = \int_0^{\infty} d\Omega \int_{\Omega}^{1/\tau} d\epsilon f_{\sigma\sigma}(\epsilon) \Gamma_L^M(\mathbf{q}, \Omega, \omega)^2 S, \tag{C5c}$$

$$d^{(r)} = \int_0^{\infty} d\Omega \int_{\Omega}^{1/\tau} d\epsilon f_{\sigma\sigma}(\epsilon) \Gamma_L^M(\mathbf{q}, \Omega, \omega)^2 T, \tag{C5d}$$

$$e^{(r)} = \int_0^{\infty} d\Omega \int_{\Omega}^{1/\tau} d\epsilon f_{\sigma\sigma'}(\epsilon) \Gamma_L^M(\mathbf{q}, \Omega, \omega)^2 U, \tag{C5e}$$

where:

$$P \;=\; R = \sum_{\mathbf{k}} G_+^2 G_-^2 = \frac{2k_F}{\pi}\tau^3, \tag{C6}$$

$$S \;=\; W(\sum_{\mathbf{k}} G_+^2 G_-)^2 = -\frac{k_F}{\pi}\tau^3, \tag{C7}$$

$$T \;=\; U = W(\sum_{\mathbf{k}} G_+ G_-^2)^2 = -\frac{k_F}{\pi}\tau^3. \tag{C8}$$

It is straightforward to see that contributions for $\sigma\sigma$ and for $\sigma\sigma'$ coming from eqs. (C5), multiplied with appropriate combinatorial factors, separately add up to zero.

A similar analysis of the three-ladder terms $d_{-+}^{(b)}$ and $e_{-+}^{(b)}$ shows that they produce singularities of at most $|\mathbf{q}|^{2L}|\mathbf{q}|^{d-2}$. All other terms come with higher powers of $|\mathbf{q}|$ and are therefore subleading. Thus, we have shown that the interaction corrections produce singularities of at most of the order $|\mathbf{q}|^{2L}|\mathbf{q}|^{d-2}$ which means they are suppressed by a factor $|\mathbf{q}|^{2L}$ compared to the zero angular momentum case.[11]

The above conclusion is easily generalized to ferromagnetic reference ensembles: If the magnetization is in z-direction, the $\uparrow\uparrow$ and $\downarrow\downarrow$ components of the order parameter have the same type of singularity as discussed above, while the leading singularities in the $\uparrow\downarrow$ components are cut-off by the exchange gap.

APPENDIX D: 4-POINT VERTICES

In this Appendix we present details of calculation of four-point susceptibility $\chi^{(4)}$ in $3d$, eqs. (11) and (12). We start with replica diagonal part, $\chi^{(4)}_{diag}$ which is calculated from the diagrams shown on the Fig. 2. The most singular contributions are produced if the frequencies structure permits all four external vertices to be renormalized by an active (retarded-advanced) ladder (4-ladder diagrams). Expressing the first diagram (Fig. 2a) in terms of integrals we get:

$$D_a = T\sum_{\mathbf{k},\Omega}[\Gamma_1^0(\mathbf{q},\omega;\Omega)]^4 G^2(\mathbf{k}+\mathbf{q},\Omega+\omega)G^2(-\mathbf{k},-\Omega). \tag{D1}$$

Here we restrict ourselves to one particular angular order parameter component corresponding to the spherical harmonics Y_1^0, and Γ_1^0 is the corresponding renormalized

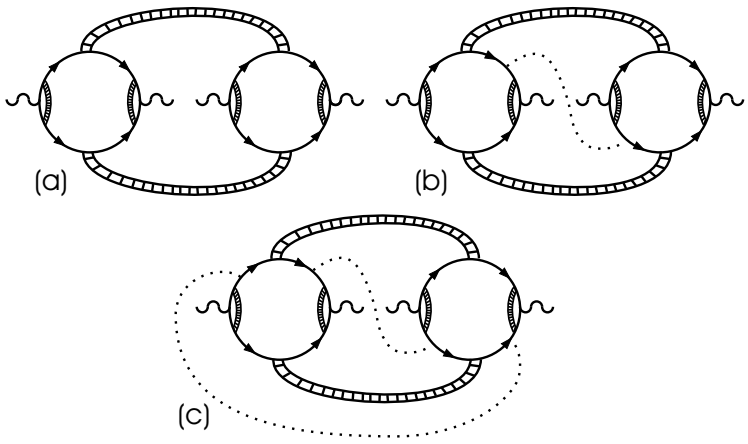

FIG. 9: Diagrams contributing to the $\chi^{(4)}_{off}$. All four vertices are renormalized, with two extra active particle-particle ladders connecting two fermionic loops. The zeroth order terms in small $\mathbf{q}$ and ω of these diagrams cancel.

vertex (A9). The $\mathbf{k}$-sum can be immediately carried out; after expanding in small wave numbers and frequencies we obtain:

$$D_a = \frac{2\ell^5\tau^2|\mathbf{q}|^4\cos^4(\alpha)}{81\pi}\sum_{\Omega}\frac{\Theta(\Omega(\Omega+\omega))}{(|2\Omega+\omega|\tau+\frac{\ell^2|\mathbf{q}|^2}{3})^4}\times \\ \times(1-9|2\Omega+\omega|\tau-\ell^2|\mathbf{q}|^2). \tag{D2}$$

An analogous calculation for diagram 2b) gives (the frequency constraint requires the extra impurity line to act as a single impurity line rather than an active ladder):

$$D_b = -\frac{\ell^5\tau^2|\mathbf{q}|^4\cos^4(\alpha)}{81\pi}\sum_{\Omega}\frac{\Theta(\Omega(\Omega+\omega))}{(|2\Omega+\omega|\tau+\frac{\ell^2|\mathbf{q}|^2}{3})^4}\times \\ \times(1-12|2\Omega+\omega|\tau-2\ell^2|\mathbf{q}|^2). \tag{D3}$$

Each of these two diagrams individually has an divergence $\sim 1/|\mathbf{q}|^2$. However, because the relative combinational factor of D_b is 2, the divergent contributions cancel, rendering the final value for $\chi^{(4)}_{diag}$ finite (Eq. (11)).

Similar cancellations among individually diverging diagrams take place in the replica off-diagonal case, with the strongest singularities coming from diagrams with the largest number of active ladders. A set of such diagrams is shown on Fig. 9. Here, at most six ladders can be active, leading to an infrared singularity in each of the diagrams of the form $1/|\mathbf{q}|$. Similar calculations to the ones carried out above reveal

that the singular contributions of diagrams (a), (b), and (c) canceled each other. The remaining contribution is finite and can be estimated from the simple diagram Fig. 3.

We emphasize once more that all the results for the singularities in the anomalous density correlation functions in the Appendices A to D have been obtained in low-order perturbation theory. Within perturbation theory one cannot prove that the terms obtained indeed represent the leading singularities to all orders. We are nonetheless confident that we indeed identified the leading terms, because in the s-wave case we reproduce the known rigorous results from Q-field theory.[16,28]

---

[1] J. A. Hertz, Phys. Rev. B **14**,1976 (1165).

[2] S. L. Sondhi, S. M. Girvin, J. P. Carini and D. Shahar, Rev. Mod. Phys. **69**,315 (1997).

[3] S. Sachdev, *Quantum Phase Transitions* (Cambridge University Press, Cambridge, 1999).

[4] See, e.g., P. Coleman, B. Maple and A. Millis, *Proccedings of the Institute for Theoretical Physics Conference on Non-Fermi Liquid Behavior in Metals*, J. Phys. Cond. Matt. **8** (1996).

[5] S. S. Saxena et al., Nature **406**, 587 (2000).

[6] C. Pfleiderer et al., Nature **412**, 58 (2001).

[7] J. R. Dorfman, T. R. Kirkpatrick and J. V. Sengers, Ann. Rev. Phys. Chem. **A45**, 213 (1994); B. M. Law and J. C. Nieuwoudt, Phys. Rev. A **40**, 3880 (1989); S. Nagel, Rev. Mod. Phys. **64**, 321 (1992)

[8] D. Belitz, T. R. Kirkpatrick and T. Vojta, Phys. Rev. B **55**, 9452 (1997).

[9] G. Y. Chitov and A. J. Millis, Phys. Rev. B **64**, 054414 (2001).

[10] A. V. Chubukov and D. L. Maslov, cond-mat/0304381.

[11] T. R. Kirkpatrick and D. Belitz, Phys. Rev. B **53**, 14364 (1996).

[12] B. L. Altshuler and A. G. Aronov, Zh. Eksp. Teoret. Fiz. **77**, 2028 (1979) [Sov. Phys. JETP **50**, 968 (1979)]

[13] T. Vojta, D. Belitz, R. Narayanan and T. R. Kirkpatrick, Z. Phys. B **103**, 451 (1997);

D. Belitz, T. R. Kirkpatrick and T. Vojta, Phys. Rev. Lett. **82**, 4707 (1999).

[14] D. Belitz and T. R. Kirkpatrick, cond-mat/0207470.

[15] D. Belitz, T. R. Kirkpatrick, M. T. Mercaldo and S. L. Sessions, Phys. Rev. B **63**, 174427 (2001).

[16] T. R. Kirkpatrick and D. Belitz, Phys. Rev. Lett. **79**, 3042 (1997).

[17] D. Belitz, T. R. Kirkpatrick and T. Vojta, Phys. Rev. B **65**, 165112 (2002).

[18] For finite-q order parameters, the coupling to fermionic modes is generically weaker, and Hertz' scheme works, at least in 3d.[36]

[19] I.F. Herbut, Phys. Rev. Lett. **85**, 1532 (2000).

[20] T. R. Kirkpatrick, D. Belitz and T. Vojta, R. Narayanan, Phys. Rev. Lett. **87**, 127003 (2001).

[21] J. Hubbard, Phys. Rev. Lett. **3**, 77 (1959).

[22] R. L. Stratonovich, Dokl. Akad. Nauk SSSR **115**, 1907 (1959) [Sov. Phys. Dokl. **2**, 416 (1959)].

[23] S. F. Edwards and P. W. Anderson, J. Phys. F **5**, 965 (1975).

[24] A. A. Abrikosov and L. P. Gorkov, Zh. Eksp. Teoret. Fiz. **39**, 1781 (1960) [Sov. Phys. JETP **12**, 1243 (1961)].

[25] A. I. Larkin, Sov. Phys. JETP Lett. **2**, 130 (1965).

[26] P. W. Anderson, J. Phys. Chem. Solids **11**, 26 (1959).

[27] H. Adachi and R. Ikeda, J. Phys. Soc. Japan **70**, 2848 (2001).

[28] D. Belitz and T. R. Kirkpatrick, Rev. Mod. Phys. **66**, 261 (1994); Phys. Rev. B **56**, 6513 (1997).

[29] Note that the 6th and higher order terms in the LGW functional are renormalization-group irrelevant even though their coefficients are singular.

[30] A. V. Chubukov, A. M. Finkelstein, R. Haslinger and D. K. Morr, Phys. Rev. Lett. **90**, 077002 (2002), have suggested that the thermal triplet superconducting transition near a ferromagnetic quantum critical point is of first order due to the interplay between spin-fluctuations and pairing.

[31] D. Boyanovsky and J. L. Cardy, Phys. Rev. B **26**, 154 (1982).

[32] T. R. Kirkpatrick and D. Belitz, Phys. Rev. Lett **76**, 2571 (1996); **78**, 1197 (1997).

[33] R. Narayanan, T. Vojta, D. Belitz and T. R. Kirkpatrick, Phys. Rev. Lett. **82**, 5132 (1999); Phys. Rev. B **60**, 10150 (1999).

[34] R. Sknepnek, T. Vojta and R. Narayanan, unpublished.

[35] Directly at the magnetic quantum critical point our theory may not be applicable because of strong non-Fermi liquid effects and the interplay between spin-fluctuations and pairing[30]. However, away from the magnetic quantum critical point the low-temperature normal state is a Fermi liquid, and our theory should apply.

[36] A. Abanov and A. V. Chubukov, Phys. Rev. Lett. **84**, 5608 (2000) argued that in 2D, the antiferromagnetic order parameter couples sufficiently strongly to soft modes to influence the critical behavior.

4. SMEARED PHASE TRANSITION IN A THREE-DIMENSIONAL ISING MODEL WITH PLANAR DEFECTS: MONTE-CARLO SIMULATIONS

Rastko Sknepnek and Thomas Vojta

Department of Physics, University of Missouri - Rolla, Rolla, MO, 65409

Abstract

We present results of large-scale Monte Carlo simulations for a three-dimensional Ising model with short range interactions and planar defects, i.e., disorder perfectly correlated in two dimensions. We show that the phase transition in this system is smeared, i.e., there is no single critical temperature, but different parts of the system order at different temperatures. This is caused by effects similar to but stronger than Griffiths phenomena. In an infinite-size sample there is an exponentially small but finite probability to find an arbitrary large region devoid of impurities. Such a rare region can develop true long-range order while the bulk system is still in the disordered phase. We compute the thermodynamic magnetization and its finite-size effects, the local magnetization, and the probability distribution of the ordering temperatures for different samples. Our Monte-Carlo results are in good agreement with a recent theory based on extremal statistics.

I. INTRODUCTION

The influence of disorder on a phase transition is an important and still partially open problem. Historically, the first attempts to address this question resulted in the belief that any kind of disorder would destroy a critical point because the system would divide itself into regions which independently undergo the phase transition at different temperatures. Therefore, there would not be a unique critical temperature for the system, but the phase transition would be smeared over an interval of temperatures. The singularities of thermodynamic quantities, which are the typical sign of a phase transition, would also be smeared (see Ref. 1 and references therein).

However, it soon became clear that this belief was mistaken: in systems with weak short-range correlated disorder the phase transition remains sharp. Harris proposed a simple, heuristic criterion[2] for the influence of disorder on a critical point: if $\nu \geq 2/d$, where ν is the correlation length critical exponent and d the spatial dimensionality, the disorder does not affect the critical behavior. In this case, the randomness decreases under coarse graining, and the system effectively looks homogeneous on large length scales. The critical behavior is identical to that of the clean system, i.e., the clean renormalization group fixed point is stable against disorder. The relative widths of the probability distributions of the macroscopic observables tend to zero in thermodynamic limit, i.e., they are self-averaging.

Even if the Harris criterion is violated the phase transition will generically remain sharp, but the critical behavior will be different from the clean case. There are two possible scenarios, a finite-randomness critical point or an infinite-randomness critical point. A critical point is of finite-randomness type if, under coarse graining, the system stays disordered on all length scales with the effective strength of the randomness approaching a finite constant. The probability distributions of thermodynamic observables reach a finite width in the thermodynamic limit, i.e., they are not self-averaging.[3,4] From a renormalization group point of view this means there is a critical fixed point with finite disorder strength. At a finite-randomness critical point, the thermodynamic observables obey standard power-law scaling behavior, but with exponents different from the exponents of the corresponding clean system. The

other scenario, an infinite-randomness critical point, occurs if the effective disorder strength in the system grows without limit under coarse graining. The system looks more and more disordered on larger and larger length scales, i.e., it is described by a renormalization group fixed point with infinite disorder. The probability distributions of the thermodynamic observables become very broad (even on the logarithmic scale) and their widths diverge when approaching the critical point. The scaling behavior is of activated rather than of conventional power-law type. A famous example of an infinite-randomness critical point occurs in the McCoy-Wu model,[5,6] a $2d$ Ising model with bond disorder perfectly correlated in one dimension and uncorrelated in the other. Recently, infinite-randomness critical points have also been found in several $1d$ random quantum spin chains and two-dimensional random quantum Ising models.[7–14]

Disorder does not only influence the physics at the critical point itself, but also produces interesting effects close to it. These effects are known as Griffiths phenomena, a topic that has regained considerable attention in recent years. Griffiths phenomena are non-perturbative effects produced by rare disorder fluctuations close to a phase transition. They can be understood as follows: Generically, the critical temperature T_c of a disordered system is lower than its clean value, T_c^0. In the temperature interval $T_c < T < T_c^0$, the bulk system is in the disordered phase. On the other hand, in an infinite size sample, there is an exponentially small, but finite probability for finding an arbitrary large region devoid of impurities. Such a region, a 'Griffiths island', can develop local order while the bulk system is still disordered. Due to its size, such an island will have very slow dynamics because flipping it requires changing of the order parameter over a large volume, which is a slow process. Griffiths[15] showed that the presence of the locally ordered islands produces an essential singularity[15,16] in the free energy in the whole region $T_c < T < T_c^0$, which is now known as the Griffiths region or the Griffiths phase.[17] In generic classical systems the Griffiths singularity is weak, and it does not significantly contribute to the *thermodynamic* observables. In contrast, the long-time dynamics is dominated by these rare regions. Inside the Griffiths phase the spin autocorrelation function $C(t)$ decays as $\ln C(t) \sim -(\ln t)^{d/(d-1)}$

for Ising systems[17–21] and as $\ln C(t) \sim -t^{1/2}$ for Heisenberg systems.[20,22] These results were recently confirmed by more rigorous calculation for the equilibrium[23,24] and dynamic[25,26] properties of disordered Ising systems.

There are numerous systems where the disorder is not point like, but is realized through, e.g., dislocations or grain boundaries. This extended disorder in a d-dimensional system can often be modeled by defects perfectly correlated in d_C dimensions and uncorrelated in the remaining $d_\perp = d - d_C$ dimensions. It is generally agreed that extended disorder will have even stronger effects on a phase transition than point-like impurities. Nevertheless, the fate of the transition in the presence of the extended impurities is not settled. Early renormalization group analysis[27] based on a single expansion in $\epsilon = 4 - d$ did not produce a critical fixed point, leading to the conclusion that the phase transition is either smeared or of first order.[28,29] Later work[30–32] which included an expansion in the number of correlated dimensions d_C lead to a fixed point with conventional power law scaling. Subsequent Monte-Carlo simulations of a $3d$ Ising model with planar defects provided further support for a sharp phase transition scenario.[33] Notice, however, that the perturbative renormalization group calculations missed all effects coming form the rare regions. These effects were extensively studied for the above-mentioned McCoy-Wu model. While it was believed for a long time that the phase transition in this model is smeared, it was later found to be sharp, but of infinite-randomness type.[9,11,34] Based on these findings, there was a general belief that a phase transition will remain sharp even in the presence of extended disorder.

Recently, it has been shown that this belief is not true. A theory[35,36] based on extremal statistics arguments has predicted that impurities correlated in a sufficiently high number of dimensions will generically smear the phase transition. The predictions of this theory were confirmed in simulations of mean-field type models[35,36] but up to now, a demonstration of the smearing in a more realistic short-range model has been missing.

In this paper, we therefore present results of large-scale Monte-Carlo simulations for a $3d$ Ising model with planar defects and nearest-neighbor interactions in both the correlated and uncorrelated dimensions. These simulations show that the sharp

phase transition is indeed destroyed by the extended disorder. The smearing of the transition is a consequence of a mechanism similar to but stronger than the Griffiths phenomena. In an Ising system with planar defects true static long-range order can develop on rare islands devoid of impurities. As a consequence, the order parameter becomes spatially very inhomogeneous and its average develops an exponential dependence on temperature. This paper is organized as follows. In section II, the model is introduced and the mechanism of the smearing is explained. Section III is devoted to the results of the Monte-Carlo simulations and a comparison with the theoretical predictions. In Section IV, we present our conclusions and discuss a number of open questions.

II. THE MODEL

A. 3D Ising model with planar defects

Our starting point is a $3d$ Ising model with planar defects. Classical Ising spins $S_{ijk} = \pm 1$ reside on a cubic lattice. They interact via nearest-neighbor interactions. In the clean system all interactions are identical and have the value J. The defects are modeled via 'weak' bonds randomly distributed in one dimension (uncorrelated direction). The bonds in the remaining two dimensions (correlated directions) remain equal to J. The system effectively consists of blocks separated by parallel planes of weak bonds. Thus, $d_\perp = 1$ and $d_C = 2$. The Hamiltonian of the system is given by:

$$\begin{aligned} H = & - \sum_{\substack{i=1,\ldots,L_\perp \\ j,k=1,\ldots,L_C}} J_i S_{i,j,k} S_{i+1,j,k} \\ & - \sum_{\substack{i=1,\ldots,L_\perp \\ j,k=1,\ldots,L_C}} J(S_{i,j,k} S_{i,j+1,k} + S_{i,j,k} S_{i,j,k+1}), \end{aligned} \tag{1}$$

where $L_\perp (L_C)$ is the length in the uncorrelated (correlated) direction, i, j and k are integers counting the sites of the cubic lattice, J is the coupling constant in the correlated directions and J_i is the random coupling constant in the uncorrelated

direction. The J_i are drawn from a binary distribution:

$$J_i = \begin{cases} cJ & \text{with probability} \quad p \\ J & \text{with probability} \quad 1-p \end{cases} \tag{2}$$

characterized by the concentration p and the relative strength c of the weak bonds ($0 < c \leq 1$). The fact that one can independently vary concentration and strength of the defects in an easy way is the main advantage of this binary disorder distribution. However, it also has unwanted consequences, viz. log-periodic oscillations of many observables as functions of the distance from the critical point.[37] These oscillations are special to the binary distribution and unrelated to the smearing considered here; we will not discuss them further. The order parameter of the magnetic phase transition is the total magnetization:

$$m = \frac{1}{V} \sum_{i,j,k} \langle S_{i,j,k} \rangle, \tag{3}$$

where $V = L_\perp L_C^2$ is the volume of the system, and $\langle \cdot \rangle$ is the thermodynamic average.

Now we consider the effects of rare disorder fluctuations in the system. Similarly to the Griffiths phenomena, there is a small but finite probability to find a large spatial region containing only strong bonds in the uncorrelated direction. Such a rare region can locally be in the ordered state while the bulk system is still in the disordered (paramagnetic) phase. The ferromagnetic order on the largest rare regions starts to emerge right below the clean critical temperature T_c^0. Since the defects in the system are planar, these rare regions are infinite in the two correlated dimensions but finite in the uncorrelated direction. This makes a crucial difference compared to systems with uncorrelated disorder, where rare regions are of finite extension. In our system, each rare region is equivalent to a two dimensional Ising system that can undergo a real phase transition independently of the rest of the system. Thus, each rare region can independently develop true static order with a non-zero static value of the local magnetization. Once the static order has developed, the magnetizations of different rare regions can be aligned by an infinitesimally small interaction or external field. The resulting phase transition will thus be markedly different from a conventional continuous phase transition. At a conventional transition, a non-zero order parameter develops as a collective effect of the entire system which is signified

by a diverging correlation length of the order parameter fluctuations at the critical point. In contrast, in a system with planar defects, different parts of the system (in the uncorrelated direction) will order independently, at different temperatures. Therefore the global order will develop inhomogeneously and the correlation length in the uncorrelated direction will remain finite at all temperatures. This defines a smeared transition. Thus we conclude that planar defects destroy a sharp phase transition and lead to its smearing.

B. Results of extremal statistics theory

In this subsection we briefly summarize the results of the extremal statistics theory[36] for the behavior in the 'tail' of the smeared transition, i.e., in the parameter region where a few rare regions have developed static order but their density is still sufficiently low so they can be considered as independent. The approach is very similar to that of Lifshitz[38] and others developed for the description of the tails in the electronic density of states. The extremal statistics theory[36] correctly describes the leading (exponential) behavior of the magnetization and other observables. A calculation of pre-exponential factors would be much more complicated because one would have to include, among other things, details of the geometry of the rare regions, surface critical behavior[39,40] at the surfaces of the rare regions, and corrections to finite-size scaling. This is beyond the scope of the present paper.

The probability w to find a large region of linear size $L_\perp$ containing only strong bonds is, up to pre-exponential factors:

$$w \sim (1-p)^{L_\perp} = e^{\log(1-p)L_\perp}. \tag{4}$$

As discussed in subsection II A, such a rare region develops static long-range (ferromagnetic) order at some reduced temperature $T_c(L_\perp)$ below the clean critical reduced temperature T_c^0. The value of $T_c(L_\perp)$ varies with the length of the rare region; the longest islands will develop long-rage order closest to the clean critical point. A rare region is equivalent to a slab of the clean system, we can thus use finite size scaling to obtain:

$$T_c^0 - T_c(L) = |t_c(L)| = AL^{-\phi}, \tag{5}$$

where ϕ is the finite-size scaling shift exponent of the clean system and A is the amplitude for the crossover from three dimensions to a slab geometry infinite in two (correlated) dimension but with finite length in the third (uncorrelated) direction. The reduced temperature $t = T - T_c^0$ measures the distance from the *clean* critical point. Since the clean $3d$ Ising model is below its upper critical dimension ($d_c^+ = 4$), hyperscaling is valid and the finite-size shift exponent $\phi = 1/\nu$. Combining (4) and (5) we get the probability for finding an island of length $L_\perp$ which becomes critical at some t_c as:

$$w(t_c) \sim e^{-B|t_c|^{-\nu}} \ \text{(for } t_c \to 0-\text{)} \tag{6}$$

with the constant $B = -\log(1-p)A^\nu$. The total (average) magnetization m at some reduced temperature t is obtained by integrating over all rare regions which have $t_c > t$. Since the functional dependence on t of the local magnetization on the island is of power-law type it does not enter the leading exponentials but only pre-exponential factors, so:

$$m(t) \sim e^{-B|t|^{-\nu}} \ \text{(for } t \to 0-\text{)}. \tag{7}$$

Now we turn our attention to the homogeneous magnetic susceptibility. It contains two contributions, one coming from the islands on the verge of ordering and one from the bulk system still deep in the disordered phase. The bulk system provides a finite, non-critical background susceptibility throughout the whole tail region of the smeared transition. In order to estimate the second part of the susceptibility, i.e., the part coming from the islands consider the onset of local magnetization at the clean critical point. Using eq. (6) for the density of islands we can estimate:

$$\chi \sim \int_0^\Lambda dt t^{-\gamma} e^{-Bt^{-\nu}} \ \text{(for } t \to 0-\text{)}. \tag{8}$$

The last integral is finite because the exponentially decreasing island density overcomes the power-law divergence of the susceptibility of an individual island. Here γ is the clean susceptibility exponent and Λ is related to a lower cutoff for the island size. Once the first island is ordered it produces an effective background magnetic field which cuts off any possible divergence in χ. Therefore, we conclude that the homogeneous magnetic susceptibility does not diverge anywhere in the tail of the

smeared transition. However, there is an essential singularity at the clean critical temperature produced by the vanishing density of ordered islands. Because if this singularity one might be tempted to call this temperature the transition temperature of our system, but this is not appropriate because at this temperature only an infinitesimally small part of the system starts to develop a finite magnetization while most of the system remains solidly in the nonmagnetic phase. We rather view the clean critical temperature as the onset of the smearing region in our model.[36]

The spatial distribution of the magnetization in the tail region of the smeared transition is very inhomogeneous. On the already ordered islands, the local (layer) magnetization $m_i = (1/L_C^2)\sum_{j,k}\langle S_{i,j,k}\rangle$ is comparable to the magnetization of the clean system. On the other hand, far away from the ordered islands m_i decays exponentially with the distance from the closest one. The probability distribution of the logarithm of the magnetization $P[\log m_i]$ will therefore be very broad, ranging from $\log m_i = O(1)$ on the largest islands to $\log m_t \to -\infty$ on sites very far away from any ordered islands. The typical magnetization m_{typ} can be estimated from the typical distance of a point from the nearest ordered island. Using eq. (6) we get:

$$x_{typ} \sim e^{B|t|^{-\nu}}. \tag{9}$$

At the distance x_{typ} from an ordered island, the local magnetization has decayed to

$$m_{typ} \sim e^{-x_{typ}/\xi_0} \sim e^{-Ce^{B|t|^{-\nu}}} \tag{10}$$

where ξ_0 is the bulk correlation length, which is finite and changes slowly throughout the tail region of the smeared transition, and C is a constant. A comparison with eq. (7) gives the relation between m_{typ} and the thermodynamic order parameter (magnetization) m as:

$$|\log m_{typ}| \sim \frac{1}{m}. \tag{11}$$

Thus, m_{typ} decays exponentially with m indicating an extremely broad order parameter distribution. In order to determine the functional form of the local order parameter distribution, first consider a situation with just a single ordered island at the origin of the coordinate system. For large distances x, the local magnetization falls off exponentially as $m(x) = m_0\ e^{-x/\xi_0}$. The probability distribution of

$y = \log[m(x)] = \log m_0 - x/\xi_0$ can be calculated from

$$P(|y|) = \left|\frac{dN}{dy}\right| = \frac{dN}{dx}\left|\frac{dx}{dy}\right| = \xi_0 \frac{dN}{dx} \sim \xi_0 \tag{12}$$

where dN is the number of sites at a distance from the origin between x and $x + dx$ or, equivalently, having a logarithm of the local magnetization between y and $y + dy$. Therefore, for large distances, the probability distribution of $\log m(x)$ generated by a single ordered island takes the form

$$P[\log(m)] = const. \text{ (for } m(x) \ll 1) \ . \tag{13}$$

In the tail region of the smeared transition our system consists of a few ordered islands whose distance is large compared to ξ_0. The probability distribution of the local magnetization, $\log(m_i)$, thus takes the form (13) with a lower cutoff corresponding to the typical island-island distance and an upper cutoff corresponding to a distance ξ_0 from an ordered island.

C. Finite-size effects

It is important to distinguish effects of a finite size L_C in the correlated directions and a finite size $L_\perp$ in the uncorrelated directions. If $L_\perp$ is finite but L_C is infinite static order on the rare regions can still develop. In this case, the sample contains only a finite number of islands of a certain size. As long as the number of relevant islands is large, finite size-effects are small and governed by the central limit theorem. However, for $t \to 0-$ very large and rare islands are responsible for the order parameter. The number N of islands which order at t behaves like $N \sim L_\perp w(t)$. When N becomes of order one, strong sample-to-sample fluctuations arise. Using (6) for $w(t)$ we find that strong sample to sample fluctuations start at

$$|t_L| \sim \left(\frac{1}{B}\log(L_\perp)\right)^{-1/\nu} \ . \tag{14}$$

Thus, finite size effects are suppressed only logarithmically.

Analogously, one can study the onset of static order in a sample of finite size $L_\perp$ (i.e., the ordering temperature of the largest rare region in this sample). For small

sample size $L_\perp$, the probability distribution $P(T_s)$ of the sample ordering temperatures T_s will be broad because some samples do not contain any large islands. With increasing sample size the distribution becomes narrower and moves toward the clean T_c^0 because more samples contain large islands. The maximum T_s coincides with T_c^0 corresponding to a sample without impurities. The lower cutoff corresponds to an island size so small that essentially every sample contains at least one of them. Consequently, the width of the distribution of critical temperatures in finite-size samples is governed by the same relation as the onset of the fluctuations,

$$\Delta T_s \sim \left(\frac{1}{B}\log(L_\perp)\right)^{-1/\nu} . \tag{15}$$

For the system under study in this paper, a finite size in the correlated direction has far less interesting consequences. In this case the rare regions are finite in all directions and cannot develop true static order. Therefore, the phase transition is rounded by conventional finite-size effects in addition to the disorder induced smearing discussed in this paper.

III. NUMERICAL RESULTS

A. The method

We now turn to the main part of the paper, Monte-Carlo simulations of a $3d$ Ising model with planar bond defects and short range interactions, as given in eq. (1). The simulations are performed using the Wolff cluster algorithm.[41]

As discussed above, the smearing of the transition is a result of exponentially rare events. Therefore sufficiently large system sizes are required in order to observe it. We have simulated system sizes ranging from $L_\perp = 50$ to $L_\perp = 200$ in the uncorrelated direction and from $L_C = 50$ to $L_C = 400$ in the remaining two correlated directions, with the largest system simulated having a total of 32 million spins. We have chosen $J = 1$ and $c = 0.1$ in the eq. (2), i.e., the strength of a 'weak' bond is 10% of the strength of a strong bond. The simulations have been performed for various disorder concentrations $p = \{0.2, 0.25, 0.3\}$. The values for concentration p and strength c of the weak bonds have been chosen in order to observe the desired behavior over a

sufficiently broad interval of temperatures. This issue will be discussed in more detail in Section IV. The temperature range has been $T = 4.325$ to $T = 4.525$, close to the critical temperature of the clean $3d$ Ising model $T_c^0 = 4.511$.

Monte-Carlo simulations of disordered systems require a huge computational effort.[42] For optimal performance one must thus carefully choose the number N_S of disorder realizations (i.e., samples) and the number N_I of measurements during the simulation of each sample. Assuming full statistical independence between different measurements (quite possible with a cluster update), the variance σ_T^2 of the final result (thermodynamically and disorder averaged) for a particular observable is given by[43,44]

$$\sigma_T^2 = (\sigma_S^2 + \sigma_I^2/N_I)/N_S \tag{16}$$

where σ_S is the disorder-induced variance between samples and σ_I is the variance of measurements within each sample. Since the computational effort is roughly proportional to $N_I N_S$ (neglecting equilibration for the moment), it is then clear that the optimum value of N_I is very small. One might even be tempted to measure only once per sample. On the other hand, with too short measurement runs most computer time would be spent on equilibration.

In order to balance these requirements we have used a large number N_S of disorder realizations, ranging from 30 to 780, depending on the system size and rather short runs of 100 Monte-Carlo sweeps, with measurements taken after every sweep. (A sweep is defined by a number of cluster flips so that the total number of flipped spins is equal to the number of sites, i.e., on the average each spin is flipped once per sweep.) The length of the equilibration period for each sample is also 100 Monte-Carlo sweeps. The actual equilibration times have typically been of the order of 10-20 sweeps at maximum. Thus, an equilibration period of 100 sweeps is more than sufficient.

B. Total magnetization and susceptibility

In this subsection we present numerical results for the total magnetization m (as usual, our Monte-Carlo estimator of m is the average of the *absolute value* of the

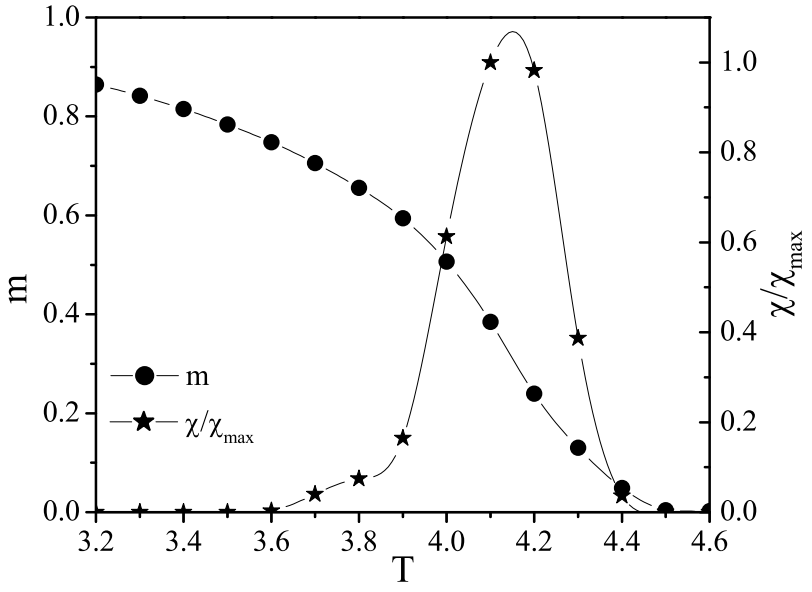

FIG. 1: Average magnetization m and susceptibility χ (spline fit) as functions of T for $L_\perp = 100$, $L_C = 200$ and $p = 0.2$ averaged over 200 disorder realizations.

magnetization in each measurement) and the homogeneous susceptibility $\chi = \partial m/\partial h$. Fig. 1 gives an overview of total magnetization and susceptibility as functions of temperature averaged over 200 samples of size $L_\perp = 100$ and $L_C = 200$ with an impurity concentration $p = 0.2$. We note that at the first glance the transition looks like a sharp phase transition with a critical temperature between $T = 4.3$ and $T = 4.4$, rounded by conventional finite size effects. In order to distinguish this conventional scenario from the disorder induced smearing of section II, we have performed a detailed analysis of the system in a temperature range in the immediate vicinity of the clean critical temperature $T_c^0 = 4.511$.

In Fig. 2, we plot the logarithm of the total magnetization vs. $|T_c^0 - T|^{-\nu}$ averaged over 240 samples for system size $L = 200$, $L_C = 280$ and three disorder concentrations $p = \{0.2, 0.25, 0.3\}$. The standard deviation of the total magnetization is below 10^{-3}. For all three concentrations the data follow the analytical prediction, eq. (7), over more than an order of magnitude in m with the exponent for the clean Ising model $\nu = 0.627$. The deviation from the straight line for small m is due to the conventional

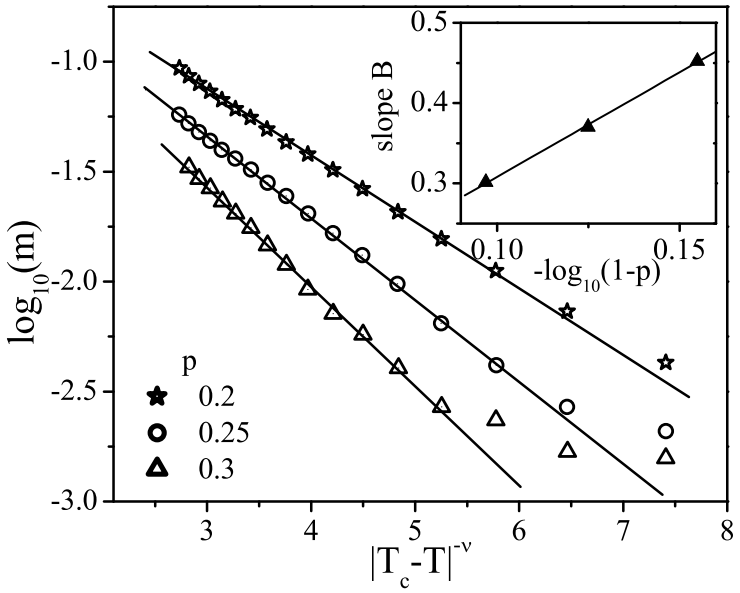

FIG. 2: Logarithm of the total magnetization m as a function of $|T_c^0 - T|^{-\nu}$ ($\nu = 0.627$) for several impurity concentrations $p = 0.2, 0.25, 0.3$, averaged over 240 disorder realizations. System size $L_\perp = 200$, $L_C = 280$. The statistical errors are smaller than a symbol size for all $\log_{10}(m) > -2.5$. Inset: Decay slope B as a function of $-\log(1-p)$.

finite size effects (see discussion in subsection III C). In the inset we show that the decay constant B depends linearly on $-\log(1-p)$. This is the behavior expected from eq. (4).

C. Finite size effects and sample-to-sample fluctuations

As discussed in subsection II C one should distinguish between two different finite size effects, i.e., effects coming form the finite size L_C in correlated direction and effects produced by the finite size $L_\perp$ in uncorrelated direction.

We start with analysis of the finite size effects in correlated directions, i.e. L_C finite and $L_\perp \to \infty$. The true static order on the rare regions is destroyed by the finite length of the island in the correlated direction. For our model $d_\perp = 1$ so no true static long range order can develop. The value of m measured in the simulations is thus due to fluctuations which are governed by the central limit theorem, i.e., $m \sim V^{-1/2}$,

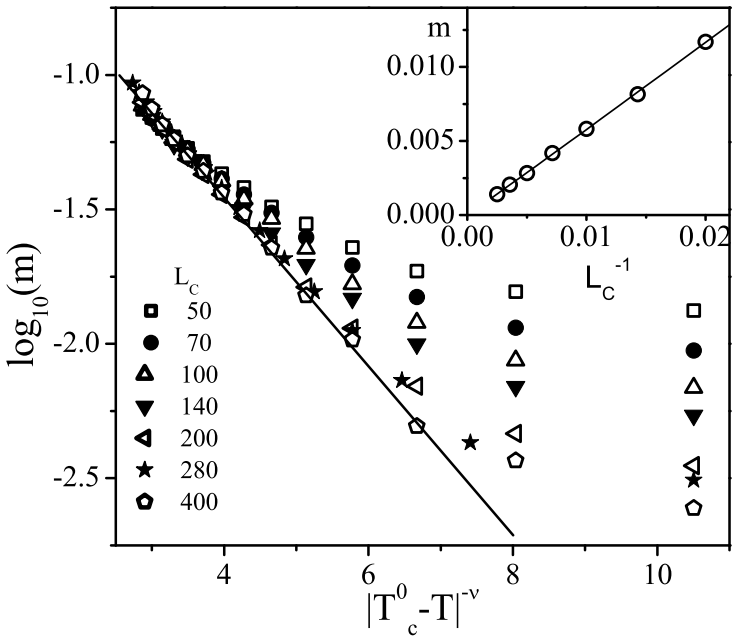

FIG. 3: Logarithm of the total magnetization m as a function of $|T_c^0 - T|^{-\nu}$ ($\nu = 0.627$) for disorder concentration $p = 0.2$ and system sizes $L_\perp = 200$, $L_C = 50 \ldots 400$. The statistical errors are smaller than about a symbol size. The solid line shows the analytic prediction, eq. (7). Inset: Total magnetization m as a function of inverse length in the correlated direction L_C for $T = 4.5$ ($|T - T_c^0|^{-\nu} = 16.91$).

where $V = L_\perp L_C^2$ is the volume of the system. This produces a conventional finite-size rounding responsible for the deviations of m from the exponential law in Fig. 2. In Fig. 3, we investigate this finite-size effect in more detail. This figure shows the total magnetization m as a function of $|T_c^0 - T|^{-\nu}$ for systems with fixed size in the uncorrelated direction $L_\perp = 200$ and various lengths in the uncorrelated direction, $L_C = 50, 70, 100, 140, 200, 280, 400$. The magnetization is averaged over 30 to 240 disorder realizations. As expected, for high temperatures, the total magnetization shows a strong dependence on L_C. The smallest systems follow the exponential behavior (7) only over a narrow range of temperatures and then cross over to the fluctuation determined value. If L_C is increased the crossover between the exponential behavior (7) and the fluctuation background shifts to higher temperatures. In order to show that the fluctuation-determined value of the total magnetization m at high

temperatures indeed follows the predictions of the central limit theorem, i.e. $m \sim V^{-1/2} = (L_\perp L_C^2)^{-1/2} \sim 1/L_C$ ($L_\perp$ is constant) we plot m as a function of $1/L_C$ ($T = 4.5$, $|T - T_c^0|^{-\nu} = 16.91$). The numerical data shown in the inset of Fig. 3 can indeed be well fitted with a straight line. These results show that the small-m deviations from the predicted behavior (7) are indeed the result of conventional finite-size rounding.

We now turn our attention to the more interesting finite size effects produced by the finite sample length $L_\perp$ in the uncorrelated direction. For sufficiently small $L_\perp$ one expects strong sample to sample fluctuations, as discussed in subsection II C. In Fig. 4 we show the logarithm of the total magnetization m as a function of $|T_c^0 - T|^{-\nu}$ for three typical disorder realizations. For comparison, the upper panel of the Fig. 4 shows the coupling constant J_i as a function of the position i for the three samples. The numbers in the graph indicate the lengths of the longest islands L_i. The system size is $L_\perp = 200$, $L_C = 280$ with disorder concentration $p = 0.2$. The solid line is the average magnetization over 240 disorder realizations. We see that all three curves qualitatively follow the average at low temperatures but start to deviate from it at higher temperatures. The temperature T_s at which the magnetization of a sample rapidly drops is associated with the ordering of the largest island in this sample. Numerically, we determine T_s as the temperature where the sample magnetizations falls below 1/3 of the average magnetization. This definition contains some amount of arbitrariness which corresponds to an overall shift of all T_s. However, the leading functional dependence of T_s on the size L_i of the longest island in the sample is not influenced by this shift. In order to demonstrate this dependence we can apply finite size scaling for the clean $3d$ Ising model (islands are regions devoid of impurities) in the slab geometry, i.e. on a sample of length L_i in one dimension and essentially infinite length in other two dimensions ($L_C \gg L_i$). In the inset of Fig. 4 we plot $|T_c^0 - T_s|^{-\nu}$ as a function of L_i. The data show good agreement with the finite-size scaling prediction. Figure 4 also demonstrates that, in the tail of the smeared transition (for $T \to T_c^0$), the average (thermodynamic) magnetization is determined by rare samples with untypically large rare regions.

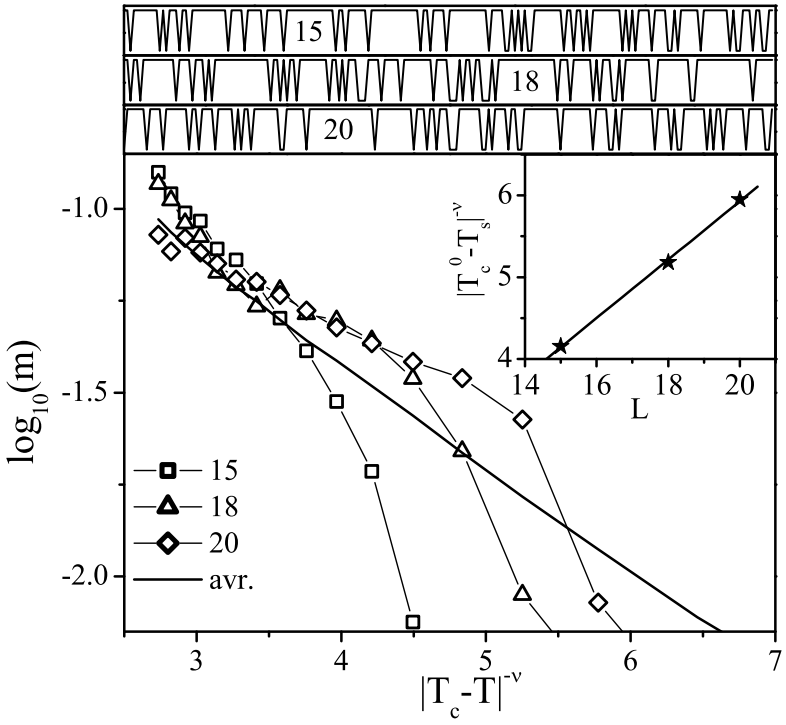

FIG. 4: Logarithm of the total magnetization m as a function of $|T_c^0 - T|^{-\nu}$ for $L_\perp = 200$, $L_C = 280$ and $p = 0.2$ for three different disorder realizations. The thermodynamic statistical error of $\log_{10} m$ of a *single* realization is about 0.1. Straight line represents the average over 240 disorder realizations. Upper panel: The coupling constant J_i in the uncorrelated direction as a function of i for the corresponding three disorder realizations. Numbers indicate length of the longest island L_i in the uncorrelated direction. Inset: Relation between the sample critical temperature T_s and the size of the island length, plotted as $|T_c^0 - T_s|^{-\nu}$ as a function of island length.

In Fig. 5, we show the probability distribution of the sample ordering temperature T_s for system sizes $L_\perp = 25, 50, 75, 100, 200$ and $L_C = 200$, computed from 700 to 780 disorder realizations (the statistical error of the T_s values is $\Delta T_S \lesssim 0.03$). The results are in good agreement with the predictions of subsection II C, i.e., the probability distribution of the sample critical temperature becomes narrower and moves toward the clean critical temperature as the sample length $L_\perp$ in the uncorrelated direction is increased. In the inset of Fig. 5, we show that the width of the probability distribution

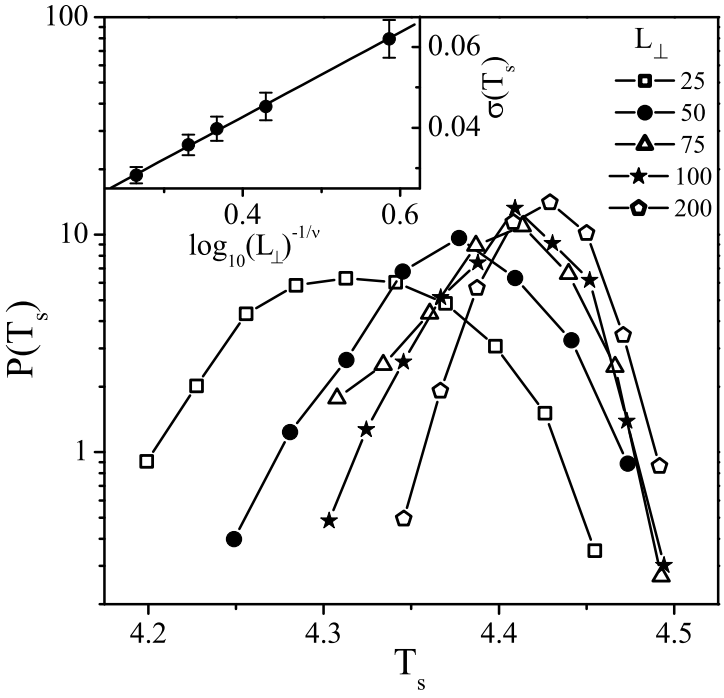

FIG. 5: The probability distribution of sample critical temperature T_s as for different sample lengths in the uncorrelated direction. The data shown is for system with $L_\perp = 25, 50, 75, 100, 200$ and $L_C = 200$. The probability distribution is calculated from 700 to 780 disorder realizations and disorder concentration $p = 0.2$. Inset: Width of the probability distribution as a function of $\log(L_\perp)^{-1/\nu}$.

(defined as its standard deviation) is proportional to $\log(L_\perp)^{-1/\nu}$ as predicted in eq. (15).

D. Local magnetization

We now turn to the local (layer) magnetization m_i (as for the total magnetization, our Monte-Carlo estimator is the average of the *absolute values* of the layer magnetizations for each measurement). Close to the clean critical point the system contains a few ordered islands (rare regions devoid of impurities) typically far apart in space. The remaining bulk system is essentially still in the disordered phase. Fig. 6 illustrates such a situation. It displays the local magnetization m_i of a particular

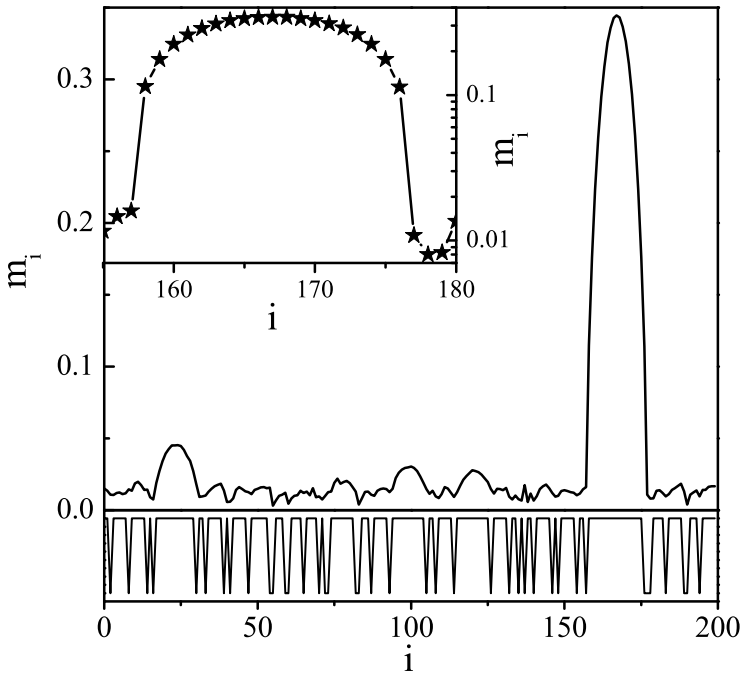

FIG. 6: Local magnetization m_i of a particular disorder realization as a function of the position i in the uncorrelated direction (system size $L = 200$, $L_C = 200$ and temperature $T = 4.425$). The statistical error is approximately $5 \cdot 10^{-3}$. Lower panel: The coupling constant J_i in the uncorrelated direction as a function of position i. Inset: Log-linear plot of the zoomed in region in the vicinity of the largest ordered island.

disorder realization as a function of the position i in the uncorrelated direction for the size $L_\perp = 200$, $L_C = 200$ at a temperature $T = 4.425$ in the tail of the smeared transition. The lower panel shows the local coupling constant J_i as a function of i. The figure shows that a sizable magnetization has developed on the longest island only (around position $i = 160$). One can also observe that order starts to emerge on the next longest island located close to $i = 25$. Far form these islands the system is still in its disordered phase. In the thermodynamic limit, the local magnetization should be exponentially small as predicted by eq. (10). However, in the simulations of a finite size system the local magnetization has a lower cut-off which is produced by finite-size fluctuations of the order parameter. These fluctuations are governed by the central limit theorem and can be estimated as $m_{bulk} \approx 1/\sqrt{N_{cor}} \approx \sqrt{L_{cl}^2/L_C^2} \approx 5 \cdot 10^{-3}$

in agreement with the typical off-island value in Fig. 6. Here, N_{cor} is the number of correlated volumes per slab as determined by the size off the Wolff cluster. L_{cl} is a typical linear size of a Wolff cluster which is, at $T = 4.425$, $L_{cl} \approx 10$). In the inset of Fig. 6 we zoom in on the region around the largest island. The local magnetization, plotted on the logarithmic scale, exhibits a rapid drop-off with the distance from the ordered island. This drop-off suggests a relatively small (a few lattice spacings) bulk correlation length ξ_0 in this parameter region.

As was discussed above, finite-size fluctuations of the local magnetization far form the ordered islands mask the true asymptotic behavior for very small m_i. In order to verify the probability distribution (13) of the local magnetization numerically, fluctuations have to be suppressed sufficiently. This would require simulating very large systems whose sizes in the correlated direction increase quadratically with the required magnetization resolution. With sizes available in our simulations we were not able to reproduce the distribution function, eq. (13), of $P(\log m_i)$ predicted to be constant at small m_i and calculated for the mean-field model.[36]

IV. CONCLUSIONS

In this final section we summarize our results and discuss how the disorder induced smearing of the phase transition found here compares to the Griffiths phenomena. We also remark on favorable conditions for observing the disorder-induced smearing in experiments and simulations. Then we shortly discuss differences between models with discrete and continuous symmetry. We end by briefly addressing the question of smearing of quantum phase transitions.

We have performed large-scale Monte-Carlo simulations of a $3d$ Ising model with short-ranged, nearest neighbor interactions and planar defects, introduced via correlated bond disorder. The results of the simulations show that the phase transition is not sharp, but rather smeared over a range of temperatures by the presence of the extended defects. The numerical results are in good agreement with the theoretical predictions (see subsection II B) based on the Lifshitz tail arguments.[35,36]

The physics behind the smearing of the phase transition discussed in this paper is similar to the physics underlying Griffiths phenomena. Both effects are produced by rare spatial regions which are devoid of impurities and therefore locally in the ordered phase while the bulk system is still disordered. The difference between Griffiths phenomena and disorder-induced smearing is a result of disorder correlations. If the disorder is uncorrelated or short-range correlated, the rare regions have finite size and cannot develop true static order. The order parameter on such a rage region still fluctuates, albeit slowly. These slow fluctuations lead to the well known Griffiths singularities[15] discussed in section I. In contrast, if the rare regions are infinite in two or more dimensions a stronger effect arises. The rare regions can develop true static long-range order independently of the rest of the system. The order parameter in such a system develops very inhomogeneously, which leads to the smearing of the phase transition. Therefore, exactly the same rare regions which would result in Griffiths phenomena if the disorder was short-range correlated lead to the smeared phase transition in the case of disorder correlated in two or more dimensions. In this sense the smearing of the transition takes the place of both the phase transition and the Griffiths region. Notice that long-range interactions increase the tendency toward smearing. If the interaction in the correlated direction falls off as $1/r^2$ or slower, even linear defects can lead to smearing, because a $1d$ Ising model with $1/r^2$ interaction has an ordered phase.[45,46]

Now we turn our attention to favorable conditions for observing the smearing in numerical simulations or experiments. This turns out to be controlled by two conditions, one for the concentration of the impurities, and one for their strength. In order to easily observe the smearing, the concentration of rare regions, eq. (6), has to be sufficiently large. This requires a relatively small concentration of impurities. If the concentration of the impurities is too high, the exponential drop-off of the island number and thus of m is very steep and the smearing effects would be very hard to observe. On the other hand, if the impurities are too weak, the smeared transition is too close to the clean critical point and the bulk critical fluctuations will effectively mask the smearing. Consequently, the best parameters for observing the smearing

are a small concentration of strong impurities. This has been confirmed in test calculations using concentrations from $p = 0.05$ to 0.5. Unfavorable parameter values may also be the reason why no smearing has been observed in previous simulations.[33,47] Specifically, in Ref. 33, simulations have been performed using a high concentration $p = 0.5$ of weak impurities ($\Delta J/J = 0.1$). The relatively small system sizes (up to $L = 27$) in that simulation were probably not sufficient to observe the smearing.

The next remark concerns models with continuous order parameter symmetry. As pointed out above, the smearing of the phase transition is caused by static order on the rare regions. Thus, systems with continuous order parameter symmetry and short-range interactions would exhibit smearing of the phase transition only if the disorder is correlated in three or more dimensions.[48] Again, long-range interactions increase the tendency toward smearing. It is known[49] that classical XY and Heisenberg systems in $1d$ and $2d$ develop long range order only if the interaction falls off more slowly than $1/r^{2d}$. Therefore a system with linear (planar) defects would show smearing of the phase transition if the interactions in the correlated direction would fall off more slowly then $1/r^2$ ($1/r^4$).

We end our discussion with the brief remark about smearing of quantum phase transitions in disordered itinerant electronic systems. Each quantum phase transition can be mapped to a classical phase transition in higher dimension, with imaginary time acting as additional dimension. For dirty itinerant ferromagnets the effective interaction between the spin fluctuations in the imaginary time direction falls off as $1/\tau^2$, and the disorder is correlated in this direction.[50] Therefore, the dirty itinerant ferromagnetic transition is smeared even for point-like defects.[36]

In conclusion, we have presented results of Monte-Carlo simulations of a $3d$ Ising model with short-range interactions and planar defects. The numerical results show that the perfect disorder correlations in two dimensions destroy the sharp magnetic phase transition leading to a smeared transition at which the magnetization gradually develops over range of temperatures.

Acknowledgments

We acknowledge support from the University of Missouri Research Board.

---

[1] G. Grinstein, in *Fundamental Problems in Statistical Mechanics VI*, edited by E. G. D. Cohen (Elsevier, New York, 1985).

[2] A. B. Harris, J. Phys. C **7**, 1671 (1974).

[3] A. Aharony and A. B. Harris, Phys. Rev. Lett. **77**, 3700 (1996).

[4] S. Wiseman and E. Domany, Phys. Rev. Lett. **81**, 22 (1998).

[5] B. M. McCoy and T. T. Wu, Phys. Rev. **176**, 631 (1968).

[6] B. M. McCoy and T. T. Wu, Phys. Rev. **188**, 982 (1969).

[7] S. K. Ma, C. Dasgupta, and C.-K. Hu, Phys. Rev. Lett. **43**, 1434 (1979).

[8] R. N. Bhatt and P. A. Lee, Phys. Rev. Lett. **48**, 344 (1982).

[9] D. S. Fisher, Phys. Rev. Lett. **69**, 534 (1992).

[10] D. S. Fisher, Phys. Rev. B **50**, 3799 (1994).

[11] D. S. Fisher, Phys. Rev. B **51**, 6411 (1995).

[12] A. P. Young and H. Rieger, Phys. Rev. B **53**, 8486 (1996).

[13] C. Pich, A. P. Young, and N. Kawashima, Phys. Rev. Lett. **81**, 5916 (1998).

[14] O. Motrunich, S.-C. Mau, D. A. Huse, and D. S. Fisher, Phys. Rev. B **61**, 1160 (2000).

[15] R. B. Griffiths, Phys. Rev. Lett. **23**, 17 (1965).

[16] A. J. Bray and D. Huifang, Phys. Rev. B **40**, 6980 (1989).

[17] M. Randeria, J. Sethna, and R. G. Palmer, Phys. Rev. Lett. **54**, 1321 (1985).

[18] D. Dhar, in *Stochastic Processes: Formalism and Applications*, edited by D. S. Argawal and S. Dattagapta (Springer, Berlin, 1985).

[19] D. Dhar, M. Randeria, and J. P. Sethna, Europhys. Lett. **5**, 485 (1988).

[20] A. J. Bray, Phys. Rev. Lett. **60**, 720 (1988).

[21] A. J. Bray and G. J. Rodgers, Phys. Rev. B **38**, 9252 (1988).

[22] A. J. Bray, Phys. Rev. Lett. **59**, 586 (1987).

[23] H. von Dreyfus, A. Klein, and J. F. Perez, Commun. Math. Phys. **170**, 21 (1995).

[24] G. Gielis and C. Maes, J. Stat. Phys. **81**, 829 (1995).

[25] S. Cesi, C. Maes, and F. Martinelli, Commun. Math. Phys. **189**, 135 (1997).

[26] S. Cesi, C. Maes, and F. Martinelli, Commun. Math. Phys. **189**, 323 (1997).

[27] T. C. Lubensky, Phys. Rev. B **11**, 3573 (1975).

[28] J. Rudnick, Phys. Rev. B **18**, 1406 (1975).

[29] D. Andelman and A. Aharony, Phys. Rev. B **31**, 4305 (1975).

[30] S. N. Dorogovtsev, Fiz. Tverd. Tela (Leningrad) **22**, 321 (1980), [Sov. Phys.-Solid State **22**,188].

[31] D. Boyanovsky and J. L. Cardy, Phys. Rev. B **26**, 154 (1982).

[32] L. D. Cesare, Phys. Rev. B **49**, 11742 (1994).

[33] J. C. Lee and R. L. Gibbs, Phys. Rev. B **45**, 2217 (1992).

[34] B. M. McCoy, Phys. Rev. Lett. **23**, 383 (1969).

[35] T. Vojta, Phys. Rev. Lett. **90**, 107202 (2003).

[36] T. Vojta, J. Phys. A: Math. Gen. **36**, 10921 (2003).

[37] D. Karevski and L. Turban, J. Phys. A **29**, 3461 (1996).

[38] I. M. Lifshitz, Usp. Fiz. Nauk **83**, 617 (1964), [Sov. Phys.-Usp. **7** 549].

[39] K. Binder, in *Phase Transitions and Critical Phenomena*, edited by C. Domb and J. L. Lebowitz (Academic Press, London, 1983), vol. 8.

[40] H. W. Diehl, in *Phase Transitions and Critical Phenomena*, edited by C. Domb and J. L. Lebowitz (Academic Press, London, 1986), vol. 10.

[41] U. Wolff, Phys. Rev. Lett. **62**, 361 (1989).

[42] W. Selke, L. N. Shchur, and A. L. Tapalov, in *Annual Reviews of Computational Physics*, edited by D. Stauffer (World Scientific, Singapore, 1994), vol. 1.

[43] H. G. Ballesteros, L. A. Fernandez, V. Martin-Mayor, A. M. Sudupe, G. Parisi, and J. J. Ruiz-Lorenzo, Phys. Rev. B **58**, 2740 (1998).

[44] H. G. Ballesteros, L. A. Fernandez, V. Martin-Mayor, A. M. Sudupe, G. Parisi, and J. J. Ruiz-Lorenzo, Nucl. Phys. B **512**, 681 (1998).

[45] D. J. Thouless, Phys. Rev. **187**, 732 (1969).

[46] J. Cardy, J. Phys. A **14**, 1407 (1981).

[47] B. Berche, P. Berche, F. Igloi, and G. Palagyi, J. Phys. A **31**, 5193 (1998).

[48] N. D. Mermin and H. Wagner, Phys. Rev. Lett. **17**, 1133 (1966).

[49] P. Bruno, Phys. Rev. Lett. **87**, 137203 (2001).

[50] J. Hertz, Phys. Rev. B **14**, 1165 (1976).

5. EXOTIC VS. CONVENTIONAL SCALING AND UNIVERSALITY IN A DISORDERED BILAYER QUANTUM HEISENBERG ANTIFERROMAGNET

Rastko Sknepnek,[1] Thomas Vojta,[1] and Matthias Vojta[2]

[1]*Physics Department, University of Missouri - Rolla, Rolla, MO 65409*

[2]*Institut für Theorie der Kondensierten Materie, Universität Karlsruhe, 76128 Karlsruhe, Germany*

(Dated: April 15, 2004)

Abstract

We present large-scale Monte-Carlo simulations of a two-dimensional (2d) bilayer quantum Heisenberg antiferromagnet with random dimer dilution. In contrast to the exotic scaling scenarios found in many other random quantum systems, the quantum phase transition in this system is characterized by a finite-disorder fixed point with power-law scaling. After accounting for strong corrections to scaling, characterized by a leading irrelevant exponent of $\omega \approx 0.48$, we find universal, i.e., disorder-independent, critical exponents $z = 1.310(6)$ and $\nu = 1.16(3)$. We discuss the consequences of these findings and suggest new experiments.

Quantum phase transitions (QPT) under the influence of quenched disorder are a topic of great current interest. Experimental examples range from localized [1] and itinerant [2] quantum magnets to heavy-fermion compounds [3], high-temperature superconductors [4], metal-insulator [5], as well as superconductor-insulator transitions [6]. These systems display rich new physics but many are still poorly understood. In the context of classical phase transitions, the interplay between disorder and critical fluctuations has a long history. Harris [7] derived a criterion for the stability of a critical point against disorder: If the correlation length exponent ν fulfills the inequality $\nu > 2/d$, where d is the spatial dimensionality, the critical behavior is not influenced by weak disorder. If a clean critical point violates the Harris criterion, the generic result of introducing disorder is a new (finite-disorder) critical point with power-law scaling and new critical exponents which fulfill the Harris criterion [8].

At QPTs, order-parameter fluctuations in space and time have to be considered. Quenched disorder is time-independent, i.e., perfectly correlated in time direction. As a result, disorder effects at QPTs are generically stronger than at classical transitions. Prominent consequences are the infinite-randomness critical points in 1d random spin chains [9] and in 1d [10] and 2d [11] random quantum Ising models. At these infinite-randomness critical points, the dynamical scaling is activated, i.e., the relation between the correlation time ξ_τ and the correlation length ξ is exponential: $\ln \xi_\tau \sim \xi^\mu$. (At a conventional critical point, this relation is a power law, $\xi_\tau \sim \xi^z$). In itinerant electrons systems, the effects of impurities can be even more dramatic. For Ising symmetry, the interplay of quenched disorder and Landau damping of the order parameter fluctuations completely destroys the sharp QPT by smearing [12]. Further unconventional phenomena include non-universal, continuously varying critical exponents, observed in the Griffiths region associated with a QPT [10, 11, 13] or at certain impurity QPTs [14]. These results lead to a general belief that all QPTs in presence of disorder are unconventional [15].

In this Letter we show that this belief is mistaken. Specifically, we demonstrate that a dimer-diluted 2d spin-1/2 bilayer quantum Heisenberg antiferromagnet has a conventional quantum critical point with power-law scaling. Moreover, the critical exponents are *universal*, i.e., dilution-independent, but only after accounting for

corrections to scaling characterized by an irrelevant exponent $\omega \approx 0.48$. The asymptotic dynamical and correlation length exponents are $z = 1.310(6)$ and $\nu = 1.16(3)$ (fulfilling the Harris criterion $\nu > 2/d = 1$ [7, 8]).

Our starting point is the spin-1/2 bilayer quantum Heisenberg antiferromagnet, as depicted in the inset of Fig. 1. The spins in each square-lattice plane interact via exchange $J_\parallel$, and the interplane coupling is $J_\perp$. The clean version of this model has been studied extensively in the past [16, 17]. For $J_\perp \gg J_\parallel$, neighboring spins from the two layers form singlets, and the ground state is paramagnetic. In contrast, for $J_\parallel \gg J_\perp$ the system develops Néel order. Both phases are separated by a QPT at $J_\perp/J_\parallel \approx 2.525$. Importantly, the Berry phase contributions from the two spins of each unit cell exactly cancel, and the continuum limit of this model is an ideal realization of the (2+1)-dimensional O(3) non-linear sigma model without Berry phases [20, 21].

Random disorder is now introduced by removing *pairs* (dimers) of adjacent spins, one from each layer. This type of disorder does *not* introduce random Berry phases, which are present in many other diluted spin systems. Here, by removing dimers, the compensation of Berry phases from adjacent sites is not disrupted by the disorder, and thus this complication is absent. The Hamiltonian of the model with dimer dilution is:

$$H = J_\parallel \sum_{\substack{\langle i,j\rangle \\ a=1,2}} \epsilon_i \epsilon_j \hat{\mathbf{S}}_{i,a} \cdot \hat{\mathbf{S}}_{j,a} + J_\perp \sum_i \epsilon_i \hat{\mathbf{S}}_{i,1} \cdot \hat{\mathbf{S}}_{i,2}, \tag{1}$$

and ϵ_i=0 (ϵ_i=1) with probability p $(1-p)$. The phase diagram of the dimer-diluted bilayer Heisenberg model has been studied by Sandvik [18] and Vajk and Greven [19], see Fig. 1. For small $J_\perp$ magnetic order survives up to the percolation threshold $p_p \approx 0.4072$, and a multicritical point exists at $p = p_p$ and $J_\perp/J_\parallel \approx 0.16$. We focus on the generic transition at $0 < p < p_p$, driven by $J_\perp$, where the results of Refs. [18, 19] are inconclusive.

As an aside, we note that site dilution (in contrast to dimer dilution) completely changes the physics for $J_\perp \gg J_\parallel$. The random Berry phases (which have no classical analogue [21]) are equivalent to impurity-induced moments [22], and those become weakly coupled via bulk excitations. Thus, for all $p < p_p$ the ground state of the system shows long-range order, independent of $J_\perp/J_\parallel$!

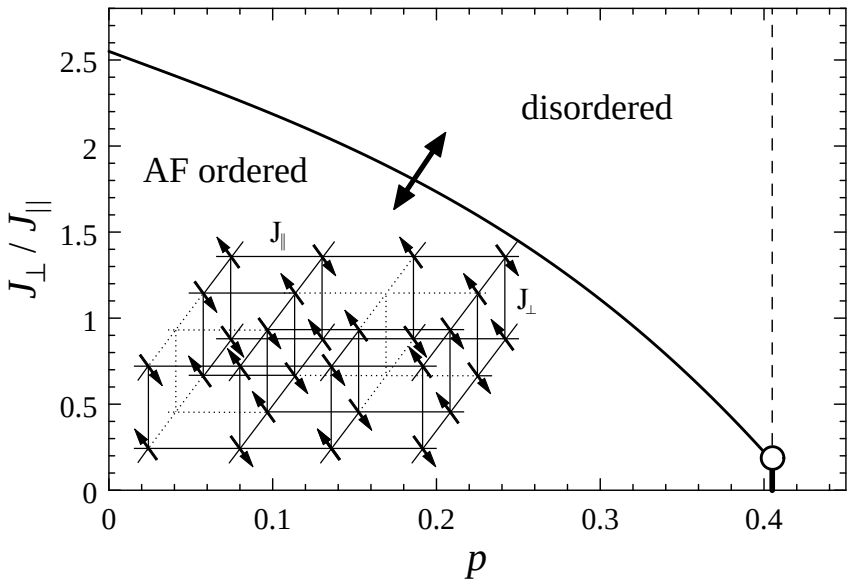

FIG. 1: Phase diagram [19] of the diluted bilayer Heisenberg antiferromagnet, as function of $J_\perp/J_\parallel$ and dilution p. The dashed line is the percolation threshold, the open dot is the multicritical point of Refs. [18, 19]. The arrow indicates the QPT studied here. Inset: The model: Quantum spins (arrows) reside on the two parallel square lattices. The spins in each plane interact with the coupling strength $J_\parallel$. Interplane coupling is $J_\perp$. Dilution is done by removing dimers.

In order to determine the critical behavior at the QPT most effectively, we simulate a 3d classical Heisenberg model which is in the same universality class as the (2+1)-dimensional O(3) non-linear sigma model discussed above. The disorder is introduced via site dilution perfectly correlated in the imaginary time direction, i.e. the impurities are 1d holes "drilled" through the system. The classical Hamiltonian reads:

$$H = K \sum_{\langle i,j\rangle,\tau} \epsilon_i \epsilon_j \mathbf{S}_{i,\tau} \cdot \mathbf{S}_{j,\tau} + K \sum_{i,\tau} \epsilon_i \mathbf{S}_{i,\tau} \cdot \mathbf{S}_{i,\tau+1}, \tag{2}$$

where $\mathbf{S}_{i,\tau}$ is an O(3) unit vector. The coupling constant K of the classical model, or more precisely, βK is related to the ratio $J_\parallel/J_\perp$ of the quantum model. Here, $\beta \equiv 1/T$ where T is an effective "classical" temperature, not equal to the real temperature which is zero. In our simulations we set $K = 1$ and drive the classical system through the transition by tuning the classical temperature T.

We determine the critical behavior of the classical model (2) by performing Monte-Carlo simulations using the highly efficient Wolff cluster algorithm [23, 24]. We study linear sizes up to $L = 120$ in space direction and $L_\tau = 384$ in imaginary time direction for four impurity concentrations $p = \frac{1}{8}$, $\frac{1}{5}$, $\frac{2}{7}$ and $\frac{1}{3}$. The results are averaged over a large number of disorder realizations ranging from 10^4 for the smallest systems to 1000 for the largest. Each sample is equilibrated using 100 Monte-Carlo sweeps (spin-flips per site). For large dilutions, $p = \frac{2}{7}$ and $\frac{1}{3}$ we perform both Wolff and Metropolis sweeps to equilibrate small dangling clusters. During the measurement period of another 100-200 sweeps we calculate the magnetization, susceptibility, specific heat and correlation functions.

A quantity particularly suitable to locate the critical point and to extract high precision values for the exponents z and ν is the Binder ratio:

$$g_{av} = \left[1 - \frac{\langle |\mathbf{M}|^4 \rangle}{3 \langle |\mathbf{M}|^2 \rangle^2} \right]_{av}, \tag{3}$$

where $\mathbf{M} = \sum_{i,\tau} \mathbf{S}_{i.\tau}$, $[\ldots]_{av}$ denotes the disorder average and $\langle \ldots \rangle$ denotes the Monte-Carlo average for each sample. This quantity has scale dimension 0. Thus, its finite-size scaling form is given by

$$g_{av} = \tilde{g}_C(tL^{1/\nu}, L_\tau/L^z) \qquad \text{or} \tag{4}$$

$$g_{av} = \tilde{g}_A(tL^{1/\nu}, \log(L_\tau)/L^\mu) \tag{5}$$

for conventional scaling or for activated scaling, respectively. Two important characteristics immediately follow: (i) For fixed L, g_{av} has a peak as a function of L_τ. The position $L_\tau^{\max}$ of the peak marks the *optimal* sample shape, where the ratio L_τ/L roughly behaves like the corresponding ratio of the correlation lengths in time and space directions, ξ_τ/ξ. At the critical point, the peak value $g_{av}^{\max}$ is independent of L. Thus, for power law scaling, plotting g_{av} at the critical temperature vs. L_τ/L_τ^{max} should collapse the data, without the need for a value of z. In contrast, for activated scaling the g_{av} data should collapse when plotted as a function of $\log(L_\tau)/\log(L_\tau^{\max})$. (ii) For samples of the optimal shape ($L_\tau = L_\tau^{max}$), plots of g_{av} vs. temperature for different L cross at the critical temperature T_c. Based on these two characteristics, we use a simple iterative procedure to determine both the optimal shapes and the location of the critical point.

We now turn to the results of our Monte-Carlo simulations. In order to distinguish between activated and power-law dynamical scaling we perform a series of calculations at the critical temperature. The upper panel of Fig. 2 shows the Binder ratio g_{av} as a function of L_τ for various $L = 5 \ldots 100$ and dilution $p = \frac{1}{5}$ at $T = T_c = 1.1955$. The statistical error of g_{av} is below 0.1% for the smaller sizes and not more than 0.2% for the largest systems. As expected at T_c, the maximum Binder ratio for each of the curves does not depend on L. To test the conventional power-law scaling form, eq. (4), we plot g_{av}/g_{av}^{max} as a function of L_τ/L_τ^{max} in the lower panel of Fig. 2. The data scale extremely well, giving statistical errors of $L_\tau^{\max}$ in the range between 0.3% and 1%. For comparison, the inset shows a plot of g_{av} as a function of $\log(L_\tau)/\log(L_\tau^{max})$ corresponding eq. (5). The data clearly do not scale which rules out the activated scaling scenario. The results for the other three impurity concentrations $p = \frac{1}{8}, \frac{2}{7}, \frac{1}{3}$ are completely analogous.

Having established that the dynamical scaling is of conventional power-law type we proceed to determine the dynamical exponent z. In Fig. 3, we plot L_τ^{max} vs. L for all four dilutions p. The curves show significant deviations from pure power-law behavior. These deviations can be attributed to corrections to scaling, produced by one or more irrelevant operators. In such a situation, a direct power-law fit of the data will only yield *effective* exponents. To determine the true *asymptotic* exponents we take the leading correction to scaling into account, i.e., we use the ansatz $L_\tau^{max}(L) = aL^z(1+bL^{-\omega_1})$ with universal (dilution-independent) exponents z and ω_1 but dilution-dependent a and b. A combined fit of all four curves gives $z = 1.310(6)$ and $\omega_1 = 0.48(3)$ where the number in brackets is the standard deviation of the last given digit. The quality of the fit is very high ($\chi^2 \approx 0.7$), and it is also robust against removing complete data sets or removing different points form the lower or upper end of each set. We thus conclude that the asymptotic dynamical exponent z is indeed universal. (Note that the leading corrections to scaling vanish very close to $p = \frac{2}{7}$; the curvature of the $L_\tau^{\max}(L)$ curves in Fig. 3 is opposite above and below this concentration.)

To determine the correlation length exponent ν, we perform simulations in the vicinity of T_c for samples with the optimal shape ($L_\tau = L_\tau^{max}$) to keep the second argument of the scaling function (4) constant. Fig. 4 shows a scaling plot of g_{av} vs.

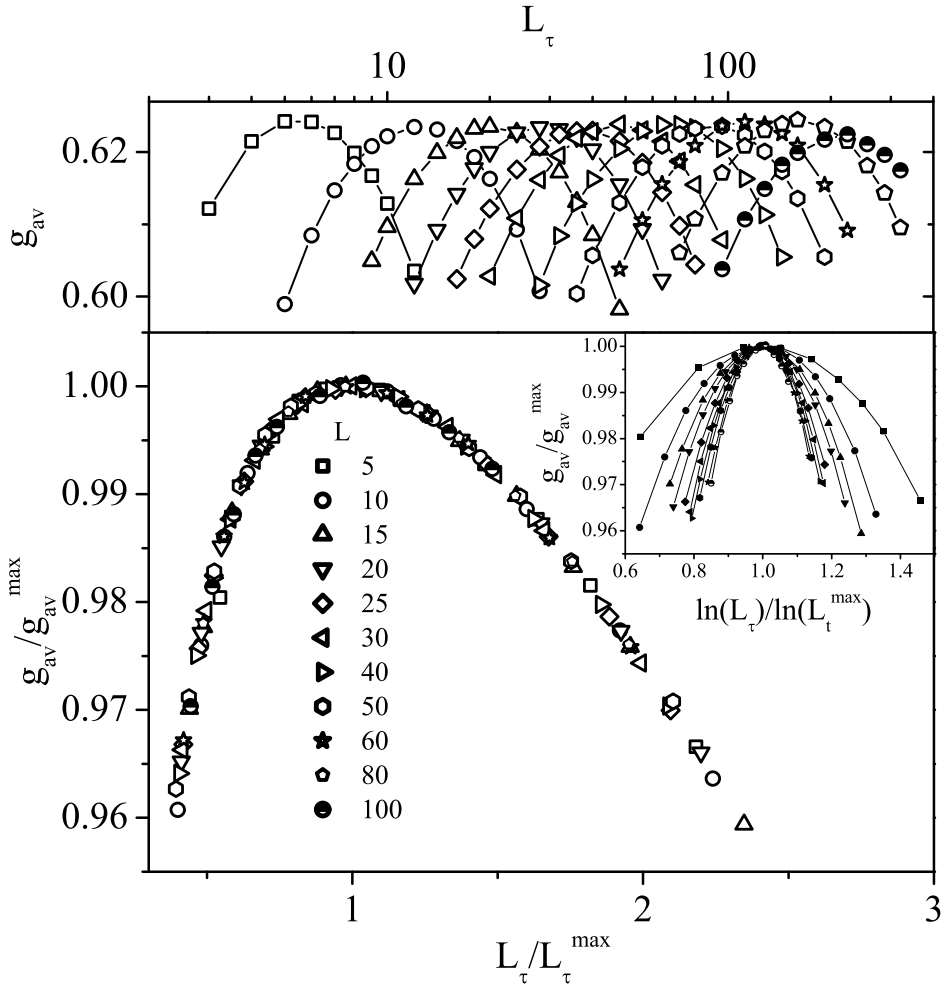

FIG. 2: Upper panel: Binder ratio g_{av} as a function of L_τ for various L ($p = \frac{1}{5}$). Lower panel: Power-law scaling plot g_{av}/g_{av}^{max} vs. L_τ/L_τ^{max} Inset: Activated scaling plot g_{av}/g_{av}^{max} vs. $\log(L_\tau)/\log(L_\tau^{max})$.

$x_L(T - T_c)$ for impurity concentration $p = \frac{1}{5}$. Again, the data scale very well, but since the scaling function lacks the characteristic maximum, the error of the resulting scaling factor x_L is somewhat larger ($1 \ldots 2\%$) than that of $L_\tau^{\max}$. The same quality of scaling was achieved for the other dilutions. Fig. 5 shows the scaling factor x_L vs. L for all four data sets. A combined fit to the ansatz $x_L = cL^{1/\nu}(1 + dL^{-\omega_2})$ where ν and ω_2 are universal, gives $\nu = 1.16(3)$ and $\omega_2 = 0.5(1)$. As above, the fit is robust and of high quality ($\chi^2 \approx 1.2$). Importantly, as expected for the true asymptotic exponent, ν fulfills the Harris criterion [7], $\nu > 2/d$=1. We also note that

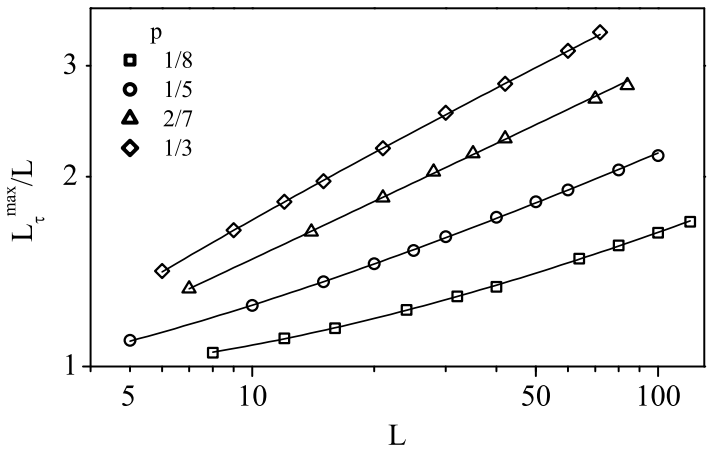

FIG. 3: L_τ^{max}/L vs. L for four disorder concentrations $p = \frac{1}{8}$, $\frac{1}{5}$, $\frac{2}{7}$ and $\frac{1}{3}$. Solid lines: Fit to $L_\tau^{max} = aL^z(1 + bL^{-\omega_1})$ with $z = 1.310(6)$ and $\omega_1 = 0.48(3)$.

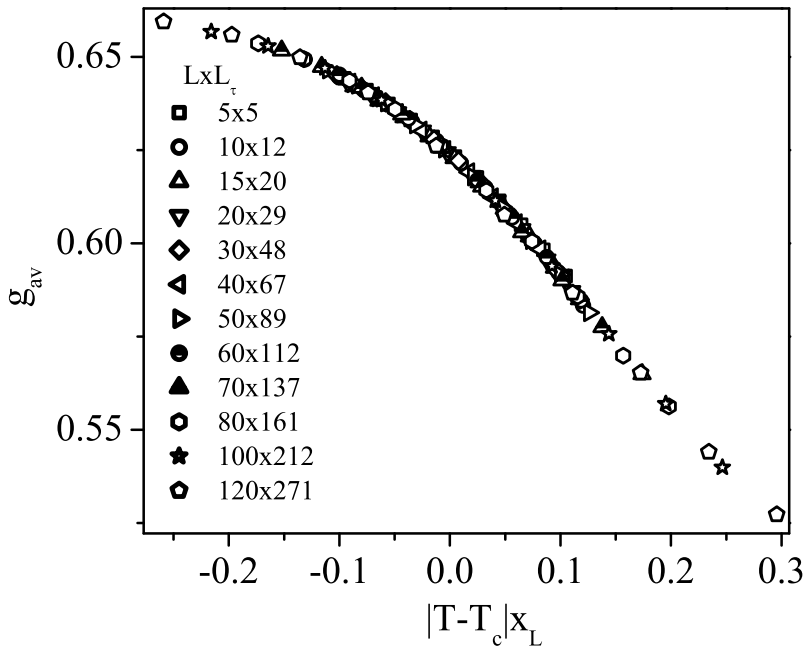

FIG. 4: Scaling plot of g_{av} vs. $(T - T_c)x_L$ for $p = 0.2$.

both irrelevant exponents ω_1 and ω_2 agree within their error bars, suggesting that the same irrelevant operator controls the leading corrections to scaling for both z and ν.

We have also calculated the exponents β and γ. However, the corrections to scaling for magnetization and susceptibility are even stronger than that of the Binder ratio, leading to larger errors for β and γ. We have found $\beta/\nu = 0.56(5)$ and $\gamma/\nu = 2.15(10)$.

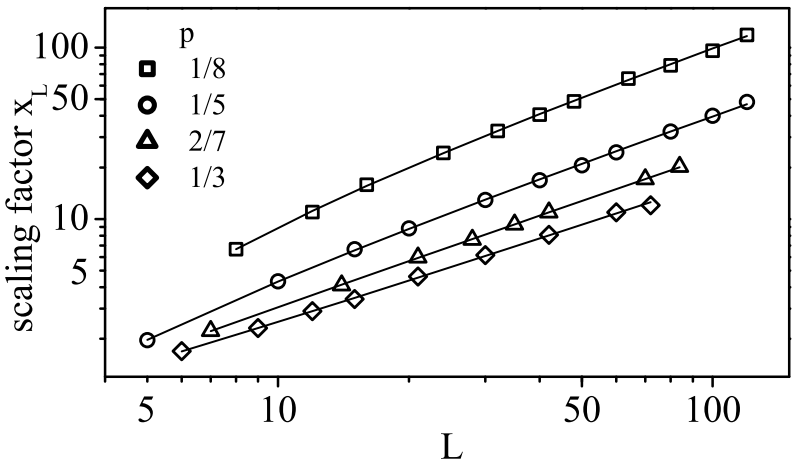

FIG. 5: Scaling factor vs. L for four disorder concentrations $p = \frac{1}{8}$, $\frac{1}{5}$, $\frac{2}{7}$ and $\frac{1}{3}$. Solid lines: Fit to $x_L = cL^{1/\nu}(1 + dL^{-\omega_2})$ with $\nu = 1.16(3)$ and $\omega_2 = 0.5(1)$.

These exponents fulfill the hyperscaling relation $2\beta + \gamma = (d + z)\nu$ which is another argument for our results being asymptotic rather than effective exponents.

In summary, we have performed Monte-Carlo simulations of a 3d classical Heisenberg model with linear impurities which is in the same universality class as the dimer-diluted bilayer quantum Heisenberg antiferromagnet. The QPT in this system is characterized by a conventional, finite-disorder critical point with power-law scaling, in contrast to the wide-spread belief that all QPTs in the presence of disorder are exotic. (Note that the Ising version of our model, the diluted 2d random transverse Ising model, shows an infinite-randomness critical point [11, 26].) Moreover, the asymptotic critical exponents are universal, i.e., dilution-independent.

Let us briefly compare our findings to previous work. The multicritical point at $p = p_p$ and $J_\perp/J_\parallel \approx 0.16$, identified in Refs. [18, 19], has a dynamical exponent $z \approx 1.3$. Within the error bars, this value coincides with the one found here for the generic $p < p_p$ transition. We see no a-priori reason for this coincidence, so far it is unclear whether or not it is accidental. Vajk and Greven [19] also quote exponent values for $p < p_c$. At dilution $p = 0.25$ they find $z = 1.07$ and $\nu = 0.89$, different from our results. However, as the authors of Ref. [19] point out, a value of $\nu < 1$ violates the Harris criterion, indicating that it represents an effective rather than an asymptotic exponent. It would also be useful to compare our findings with analytical

results. To the best of our knowledge, the only quantitative result is a resummation of the 2-loop ϵ-expansion [25]. The predicted critical exponents significantly differ from ours. However, they also violate the Harris criterion, casting doubt on their validity.

Finally, we comment on experiments. If chemical doping replaces magnetic by non-magnetic ions in a 2d antiferromagnet, e.g., Cu by Zn in $YBa_2Cu_3O_6$, the case of site rather than dimer dilution is realized. The most promising way to effectively achieve bond dilution is the introduction of strong antiferromagnetic inter-dimer bonds at random locations. Thus we propose to study magnetic transitions in bond-disordered systems; those transitions can be expected to be in the same universality class as the one studied here. One candidate material – albeit 3d – is (Tl,K)$CuCl_3$ under pressure; interesting quasi-2d compounds are $SrCu_2(BO_3)_2$ or $BaCuSi_2O_6$, where suitable dopants remain to be found.

We acknowledge support from the University of Missouri Research Board and from the DFG Center for Functional Nanostructures Karlsruhe.

[1] W. Wu *et al.*, Phys. Rev. Lett. **67**, 2076 (1991).

[2] J. DiTusa *et al.*, cond-mat/0306541.

[3] C. L. Seaman *et al.*, Phys. Rev. Lett. **67**, 2882 (1991); B. Andraka and A. M. Tsvelik, Phys. Rev. Lett. **67**, 2886 (1991); M. C. de Andrade *et al.*, Phys. Rev. Lett. **81**, 5620 (1998).

[4] C. Panagopoulos *et al.*, Phys. Rev. B **66**, 064501 (2002).

[5] S. V. Kravchenko *et al.*, Phys. Rev. B **51** 7038 (1995); E. Abrahams, S. Kravchenko, and M. Sarachik, Rev. Mod. Phys. **73**, 251 (2001).

[6] A. F. Hebard and M. A. Paalanen, Phys. Rev. Lett. **65**, 927 (1990).

[7] A. B. Harris, J. Phys. C **7**, 1671 (1974).

[8] J. Chayes *et al.*, Phys. Rev. Lett. **57**, 2999 (1986).

[9] S. K. Ma, C. Dasgupta, and C.-K. Hu, Phys. Rev. Lett. **43**, 1434 (1979); R. N. Bhatt and P. A. Lee, *ibid.* **48**, 344 (1982); D. S. Fisher, Phys. Rev. B **50**, 3799 (1994).

[10] D. S. Fisher, Phys. Rev. Lett. **69**, 534 (1992); Phys. Rev. B **51**, 6411 (1995); A. P.

Young and H. Rieger, *ibid.* **53**, 8486 (1996);

[11] C. Pich *et al.*, Phys. Rev. Lett. **81**, 5916 (1998); O. Motrunich *et al.*, Phys. Rev. B **61**, 1160 (2000).

[12] T. Vojta, Phys. Rev. Lett. **90**, 107202 (2003).

[13] R. B. Griffiths, Phys. Rev. Lett. **23**, 17 (1969); B. M. McCoy, Phys. Rev. Lett. **23**, 383 (1969).

[14] A. Georges and A. M. Sengupta, Phys. Rev. Lett. **74**, 2808 (1995), and references therein.

[15] Y.-C. Lin, R. Melin, H. Rieger, and F. Igloi, Phys. Rev. B **68**, 024424 (2003) have shown that the *stable low-energy fixed point* of random Heisenberg models in $d \geq 2$ is conventional.

[16] K. Hida, J. Phys. Soc. Jpn. **59**, 2230 (1990); A. J. Millis and H. Monien, Phys. Rev. Lett. **70**, 2810 (1993).

[17] A. W. Sandvik and D. J. Scalapino, Phys. Rev. Lett. **72**, 2777 (1994); P. V. Shevchenko, A. W. Sandvik and O. P. Sushkov, Phys. Rev. B **61**, 3475 (2000).

[18] A. W. Sandvik, Phys. Rev. Lett. **89**, 177201 (2002).

[19] O. P. Vajk and M. Greven, Phys. Rev. Lett. **89**, 177202 (2002).

[20] S. Chakravarty, B. I. Halperin and D. R. Nelson, Phys. Rev. B **39**, 2344 (1989).

[21] S. Sachdev, *Quantum Phase Transitions*, Cambridge University Press, Cambridge (1999).

[22] S. Sachdev and M. Vojta, in Proceedings of the XIII International Congress on Mathematical Physics, eds. A. Fokas *et al.*, International Press, Boston (2001).

[23] U. Wolff, Phys. Rev. Lett. **62**, 361 (1989).

[24] Since the classical model is not frustrated, we can use cluster algorithms to reduce critical slowing down.

[25] V. Blavats'ka, C. von Ferber, and Yu. Holovatch, Phys. Rev. B **67**, 094404 (2003).

[26] T. Senthil and S. Sachdev, Phys. Rev. Lett. **77**, 5292 (1996).

VITA

Rastko Sknepnek was born on December 14, 1976 in Pančevo, Serbia and Montenegro (formerly Yugoslavia). He received his diploma in theoretical physics from the Faculty of Physics, Belgrade University in May 2000. In the same year he joined the group of Prof. Dr. Michael Schreiber as a graduate student at the Physics Department, Chemnitz University of Technology, Germany. His research was supervised by Dr. Thomas Vojta, at the time senior research assistant in Prof. Schreiber's group. In February 2002 he transfered to the University of Missouri-Rolla following Dr. Vojta who has taken a faculty position in the Physics Department.